REMOTE SENSING ESTIMATION OF SPATIAL AND TEMPORAL VARIABILITY OF ACTUAL EVAPOTRANSPIRATION USING SEBS ALGORITHM IN THE SEMI-ARID BAROTSE SUB-BASIN, SOUTH-WESTERN ZAMBIA

Wilson Kakusa Phiri

A thesis submitted to the University of Zambia, School of Mines, in partial fulfilment of the requirement for the Master of Science Degree in Integrated Water Resources Management

University of Zambia
LUSAKA

DECLARATION

This thesis was written and submitted in accordance with the rules and regulations governing the award of Master of Science in Integrated Water Resources Management of the University of Zambia. I further declare that the thesis has neither in part nor in whole been presented as substance for award of any degree, either to this or any other University. Where other people's work has been drawn upon, acknowledgement has been made.

Signature of author: .....

Date: .....

APPROVAL

This thesis of Wilson Kakusa Phiri is approved as fulfilling the requirements of the Degree of Master of Science in Integrated Water Resources Management of the University of Zambia.

Signature: Chairperson: .....

1st Examiner: .....

2nd Examiner: .....

External Examiner: .....

ABSTRACT

Evapotranspiration (ET) is a dominant hydrologic flux in the water budget of semi-arid areas. Thus, accurate estimation of its dynamics in such environments is critical for improving water resources management. In this study the physically-based Surface Energy Balance System (SEBS) model was applied to estimate the spatial and temporal variability of actual ET (AET) in the semi-arid Barotse Sub-basin, South-Western Zambia. The model was run using atmospherically rectified Moderate-resolution Imaging Spectroadiometer (MODIS) satellite imagery on clear-sky warm-wet, cool-dry and hot-dry days. Furthermore, based on sunshine hours and daily AET, monthly fluxes were generated. The modelled evaporative fluxes were evaluated against Penman-Montieth potential ET (PET) and independently modelled AET from the Global Circulation Model (GCM) of the European Centre for Medium-Range Weather Forecast (ECMWF).

Results showed that actual evaporative fluxes were ~64.3% and 29.4% of PET on cool-dry and hot-dry days respectively. However, these fluxes were ~104.2% of PET on warm-wet days. The systematic lack of physical agreement on these days implied that SEBS estimates were not necessarily implausible but that the assumptions on which PET is based differed from the surface conditions. This highlighted the uncertainties of evaluating AET against PET. The comparison with ECMWF estimates showed better agreement on many days at Sesheke weather station than at Kamanga. At a monthly time-step, however, this comparison showed lack of good agreement ascribed to input data and surface parameterisation. Sensitive analysis showed that model outputs varied by up to 3 mm day^{-1} when estimated air temperature in the term $\Delta(T_0-T_a)$ was varied by 8 K whereas the use of NDVI versus landuse-based surface roughness revealed a reduction of ET of up to 1.5 mm day^{-1} on forests when the latter was used. Flux analysis showed that water bodies and regularly flooded vegetation had the highest rates of ~6.9 and 5.9 mm day^{-1} on warm-wet days respectively. The lowest rates occurred over mosaic vegetation/croplands and closed to open grassland with a high variation of up to 64.1 and 71.1% respectively between warm-wet and hot-dry days.

On the overall, this study showed that the SEBS model can be successfully used to estimate evaporative fluxes in heterogeneous areas and improve water resources management. In order to accurately apply this model in such areas, however, there is need to use spatial input data and robust ways of estimating surface roughness.

DEDICATION

To my mum, Mrs. Justina Phiri, who gives me lectures on working hard in silence and discipline;

and

To my uncle, the late Justice Tamula Kakusa,who saw the 'eagle' in me and taught me how to soar.

ACKNOWLEDGEMENTS

I would like to thank my supervisor, Professor Imasiku Nyambe, for his support and professional guidance during the preparation of this thesis. His unwavering commitment to and passion for producing excellent and thorough research works inspired me to work harder. Not once but many a time, he was always prepared to go out of his way to help me stay focused on finishing this research. I will forever be indebted to him for my acquisition of the eye and a pair of infrared spectacles of a researcher needed to see through darkness.

This research was successfully completed courtesy of the financial and technical support of Tiger Africa Capacity Building Initiative for the application of satellite remote sensing to support water resources management in Africa under Project Number 026. I sincerely thank Tiger Africa for generously giving me the opportunity and financial support to attend the 12th WaterNet Conference in Maputo, Mozambique, the training course on Advanced Earth Observation Methods in Water Resources Management during the 4th Tiger Capacity Building Facility II Training Workshop at the South African National Space Agency (SANSA), South Africa, the training course on Synergic Use of Advanced Earth Observation in Water Resources Management in Lusaka, Zambia, and the 9th International Conference of African Association of Remote Sensing and the Environment (AARSE) in El Jajida, Morocco. These experiences provided me with opportunities to acquire invaluable skills that helped me to complete this thesis. For all this I say, *inshallah,* viva Tiger Africa!

I would like to forward my gratitude to the Danish International Development Agency (DANIDA), Royal Danish Embassy in Lusaka and Ministry of Mines, Energy and Water Development (MMEWD) through the University of Zambia Integrated Water Resources Management Centre (UNZA-IWRM Centre) in the School of Mines for the generous financial resources rendered to me for use in the fieldwork campaign. Without this support it would have been very difficult for me to finish this work.

My special thanks also go to Mr. Joel Kabika (PhD student-UNZA) and Mr. Kawawa Banda (PhD student-Danish Technical University, Denmark) for the support during data collection and helpful comments at the writing stage of this thesis. Ms Ingrid Kawesha, (Administrative Secretary at UNZA-IWRM Centre) is also specially thanked for logistical and moral support.

I extend my thanks to Dr. Timmerman Joris, Dr. Tsehaie Woldai and Mr. Mustapha Gokmen from the International Institute for Geo-information Science and Earth Observation (ITC), Enschede, The Netherlands, for their comments and answering my numerous queries related to this research.

My heartfelt thanks goes to my lovely and caring wife, Mercy Mwansa Phiri, and our children, Trevor and Leah for their patience and support during the whole study period when I was way from the comfort of our home.

I also thank my fellow MSc. IWRM students at UNZA, Mr. Solomon Mbewe, Mr. Ben Makayi and Ms. Choolwe Shalwindi for their encouragement during the time we spent together studying and researching. I extend my thanks to Mr. Humphrey Mubita (Acting District Water Officer - Sesheke) for the invaluable help he rendered to me during data collection in the hinterlands of Sesheke District. His friendly personality, versatility and in-depth knowledge of the geography of the local area proved to be very valuable during the field work campaign.

TABLE OF CONTENTS

LIST OF FIGURES

LIST OF TABLES

LIST OF ACRONYMS

AATSR:	Advanced Along Track Scanning Radiometer
ASTER:	Advanced Space borne Thermal Emission and Reflection Radiometer
CWSI:	Crop Water Stress Index
BAS:	Bulk Atmospheric Similarity
DEM:	Digital Elevation Model
DOY:	Day of the Year
ESA:	European Space Agency
ECMWF:	European Centre for Medium-Range Weather Forecast
GCM:	Global Circulation Model
FAO:	Food and Agriculture Organisation
ILWIS:	Integrated Land and Water Information System
LAI:	Leaf Area Index
LANDSAT:	LAND remote sensing SATellite
LIDAR:	Laser Imaging Detection and Ranging
MERIS:	Medium Resolution Imaging Spectrometer
METRIC:	Mapping ET at high Resolution and with Internalized Calibration
MODIS:	Moderate-resolution Imaging Spectoradiometer
MOS:	Monin-Obukhov Similarity
NDVI:	Normalised Difference Vegetation Index
NIR:	Near-Infrared
PAN:	Panchromatic
PBL:	Planetary Boundary Layer
RTM:	Radiative Transfer Models
SEBAL:	Surface Energy Balance Algorithm for Land
SEBS:	Surface Energy Balance System
SEBI:	Surface Energy Balance Index
S-SEBI:	Simplified Surface Energy Balance Index
SMAC:	Simplified Method for Atmospheric Correction
SVAT:	Soil Vegetation Atmospheric Transfer models
TIR:	Thermal-Infrared
TSEB:	Two-Source Energy Balance
WMO:	World Meteorological Organisation

LIST OF SYMBOLS

Symbol	Meaning	Unit
AET	Actual evapotranspiration	mm day^{-1}
C_d	Drag coefficient of the foliage	-
C_p	Specific heat capacity of dry air	$JKg^{-1}K^{-1}$
C_t	Heat transfer coefficient of the leaf	-
d_o	Zero-plane displacement height	m
ET_o	Reference evapotranspiration	mm day^{-1}
e_a	Actual vapour pressure	kPa
e_s	Saturation vapour pressure	kPa
f_c	fraction vegetation cover	-
g	Acceleration due to gravity	ms^{-2}
G_o	Ground heat flux	Wm^{-2}
H	Sensible heat flux	Wm^{-2}
H_{dry}	Sensible heat flux at dry limit	Wm^{-2}
H_{wet}	Sensible heat flux at wet limit	Wm^{-2}
k	von Karman`s constant	-
K ↓	Incoming shortwave radiation	Wm^{-2}
kB^{-1}	Excess resistance to heat transfer	-
L	Monin-Obukhov length	m
L ↓	Incoming longwave radiation	Wm^{-2}
L ↑	Outgoing longwave radiation	Wm^{-2}
n_{ec}	within canopy wind speed extinction coefficient	-
P	Air pressure	Pa
PET	Potential evapotranspiration	mm day^{-1}
Po	Air pressure at sea level	Pa
q	Specific humidity of air	-
r_{ah}	Aerodynamic resistance to heat transport	sm^{-1}
R_d	The gas constant for dry air	$JKg^{-}K^{-1}$
R_v	The gas constant for water vapour	$JKg^{-}K^{-1}$
RH	Relative humidity	%
r_o	Broadband albedo	-

R_n	Net radiation	Wm^{-2}
T	Temperature	^oC
u	Horizontal wind speed	ms^{-1}
u_*	Frictional velocity	ms^{-1}
Z	Height above surface	m
Z_{oh}	Roughness height for momentum transfer	m
Z_{om}	Roughness height for momentum transfer	m
Ψ_h	Stability correction for heat transport	-
Ψ_m	Stability correction for momentum transport	-
β	Bowen ratio	-
θ	Potential temperature	K
θ_v	Virtual potential temperature	K
Δ	Slope of saturation vapour pressure	KPa^oC^{-1}
Λ	Evaporative fraction	-
ε_a	Emissivity of the atmosphere	-
ε_s	Land surface emissivity	-
σ	Stefan-Boltzman constant	$Wm^{-2}K^{-4}$
ρ_{air}	Mean air density at constant pressure	Kgm^{-3}
λET	Latent heat flux	Wm^{-2}
γ	Psychrometric constant	PaK^{-1}
τ	Transmissivity	-
Γ_c	Soil heat flux ratio for a full vegetation canopy	-
Γ_s	Soil heat flux ratio for bare soil	-

CHAPTER 1: INTRODUCTION

1.1 Background

Evapotranspiration (ET), the sum of transpiration through plant canopy and evaporation from soil and plant surfaces (Singh, 1988; Mu et al., 2007), is a major component of the hydrologic budget (Brutsaert, 1982; Irmark, 2008; Khan et al., 2010). It is estimated that, on the average, two-thirds of the precipitation is returned to the atmosphere by evapotranspiration (Brutsaert,1982; Irmark, 2009) though this ratio varies from nearly 100 percent in the deserts to one-third or less where precipitation is high and ET relatively small (Johnson et al., 1977). It is for this reason that ET plays an important role in explaining water balance dynamics, land-atmosphere and mass-energy interactions, and improving agricultural water management (Rwasoka et al., 2011). Consequently, the accurate measurement of ET has an increasing importance in diverse disciplines such as hydrology, agronomy and meteorology (Anderson et al., 2003; Moran, 2004; Suleiman and Crago, 2004) as it provides the basis for precision irrigation, determining crop water stress and water use of vulnerable ecosystems, and predicting climate variability (van der Kwast et al., 2009). In arid and semi-arid areas, where ET is a dominant hydrologic flux (Kongo et al., 2006; Khan et al., 2010), precise quantification of its spatial and temporal variability is critical for estimating surface and groundwater resources (Huxman et al., 2005) and enhancing water resources management.

Notwithstanding its importance, ET is the least understood (Wilson et al., 1992), and one of the difficult components of the hydrologic water budget to quantify and monitor (Gash and Shuttleworth, 2007). In fact, among the components of the hydrological cycle, ET is one of the most challenging to estimate directly owing to the complex interactions among the components of the land-plant-atmosphere system (Hughes, 2001). This makes the determination of spatially distributed ET a complex task, especially at a basin or catchment scale. For this reason, ET has often been treated as a lumped residual flux from hydrologic models or quantified indirectly from local weather stations. The prevalent methods of estimating ET provide potential evapotranspiration (PET) or reference evapotranspiration (ET_o) and sometimes crop evapotranspiration (ET_c) as a product of weather-based reference evapotranspiration and crop coefficient at points, rather than spatial-temporal information about actual evapotranspiration (AET) (Allen et al., 2005c; Khan, et al., 2010).

Point based methods assume that land surfaces are homogeneous (Allen et al., 1998). Yet it is common, not least from the catchment scale, to find different types of land cover co-existing within a few square meters. These vegetation species will have different features such as rooting depth and stomata resistance all of which complicate the computation of ET over large areas. Besides, water loss by transpiration through the stomata on the leaf is not only dependent on the physiology of plant species but also the stage of growth of the plant and external factors such as radiation, air temperature and humidity, and wind (Gibson et al., 2010). This means that under the same physical conditions, plant species will have different rates of ET with respect to their physiology and stage of growth. Typically, in heterogeneous regions, a vegetated land area might exits adjacent to or forms a composite mix with land surfaces such as rivers, wetlands, cultivated land, bare land and built-up areas. Given such a scenario, point based methods fail to adequately account for the spatial distribution of ET. The problem becomes worse when these points (weather stations) are sparsely spread over a catchment. This is the typical case of the larger part of the Zambezi Basin (Cohen et al., 2010), in which the semi-arid Barotse Sub-basin of South-Western Zambia is located.

The apparent shortcomings of point based methods underscore the importance of employing techniques that effectively capture the spatial distribution of ET. In the recent past, remote sensing for spatially distributed ET has become a pragmatic approach, especially with the availability of large amounts of remote sensing data and development of various modelling techniques (Khan et al., 2010). This development has presented unprecedented opportunities for understanding the dynamics of surface-atmospheric interaction. A host of remote sensing techniques, algorithms and models have over the years been proposed for the estimation of ET by various researchers (e.g Kustas et al., 1994; Carlson et al., 1995; Bastiaanssen et al., 1998a; Jiang and Islam, 2001; Su, 2002; Nishida et al., 2003; Boegh and Soegaard, 2004). The gist of the remote sensing approach for estimating ET is to accurately quantify radiation and turbulent heat fluxes using radiometric measurements from satellite sensors. The more advanced and successful of these are based on the thermal infrared signals that contain information on the spatial distribution of the land surface temperature (Wang et al., 2006).

Application of remote sensing techniques can be an important source of obtaining data about the dynamic state of the components of the hydrological budget especially in areas where in-situ measurements are limited. This is because remote sensing data have the advantage of detailed area coverage (spatial resolution), regular updates (temporal resolution) and can ‘see’

in a wide range of the electromagnetic spectrum (spectral resolution).Today massive amount of this data is generated at different resolutions from numerous satellite sensors. Consequently, among the broad spectrum of its uses, remote sensing data is increasingly becoming an important source of information that inform sound water use planning, monitoring and management at a field, catchment and regional scale (Mu et al., 2007).

1.2 Statement of the problem

The amount of soil moisture available to the root crop, fresh water available for recharging aquifers and surface water available for human uses in the semi-arid Barotse Sub-basin, as in many other hot semi-arid areas (Huxman et al., 2005), depends largely on the balance between precipitation and ET. Characterized by limited precipitation and high rates of ET (Zambia Meteorological Department-ZMD, 1992), the semi-arid Barotse Sub-basin is prone to surface water and soil moisture deficits (droughts). This scenario poses a threat to the existence of human and animal life as a small portion of usable water is left at the land-atmosphere interface. Although rural water supply in this area depends largely on borehole water, the significantly high rate of ET and limited rainfall inevitably affects the amount of freshwater available for recharging aquifers. Thus, accurate measurement of AET in this semi-arid environment is not only critical for the understanding of spatial and temporal variability of surface fluxes but also for the assessment of groundwater recharge. The latter is the basis for determining issues related to groundwater sustainability such as the optimum rate of abstraction per year.

Despite the fact that ET is the second dominant hydrologic flux in the water balance of the semi-arid Barotse Sub-basin, data on its spatial and temporal variability is scarcer than rainfall data (cf. Cohen et al., 2010). The estimates of ET over large and varied areas of the basin are based on limited point measurements. Consequently, the spatial-temporal variability of ET is roughly quantified and thus not clearly understood. This situation is at variance with the need to understand distributed hydrologic fluxes for improved water resources management at a catchment or basin level. It is important to use spatial modelling techniques to accurately quantify the spatial-temporal distribution of AET especially in water stressed areas, as it is a key component in agriculture water resources management, planning sustainable use of limited water resources and modelling groundwater recharge rates, all of which are critical issues in the semi-arid Barotse Sub-basin (Kabika et al., 2010).

1.3 Purpose of the study

The purpose of this study is to estimate the spatial and temporal variability of actual evapotranspiration using remote sensing techniques and SEBS algorithm in the semi-arid Barotse Sub-basin of South-Western Zambia with the view to contributing towards improved water resources management, monitoring and water use planning.

1.3.1 General objective

The overall objective of this study is:

1. Using remote sensing and the SEBS algorithm to estimate the spatial and temporal variability of AET in the semi-arid Barotse Sub-basin.

1.3.2 Specific objectives

The specific objectives for this study are:

1. Estimating AET over different land cover using SEBS algorithm and MODIS images on typical clear-sky warm-wet, cool-dry and hot-dry days;
2. Generating monthly evaporative fluxes from daily AET and sunshine hours;
3. Determining daily PET from meteorological data using the FAO Penman-Montieth method; and
4. Evaluation of the SEBS modelled evaporative fluxes against calculated PET and independently modelled AET from the GCM of ECMWF.

1.3.3 Research questions

The research questions are:

1. What are the daily estimates of AET over the different land cover types on clear-sky warm-wet, cool-dry and hot-dry days in the semi-arid Barotse Sub-basin?
2. To what extent does AET vary over typical warm-wet, cool-dry and hot-dry months in the semi-arid Barotse Sub-basin?
3. What are the daily estimates of PET in the semi-arid Barotse Sub-basin using the FAO Penman-Montieth method? and
4. Do the SEBS actual evaporative fluxes show physical agreement with PET and ECMWF estimates?

1.4 Significance of the study

It is an established fact that estimation of ET from a soil and vegetated surface is one of the basic requirements needed for computing water balances and assessing water availability and requirements especially in arid and semi-arid areas (Pereira et al., 1996). The case for estimating spatial and temporal variability of AET in the semi-arid Barotse Sub-basin is more compelling given that this area is one of the regions in Zambia prone to droughts and highly susceptible to projected threats of severe climate variability and change (Flint, 2006). Since much of the semi-arid Barotse Sub-basin is already experiencing below normal annual rainfall and high rate of ET (i.e. point based estimates), the projected climate variability and change will intensify ET patterns of this area (Huntington, 2006) thereby severely limiting the amount of freshwater available for human use. It is also very likely that even groundwater quantities, which form the major and reliable source of usable water in this area, will be affected over time, as high rates of ET determines the amount of freshwater recharge and discharge from aquifers (Huxman et al., 2005). Given that freshwater is presently a scarce resource in the semi-arid Barotse Sub-basin, the intensification of ET may create untold misery, hunger and disease. However, through quantitative assessment of spatial and temporal dynamics of AET valuable data can be generated for the semi–arid Barotse Sub-basin that can inform sound practices in water resources management and mitigation strategies. Therefore, this study is useful to a wide range of interest groups particularly those interested in the field of environmental application (optimizing irrigation water use, irrigation system performance, crop water deficit, drought mitigation strategies and water resources monitoring and utilizations) such as the Ministry of Mines, Energy and Water Development in charge of planning and development of the water resources in Zambia. This assertion is based on the fact that the accurate estimation of ET in semi-arid environments or water-limited areas is of critical importance for determining water requirements for crops (Allen et al., 1998; Irmark, 2008; Irmark, 2009; van der kwast et al., 2009) and enhancing water resources planning, monitoring and management as it constitutes a dominant hydrologic flux (Khan et al., 2010).

CHAPTER 2: LITERATURE REVIEW

2.1 Defining the concept of evapotranspiration

The term 'evapotranspiration' is a fusion of the two words [Evapo (Transpire) ration], that is, evaporation and transpiration. Therefore, according to Irmark (2008), evapotranspiration in agro-ecosystems is the sum of two terms; (1) transpiration, in which water entering the plant roots is carried to stems and leaves for building plant tissue via photosynthesis and then passes through the leaves of the plant into the atmosphere, and (2) evaporation, which is water evaporating from soil and plant leaf surfaces holding water droplets from rain, irrigation, or dew formation. In simple terms, it is defined as the discharge of water from land surfaces to the atmosphere by evaporation from soil surfaces and by transpiration from the plants via stomatal openings (Singh, 1988; Brutsaert, 1982; Mu et al., 2007). It is worth pointing out that its usage underscores the basic fact that, in reality, evaporation and transpiration cannot be separated because they occur simultaneously (Allen et al., 1998).

In the analysis of ET, a conceptual distinction is made between potential evapotranspiration (PET) and actual evapotranspiration (AET). According to Brutsaert (1982), PET is the maximum intensity of ET from a large surface covered completely and homogeneously with actively growing plants under conditions of unlimited availability of soil water. The World Meteorological Organization (WMO, 1992) defines PET as the maximum quantity of water capable of being evaporated in a given climate from a continuous expanse of vegetation covering the whole ground and well supplied with water. Allen et al. (1998) refer to it as the crop ET under standard conditions and define it as the ET from disease-free, well-fertilised crops, grown in large fields, under optimum soil water conditions and achieving full production under the given conditions. In simple terms, PET is viewed as the ET from a vegetated surface when the water supply to plants is unlimited (Irmark, 2008).

On the other hand, AET can be defined as the quantity of water vapour evaporated from the soil and plants when the ground is at its natural moisture content (WMO, 1990). Brutsaert (1982) defines AET as the amount of water lost from a system given existing evaporative energy conditions (i.e PET) and the available water provided by precipitation and storage in the soil. Allen et al. (1998) define it as the amount of water transpired from plants and evaporated from soil surface under actual meteorological conditions and under non-optimal

soil, biological, management and environmental conditions. This means that it is a dynamic measure of the evaporative flux which varies depending on the prevailing climatic conditions, type of land cover and the existing amount of soil water (WMO, 1992).

2.2 Factors that influence the process of evapotranspiration

There are a number of factors that affect ET. These include weather parameters such as solar radiation, air temperature, humidity and wind speed, and land surface characteristics such as type and density of vegetation cover, rooting depth and reflective land cover characteristics (Allen et al., 1998; Irmark, 2008). According to WMO (1992) factors affecting the rate of ET from any surface can be broadly divided into two groups: meteorological factors and surface factors, either of which may be rate-limiting. The meteorological factors may, in turn, be subdivided into energy and aerodynamic variables.

Energy is needed to change water from liquid to the vapour phase. Clearly, ET is influenced by the amount of energy available to vapourise water (Allen et al., 1998). In nature, this energy is largely supplied by solar and terrestrial radiation. The spatial and temporal distribution of this solar radiation on the globe is governed by a number of factors. Firstly, the potential amount of radiation that can reach the evaporating surface is determined by its location and time of the year. In this case, potential radiation differs at various latitudes and in different seasons due to differences in the position of the sun. Secondly, the actual solar radiation reaching the evaporating surface depends on the turbidity of the atmosphere and the presence of clouds which reflect and absorb major parts of the radiation. It is important to note, however, that not all available energy reaching the surface is used to vapourise water. Some of it is used to heat up the atmosphere and the soil profile (Brutsaert, 1982).

On the other hand, aerodynamic variables such as wind speed at the surface and vapour pressure difference between the surface and the lower atmosphere, control the rate of transfer of the evaporated water vapour (Albertson et al., 2001). For instance, wind and air turbulence is responsible for removing vapour above the vapourating surface. Unless the saturated air above the vapourating surface is continuously replaced with drier air, the driving force for water vapour removal and ET rate decreases. Consequently, an increase in wind speed will increase the rate of evaporation, unless air movement also results in a reduction in temperatures (Allen et al., 1998). It is also useful to distinguish between situations where free water is present on the surface and those where it is not. In this regard, factors of importance

include the amount and state of the water and also those surface characteristics which affect the transfer process to the air or through the body surface. Resistance to moisture transfer to the atmosphere depends, for example, on surface roughness (Albertson et al., 2001). In arid and semi-arid areas, the size and shape of the evaporating surface is also extremely important. Transpiration from vegetation, in addition to the meteorological and surface factors already noted, is largely determined by plant characteristics and responses. These include, for example, the number and size of stomata (openings in the leaves), and whether these are open or closed. Stomatal resistance to moisture transfer shows a diurnal response but is also considerably dependent upon the availability of soil moisture to the rooting system. The availability of soil moisture for the roots and for the evaporation from bare soil depends on the capillary supply, namely, on the texture and composition of the soil (Allen et al., 1998).

2.3 Methods of estimating evapotranspiration

There are basically three broad groups of estimating ET: direct measurements, hydrologic modelling and remote sensing techniques (Gieske, 2003). Traditionally, however, ET has been estimated using empirical equations which retrieved the reference evapotranspiration based on the so called reference surface (grass or alfalfa under well-watered conditions) and a crop coefficient. Many formulae have been proposed on how to retrieve the reference evapotranspiration, and some of these include the Penman, Thornthwaite, Hargreaves, Priestly and Taylor and FAO Penman-Montieth equations (Penman, 1948; Thornthwaite, 1948; Priestley and Taylor, 1972; Allen et al., 1998). In this study only the FAO Penman-Montieth method (FAO56-PM), which is the internationally recommended standard for estimating the reference evapotranspiration for a grass surface (Allen et al., 1998), is reviewed. An extensive review of this approach and other empirical equations that can be used for retrieving the reference evapotranspiration is available on this web site: http//www.sjrwmd.com/technicalreports/pdfs/sp/sj2001-sp8.pdf. Therefore, a brief review of the FAO Penman-Montieth method from the website is given here.

2.3.1 Conventional methods of calculating ET: FAO Penman-Montieth Equation

The Food and Agricultural Oraganisation-Penman-Montieth method (FAO 56-PM), which incorporates the Penman-Montieth model, is one of the traditional equations used for estimating ET and is recommended for use worldwide (Allen et al., 1998). In this method the ET for a crop canopy is estimated using a reference ET (ET_o) and a crop coefficient (Kc). The

FAO 56-PM is an hourly or daily grass reference ET equation derived from the American Society of Civil Engineers-Penman-Montieth (ASCE PM-90) by assigning certain parameter values based on a specific reference surface (Allen et al., 1998). This surface has an assumed height of 0.12 m, a fixed surface resistance (r_a) of 70 s m^{-1}, and an albedo of 0.23. The zero plane displacement height and roughness lengths are estimated as a function of the assumed crop height, so that surface resistance becomes a function of only the measured wind speed. The height for the temperature, humidity, and wind measurements is assumed to be two (2) metres. The latent heat of vaporization (λ) is assigned a constant value of 2.45 MJ kg^{-1} (Allen et al., 1998). Thus, from the original Penman-Montieth combination model, the FAO 56-PM was formulated by assigning these values. The FAO 56-PM model is given as shown in equation (1) (Allen et al., 1998).

$$ET_o = \frac{0.408\,\Delta(R_n - G_o) + \gamma\frac{900}{T+273.15}U_2(e_s - e_a)}{\Delta + \gamma\,(1+0.34U_2)} \quad \text{..... Eq. 1}$$

Where ET_o is daily reference evapotranspiration, R_n is net radiation, G_o is soil heat flux, U_2 is wind speed at two metres, e_s is saturation vapour pressure, e_a is actual vapour pressure, $e_s - e_a$ is vapour pressure deficit, Δ is the slope of vapour curve, T is temperature of the air.

Allen et al. (1998; 2005a), emphasised that the FAO 56-PM reference evapotranspiration would provide reasonable estimates of evapotranspiration under various climatic conditions.
It has also been reported that compared to other point based methods, the formulations based on the Penman-Montieth model have greater performance for ET estimations, and thus can be used as the standard for evaluating other methods (Imark, 2009).

Despite its strengths, the FAO Penman-Montieth has some limitations. It is a known fact that surface resistance can vary according to the day and the weather conditions and crop coefficient determination is affected by many factors (Neale and Vinokullo, 2005). This means that the spatial and temporal variations of the surface characteristics cannot be taken into account with high accuracy by this method (Courault et al., 2005). As earlier noted, AET corresponds to the real water consumption according to weather parameters, crops factors, management and environmental conditions. This means that over a large basin, the big leaf assumption which the FAO Penman-Montieth assumes is rarely valid. There are often many vegetation types co-existing and always some parts or periods where or when the vegetation is not 'closed'. Both the soil surface and the vegetation leaves evaporate or transpire moisture

to the atmosphere and their relative importance changes dynamically as the vegetation develops (Shuttleworth and Wallace, 1985; Zhang et al., 2008). The ideal approach is that applicable at all times and places and able to reflect the changes of surface conditions. Thus, other point based methods, such as the double-layer Shuttleworth-Wallace Model, which tries to include these changes have over the years been proposed (Zhang et al., 2008). However, remote sensing data with increasing imagery resolution has been hailed as a better option that can provide this type of information over various temporal and spatial scales. Thus, the general trend shows that there has been a shift towards developing robust physically-based method of estimating ET (Courault et al., 2005), especially using remote sensing techniques as will be shown in this thesis.

A number of ET studies employing remote sensing techniques have compared results with those derived using the FAO-56PM and other point based methods. Allen (2000) compared ET calculated using the FAO-56PM method with predictions by the SEBAL remote sensing approach. Predictions were within 20% of ET based on an energy feedback remote-sensing application using NOAA-AVHRR and Landsat data (Gibson et al., 2010). In comparing ET estimates from satellites, hydrological models and field data, Kite and Droogers (2000) found that satellite methods and the FAO-24 (another approach based on the Penman-Montieth model) had the greatest variability, whereas FAO-56PM, hydrological models and field methods showed more consistency (Gibson et al., 2010).

2.3.2 Direct method of estimating evapotranspiration

A lysimeter is one of the instruments that can be used to estimate ET directly. The device consists of a large container placed below the ground surface and filled with soil, on which crops are grown under natural condition. The whole container is supported on a weighting device which records any change in moisture storage. Water is allowed to drain freely from the large container into a collecting device which can be used to measure percolation losses. Close to the lysimeter a rain gauge is located to measure all incoming precipitation. Estimates of ET (or evaporation in the case of bare soil) can then be made by measuring and balancing all the other water budget components of the container, namely, precipitation, underground water drainage, and change in water storage of the block of soil. Usually, surface runoff is eliminated (Prueger et al., 1997). A lysimeter is a multi-purpose instrument for the study of several phases of the hydrological cycle under natural conditions (WMO, 1992). Lysimeters offer a dependable means of measuring water loss from soil and crop canopy surfaces directly

and their results can be used in comparison with AET obtained from satellite data. Lysimeters can also be used for the estimation of PET of the plant covered soil, if the soil moisture is kept at field capacity (Allen et al., 1998).

Despite having the advantage of estimating ET directly, lysimeters have a number of drawbacks (Malone et al., 1999). One such shortcoming is that it only calculates ET for one particular crop at a time or for bare soil. Yet it is known that variations in ET over a whole catchment can be quite large due to variations in topography and vegetation cover. This means that the problem that affects the accuracy of lysimeters emanate from the difficulties in meeting the installation requirements for the data to be comparable to field conditions (Frank, 2008). Lysimeters will not be representative of the surrounding area if the crop in the lysimeters is either taller, shorter, denser or thinner or if the lysimeter is on the periphery of no-cropped area (Chang, 1968). Therefore, the challenge is to make the conditions in the lysimeters closer to that of the surrounding environment (Malone et al., 1999).

Bowen-ratio energy balance method is another way that is used to measure ET directly. This method combines measurements of certain atmospheric variables (temperature and vapour concentration gradients) and available energy (net radiation and changes in stored thermal energy) to determine estimates of ET (Lloyd, 1992). It therefore, incorporates energy-budget principles and turbulent-transfer theory. The theory of this method was developed by Bowen (1926). Its practical use, however, has been possible in recent times due to the availability of accurate instrumentation (Payero et al., 2003). To implement the method, data loggers with temperature and humidity sensors are required (Allen et al., 1998). The Bowen ratio is estimated using the formula given in equation (2) (Dingman, 2002).

$$\beta = \gamma \frac{T_2 - T_1}{e_2 - e_1} \quad \text{.....Eq. 2}$$

Where γ is the psychometric constant, T_2 and T_1 are measured air temperature at heights Z_1 and Z_2, e_2 and e_1 are measured water vapour pressures at Z_1 and Z_2 (Dingman, 2002). Once the Bowen ratio is determined, it is used to solve the energy balance as given in equation (3) (Perez et al., 2008).

$$\lambda E = \frac{R_n - G}{1 + \beta} \quad \text{.....Eq. 3}$$

Where R_n is net radiation, G is the ground heat flux, ƛE is the latent heat flux, ƛ is latent heat of vapourisation, E is actual evapotranspiration (Perez et al., 2008).

The advantage of the Bowen ratio method is the ability to measure AET and elimination of wind and turbulent transfer coefficients while the disadvantages are sophistication and fragility of sensors and data logging equipment. The need of adequate upwind fetch also place limits of the method (Payero et al., 2003).

The Eddy Covariance (E.C) is yet another atmospheric flux measurement technique and it measures and calculates vertical turbulent fluxes within atmospheric boundary layers. It is a statistical method used in meteorology and other applications that analyzes high-frequency wind and scalar atmospheric data series, and yields values of fluxes of these properties. Such flux measurements are widely used to estimate momentum, heat, water, and carbon dioxide exchange, as well as exchange of methane and other trace gases (Massman, 2000). The basics of this approach is that the fluctuations of the vertical wind (w') and the deviation (q') from the mean absolute humidity (q) are measured directly with fast response sensors. The E.C expression for ET is given in equation (4) (Brutsaert, 1982).

$$ET = \frac{\overline{w'q'}}{Pw} \quad \text{……..…....…….……Eq. 4}$$

In Equation (4), the over bar represents the average period and the primes indicate the deviation from the mean values during the averaging period. Although E.C method has the advantage of estimating AET directly, it suffers from the disadvantage of errors caused by sensor separation and inadequate frequency response of the sensors (Ham and Heilman, 2003).

2.3.3 Water balance and hydrologic modelling approach

The Water Balance (WatBal) method involves applying the water balance equation to the catchment area of interest over a time period (ΔT) and solving the equation for ET as given by in equation (5) (Dingman, 2002).

$$ET = P + Q_{in} + G_{in} - Q_{out} + G_{out} - \Delta S \quad \text{……..…....…..….Eq. 5}$$

Where P is precipitation, Q_{in} is inflow of the surface water, Q_{out} is outflow of the surface water, G_{in} is ground water inflow, G_{out} is ground water outflow and ΔS is change in the amount of water stored over the time period (Dingman, 2002).

The Soil Water Balance method is alternative to the WatBal approach. Both potential and actual ET can be measured with the soil water balance method (Allen et al., 1998). The water balance of the soil accounts for the incoming and outgoing fluxes of a soil compartment. This compartment can be one-dimensional (e.g. the root zone, or the soil profile to a greater depth). The soil water balance equation over a certain period can then be written as the change in water storage, (ΔW). Defining ΔW as 'In - Out', after a certain period of time, change in storage is estimated as given by equation (6) (Feddes and Lenselink, 1994).

$$\Delta W = I + P - P_i + G - R - ET \quad \text{.....Eq. 6}$$

Where, I is irrigation, P is precipitation, Pi is intercepted precipitation, G is upward flow through the bottom, R is percolation through the bottom, ET is evapotranspiration (Feddes and Lenselink, 1994).

Re-arranging equation (6) yields the estimate of evapotranspiration as given in equation (7) (Feddes and Lenselink, 1994).

$$ET = I + P - P_i + G - R - \Delta \quad \text{..... Eq. 7}$$

Because the soil water distribution over the profile is usually not uniform, ΔW in equation 6 can be expressed as given in equation (8) (Feddes and Lenselink, 1994)

$$\Delta W = \sum_{i=t}^{n} \Delta\theta_i D_i \quad \text{..... Eq. 8}$$

Where n is number of soil layers, $\Delta\,\Theta_i$ is change in volumetric soil water content of layer i, D_i is depth of the i-th soil layer (Feddes and Lenselink, 1994).

It is obvious that all errors in estimating the terms of Equation 5 and 7 will be reflected in the estimate of ET. The problem with both equations is that it is difficult to evaluate the quantity of ground inflow and outflow properly. Therefore, although the approach looks simple in theory, in reality it is difficult to measure the true values of the components in the equation.

However, if the components are reasonably estimated, the method can provide accurate estimation of ET (Feddes and Lenselink, 1994).

Hydrological Models can estimate ET through simulation of river or stream flow at a catchment level. These models achieve this by simulating the transformation of precipitation into stream flow taking into account all the intermediate processes such as ET, interception, infiltration, runoff and groundwater flow including all the artificial effects of dams, reservoirs, diversions and irrigation schemes (Beven, 2001). Thus, they are able to estimate evapotranspiration at any point and time. Some of these include hydrological surface flow models such as SWAP, SWAT, TOPMODEL, MIKE SHE, and a host of many others which have been developed over the years to meet various needs and the complexity of the phenomenon which they seek to address (Kite and Drooger, 2000; Beven, 2001). The following web site: http//www.hydrologicmodels.tamu.edu/models provides an inventory and details of these models. Many of these have evolved and accommodate the latest data sources including remote sensing and geographic information system data (Lane et al., 2004).

2.3.4 Remote sensing techniques for estimating ET

It is not a practical choice to estimate spatially distributed surface fluxes over large geographical areas with the classical field scale methods (lysimeters, Bowen ratio, eddy correlation system, soil water balance) so far described (Courault et al., 2005). Thus, nowadays attention has shifted towards deriving methods capable of capturing the spatial and temporal distribution of AET over various scales using remote sensing data. With the increase in satellite imagery and resolution, various methods of retrieving surface fluxes using remote sensing data have evolved over time. Courault et al. (2005) note that it is difficult to classify these methods because some of them are intermediate approaches which combine empirical and physical relationships. They have, however, proposed four model categories: empirical, direct methods; residual methods of the energy budget; deterministic methods; and vegetation index methods. Su (2006a), on the other hand, is of the view that the ET methods can be categorised into two types of methodologies in remote sensing of turbulent heat fluxes and evaporation i.e. (semi-) empirical versus analytical. What is clear in all these proposed categories is that they capture a progressive development in the complexity of model parametrisation and input requirements. Here a review of these approaches is presented, with particular emphasis on their physical bases and assumptions.

Empirical direct methods are based on the direct use of remote sensing observations in semi-empirical models developed to estimate ET (Courault et al., 2005). Common empirical direct method uses the simplified relationship using thermal infra-red (TIR) remote sensing and meteorological data (Bastiaanssen et al., 1998a, 1998b; Brutsaert et al., 1993; Courault et al., 2005). The use of such simplified relationships for estimating water requirements among terrestrial plants began in the late 1970`s with researchers such as Jackson et al. (1977) and later by Seguin and Ittier (1983), who computed crop water stress index (CWSI) using thermal infrared observations which were premised on the assumption that as water becomes limiting, transpiration is reduced and the plant temperature increases (Su, 2006a). A typical basis of this simple relationship is presented by Courault et al. (2005). They assert that empirical direct method assumes that it is possible to directly relate daily ET to the instantaneous difference $(Ts - Ta)_i$ measured around midday as given in equation (9).

$$ET_d = R_n + A - B(T_s - T_a)_i \quad \text{.....Eq. 9}$$

Where Rn is net radiation, A and B being constant depending on the local situation, and the value (Ts – Ta) is the stress degree day (Courault et al., 2005).

Thus, direct method relies on the assumptions that the ratio of sensible heat to net radiation is constant all along the day, and the daily value of soil heat flux is negligible (Gd =0) and that Ts can be extracted from measurements acquired in the thermal infrared range (TIR) with airborne or satellite sensors, after atmospheric correction (Courault et al., 2005). Through such a scheme, as Gibson et al. (2010) point out, the idea behind the simplified method is that the net integrated daily ET at the surface can be estimated from a few easily obtainable measurements: surface radiant temperature measured (Ts*)*, a corresponding air temperature, and the net radiation expressed as an integrated value over a 24-hour period. In the same light, another significant relationship studied by Moran et al. (1994) and Carlson et al. (1995) is that between surface temperature (Ts) and Normalised Vegetation Index (NDVI). They found that since the amount of vegetative cover affects transpiration and that vegetation indices are also related to surface temperature, higher ET tends to be associated with lower temperatures (Courault et al., 2005).

Residual methods of the energy budget combine some empirical relationships and physical modules (Courault et al., 2005). The methods are based on a complete energy balance for each pixel where ET is predicted from the residual amount of energy remaining from the

classical energy balance, which governs the ET process at the vegetation surface, and is expressed mathematically as given in equation (10).

$R_n = G + H + \lambda ET$ (Wm^{-2}) ……..……...……...……..…..…Eq. 10

Where R_n= net radiation, H= sensible heat, G= soil heat flux and λET= latent heat flux (λ is the latent heat of vaporization and E is the actual evapotranspiration) (Courault et al., 2005).

Equation (10) shows that the net incoming solar radiation at any location is converted into heat energy, heating the air above the soil (sensible heat flux) surface and the soil itself (soil heat flux), and into latent heat of ET from the soil surface. The rationale behind the residual method is that if the net incoming radiation and the energy consumed in heating the air and the soil can be measured, then the latent heat of evaporation from the soil can be estimated and the rate of evaporation of water deduced (Courault et al., 2005). Therefore, using remote sensing techniques for instance, net radiation (Rn) can be computed from satellite-measured narrow-band reflectance and surface temperature; Ground heat flux (G) can be estimated from Rn, surface temperature, and a vegetation index; and Sensible heat flux (H) can be estimated from surface temperature ranges, surface roughness, and wind speed using buoyancy corrections leaving ET as the only unknown (Allen et al., 2005c).

The Surface Energy Balance Index (SEBI) method proposed by of Menenti and Choudhury (1993) is one of the residual methods. It is based on crop water stress index. In this method the dry limit is assumed to have a zero surface ET (latent heat flux) for a given set of boundary layer characteristics so that the sensible heat flux equal to the surface available energy. The minimum surface temperature can be evaluated from the wet limit, where surface is regarded as to evaporate potentially and the potential ET is calculated from Penman-Montieth equation with a zero internal resistance. The relative evaporative fraction can then be calculated by interpolating the observed surface temperature with the maximum and minimum surface temperature (Van Den Hurk, 2001).

The Surface Energy Balance Algorithm for Land (SEBAL) (Bastiaanssen et al., 1998a, 1998b; Tasumi et al., 2005) is another residual model that uses remote sensing directly to estimate input parameters, and ET is estimated as a residual of the energy balance. It was designed for regional estimation of the energy partitioning with minimum ground data. It uses surface temperature, surface reflectance, and NDVI as well as their interrelationships to

deduce surface fluxes (Bastiaanssen et al., 1998a; Tasumi et al., 2005). The atmospheric variables (air temperature and wind speed) are estimated from remote sensing data by taking into account the spatial variation induced by hydrological and energetic contrast (Courault et al., 2005). SEBAL uses the spatial relation between surface temperature (Ts) and air temperature (Ta) to estimate air temperature (when (Ts – Ta) ~ 0, H~0), Ta can be estimated from Ts values from TIR images. In this regard, determination of wet and dry surfaces on the studied area is necessary to extract threshold values. Semi-empirical relationships in the SEBAL are used to estimate emissivity and roughness length from NDVI. The sensible heat flux is computed by inverting the sensible heat flux expression over both dry (LE = 0) and wet (H = 0) land (Courault et al., 2005). Due to the difficulty in finding exactly right pixels of dry and wet conditions in certain images, its application is limited in certain instances. Furthermore, surface roughness is poorly described so that SEBAL is only suitable for flat terrain (Allen et al, 2005a). To solve related limitations of the SEBAL, some correction have been made by Su (2005) to make it more practical by remedying a theoretical problem of SEBAL model, and adding a scheme to apply Numerical Weather Prediction (NWP) fields with an up-scalling and downscaling approach.

The Simplified Surface Energy Balance Index (S-SEBI) method was developed by Roerink et al. (2000) to derive the surface energy fluxes from remote sensing measurements. This method estimates surface fluxes by determining a reflectance dependent maximum temperature for dry conditions and a reflectance dependent minimum temperature for wet conditions without the need for additional meteorological data if the surface extremes are present on the image studied (Van den Hurk, 2001; Courault et al., 2005). It is reported that it shows reasonable success for application in semi-arid areas (Roerink et al., 2000; Su, 2006b). However, S-SEBI has a disadvantage of not explicitly incorporating the aerodynamic character of the land surface, such as land surface roughness. As a result, it has limited application at a regional scale. It works appropriately for high resolution images such as Landsat and, as noted, in somewhat drier areas (Roerink et al., 2000; Brunner et al., 2004).

METRIC (Mapping EvapoTranspiration at high Resolution and with Internalized Calibration) is an image-processing model that calculates ET as a residual of the surface energy balance (Morse et al., 2006; Allen et al., 2007). It is a variant of SEBAL which was formulated for application to mountainous terrain and to provide tighter integration with ground-based reference ET (Allen et al., 2005b, 2007). According to Allen et al. (2007),

METRIC uses two anchor conditions from within an image to fix boundary conditions for the energy balance and to internally calibrate the sensible heat computation, which eliminates the need for in-depth atmospheric correction of temperature or albedo. The internal calibration reduces impacts of any biases in estimation of aerodynamic stability correction or surface roughness. The calibration is done by manually selecting a hot and a cold pixel to define the range of vertical temperature gradients (dT) above the ground surface. The cold condition is typically a well-irrigated alfalfa field where ET equals the reference ET whereas the hot condition is a dry, bare agricultural field where ET approaches zero.

METRIC has been used with high resolution Landsat images in southern Idaho, southern California and New Mexico to quantify 24-hour, monthly and seasonal ET for water rights accounting, operation of ground water models, and determination of crop coefficient (Allen et al., 2007). Comparisons between ET calculated by METRIC, ET measured by lysimeter and predicted using traditional methods have been made on a daily and monthly basis for a variety of crop types and land-uses. The results have shown that the method promises to be an efficient, accurate and inexpensive procedure for estimating ET from irrigated lands (Allen et al., 2007).

Other models using the residual method have also been developed, such as Neale and Vinokullo (2005), who present a hybrid energy balance model that couples the surface energy balance approach with a simple empirical reflectance-based crop coefficient model, for the estimation and prediction of ET over a growing season using satellite imagery as part of the Soil Moisture Atmosphere Coupling Experiment (SMACEX). In the same experiment, French et al. (2005) considered two flux estimation approaches, the SEBAL model and the Two-Source Energy Balance model (TSEB) proposed by Norman et al. (1995). In the TSEB model each pixel is categorized as vegetated or bare soil according to NDVI or another vegetation index and assumes clustered rather than distributed vegetation. Direct comparison against ground Eddy Covariance data suggests that the TSEB approach is helpful over sparsely vegetated terrain (Gibson et al., 2010). Crago and Crowley (2005) used the complementary relationship between actual and potential ET to derive ET estimates from minimal data.

Deterministic methods are based on detailed models such as Soil-Vegetation-Atmosphere Transfer models (SVAT), which estimate different components of the energy budget

(Courault et al., 2005). In these models, remote sensing data are introduced at different stages either as input parameters to characterize the different surfaces, or in assimilation procedures which aim at retrieving adequate parameters for the ET estimation (Courault et al., 2005; Braun et al., 2001, Olioso et al., 2005; Rivalland et al., 2005). Deterministic models aim at integrating all components of the water budget for monitoring and management purposes (Courault et al., 2005).

Vegetation Index (VI) methods, which are also known as inference methods, are based on the use of remote sensing to compute a reduction factor such as a crop coefficient for the estimation of the AET (Chen et al., 2004; Allen et al., 2005a; Courault et al., 2005; Consoli et al., 2006). Actual ET is then calculated as the product of this reduction factor and potential ET obtained from ground measurement (Courault et al., 2005). In some cases vegetation index methods are combined with deterministic models (Gibson el al., 2010). Boegh and Soegaard (2004) describe how the relationship between the soil water balance and the vegetation growth is represented by coupling a hydrological model (MIKE SHE) and a vegetation-SVAT model to simulate the interactions between soil, vegetation and atmosphere including the seasonal variation in plant structure and function (Gibson et al., 2010).

2.3.5 The SEBS for estimating turbulent heat fluxes and evaporative fraction

Though considered a residual method by Courault et al. (2005), the SEBS (Su, 2002) is regarded as an analytical method. According to Su (2006b), analytical methods take into account detailed physical processes at a scale of interest and usually involve complex relationships, and require various input variables such as those which can be observed directly by radiometric measurements and meteorological variables at reference height. Timmermans (2011- personal communication) is of the view that since the SEBS estimates ET from the evaporative fraction derived from the energy balance at limiting cases, it cannot therefore be regarded as a residual method.

In the formulation of the concept of energy balance at limiting cases, Su (2005) argues that although it is possible to estimate the latent heat flux as a residual by means of the energy balance equation after derivation of the sensible heat, there are associated uncertainties in the derived latent heat flux and consequently in the evaporative fraction. He contends that this is because the sensible heat flux is, under given surface conditions, determined solely by the surface temperature and the meteorological conditions at the reference height and is not

constrained by the available energy. Thus, if the surface temperature or the meteorological variables have large uncertainty, these would be propagated into the resultant latent heat flux and evaporative fraction without any avoidance. In view of this, Su (2002) proposed the removal or limiting of this uncertainty by considering energy balance at the limiting cases. He showed that this is achievable because the actual sensible heat flux is constrained in the range set by the sensible heat flux at the wet limit derived from a combination equation, and the sensible heat flux at the dry limit set by the available energy (Su, 2002). In this regard, Su (2005) notes that SEBS is similar to earlier algorithm such as the SEBI concept of Menenti and Choudhury (1993) but explicitly integrates the formulation of roughness height for heat transport. The earlier works (Jackson et al., 1977; Menenti and Choudhury, 1993) used fixed values of this parameter and as such had limited application at a regional scale because of the variability of roughness height for heat transport with different surfaces (Su, 2005). Thus, according to Su (2002), SEBS extends the SEBI concept with a dynamic model for thermal roughness (Su et al., 2001), the Bulk Atmospheric Similarity (BAS) theory of Brutsaert (1999) for Planetary Boundary Layer (PBL) scaling, and the Monin–Obukhov Atmospheric Surface Layer (ASL) similarity for surface layer scaling such that SEBS can be used for both local scaling and regional scaling under all atmospheric stability regimes, thereby providing a link for radiometric measurements and atmospheric models at various scales. Furthermore, as earlier noted, a new improvement included in the SEBS model is the determination of the evaporative fraction on the basis of the energy balance at limiting cases. Daily ET is calculated from the total daily energy by assuming that the determined evaporative fraction is constant all throughout the day (Su, 2002).

The SEBS algorithm requires three sets of inputs for the estimation of atmospheric turbulent fluxes and evaporative fractions (Su, 2002). The first set consists of land surface or biogeophysical parameters such as albedo, emissivity, temperature, fractional vegetation cover, leaf area index and the height of the vegetation (roughness height). These parameters can be derived from the reflectance and radiance measurement of the satellite imagery. The second set is meteorological data. This includes air pressure, temperature, humidity, and wind speed at a reference height. This data can be obtained from a standard meteorological station. However, according to Su (2005) this data set can also be variables estimated by a large-scale meteorological model. The third data set required in the SEBS model includes radiation components, that is, downward solar radiation and downward longwave radiation. This data

can be obtained from direct measurements, global model outputs or can also be parameterized when ground measurements are not available (Su, 2005).

The SEBS model has been validated under a wide range of environmental conditions for the estimation of ET, sensible heat flux and drought monitoring both at regional and catchment scales and over different temporal scales. It was tested against AET rates in the semiarid inland basin in North Western China (Li, 2001; Su et al., 2003), in Spain-Barrax (Su and Jacobs, 2001), for drought disaster monitoring (Su et al., 2003), and in the estimation of sensible heat flux in Spain (Jia et al., 2003). It was also evaluated well as compared with other remote sensing techniques over irrigated fields (Su et al., 2001; Su et al., 2003). Recently, validations of SEBS have been reported by Su (2005) and Su et al. (2007) using data from SMACEX experiments and CEOP references sites.

2.4 Gap analysis arising from literature review

Given the various methods reviewed and what is available on the ground, point based methods cannot be used to adequately characterise the spatial and temporal variability of AET over the semi-arid Barotse Sub-basin as it is a heterogeneous environment. Some remote sensing techniques, which have been cited in this study, cannot also be used to accurately estimate the land cover evaporative fluxes in the study area because of their inherent weaknesses in their assumptions. Table 1 shows a summary of strengths and weaknesses of some the approaches used to estimate ET. Being a physically based model, however, the SEBS model is capable of estimating spatial and temporal dynamics of turbulent heat fluxes and evaporative fraction at various scales with acceptable accuracy (Su, 2002; Su et al., 2003; Jia et al., 2003; Su, 2005; Su et al., 2007). It is for this reason that this approach was preferred over the others to be used in the estimation of evaporative fluxes in the semi-arid Barotse Sub-basin.

On the application side, the SEBS model has been employed in a number of studies for the estimation of distributed evaporative fluxes at a basin or catchment scale and includes, among others, the following works which are related to this study:

Hailegiorgis (2006) analysed summer time ET using SEBS algorithm in Regge and Dinkel, The Netherlands. He used summer time Landsat images, meteorological and groundwater data to assess the spatial and temporal variation of AET. The AET estimates from SEBS

revealed the spatial-temporal variability of ET over landuse classes. In the absence of ground truth data of actual ET needed for validation, he used the reference ET and crop coefficient (Kc) and found good agreement which strengthened the SEBS results.

Shan et al. (2007) applied the SEBS model together with the HANTS algorithm to generate a time series of evaporative fraction, albedo and AET over the arid inland Heihe River Basin in North-West China. They found out that based on the generated time series of evaporative fraction and albedo, actual ET can be implemented in HANTS algorithm over the time continuously to characterise the spatial-temporal land cover ET. They also found that the actual ET derived using time series of evaporative fraction and albedo was in agreement with the temporal distribution of NDVI, implying that actual ET achieves peak value with an increase in NDVI.

Alvarez (2007) applied the SEBS algorithm in the estimation of AET in the study of effect of land cover changes on water balance of the Palo Verde Wetland, Costa Rica. He showed, among other findings, that MODIS images are very useful in the estimation of AET time series, and that using this data, the evaporative loses in all the wetland can be calculated using the SEBS model.

Mohamed et al. (2010) studied remote sensing based estimation of AET among different land cover types in the Mkindo Catchment in Tanzania and found that different land uses/ cover types have different evaporative water use signature at a daily and monthly time scale and that forests and irrigated land had relatively higher evaporative water use compared to other land cover types in the catchment. They found that the SEBS estimates of AET had good correlation with computed PET.

Rwasoka et al. (2011) carried out a study on the estimation of AET using the SEBS algorithm in the Upper Manyame Catchment in Zimbabwe. They found out that the SEBS estimates of AET were on the average physically consistent when compared with the calculated PET. They also found that modelled estimates of AET were slightly underestimated at one station and relatively overestimated on the other when compared to AET calculated using the advection aridity equation, and that water bodies, closed broadleaved deciduous and open broadleaved deciduous forests had relatively higher mean AET rates than open grasslands.

Table 1: Summary of the weaknesses and strengths of the point-based and remote sensing techniques used to estimate ET (modified from Courault et al., 2005; Shuttleworth and Wallace, 1985)

Model	Scale	Strengths	Weaknesses
A. Point-based			
Lysimeter	Sample	Offers means of measuring water loss from soil and plant canopy directly; results can be used as a standard against which to compare and validate other models	Difficult to make the conditions in lysimeters closer to that of the surrounding area, requires expert supervision, modern and precise ones are expensive
Bowen ratio	Field	Relatively inexpensive proprietary system can be purchased that work for both short crops and natural vegetation	Problematic over tall vegetation when atmospheric gradients are low, often cannot be used at dawn and dusk when the Bowen ratio is -1
Eddy covariance	Field	Useful for field-scale measurement in research application, can be operated using relatively expensive logger and collocated sensors	Prone to systematic underestimation of fluxes; errors due to sensor separation and inadequate frequency response of the sensors
B. Remote sensing techniques			
Simplified relationships	Field to regional	operational from local to regional	spatial variation of coefficients
Residual (SEBI, S-SEBI & SEBAL)	Field to regional	Low cost, need no additional climatic data	surface characteristic are empirically estimated, works better in flat areas, requires the presence of wet and dry pixels
Inference models (Kc & NDVI)	Field to regional	Operational if combined with ground measurements or models estimating accurate reference ET	Requires calibration for each crop, K_c varies according to water stress
Determinists (SVAT)	Field to regional	Estimation of intermediate variables (e.g LAI), possible links with climate, hydrological models, assimilation to find some parameters	Requires more parameters that are not easy to estimate, and accurate remote sensing data

N.B: The generic meaning of scale; Sample = area of the soil and vegetation and sample, typically a few square metres, Field = typically a few hundreds of square metres, Regional = typically several hundred square kilometres

The concept behind this study is related to the work of Rwasoka et al. (2011) and Mohamed et al. (2010). In comparison to the former`s work, however, this study estimated the variation of evaporative fluxes over different land cover types on carefully selected clear-sky warm-wet, cool-dry and hot-dry days and further determined monthly actual fluxes for a hydrological year using daily estimates and the sunshine hours. The modelled results were evaluated against calculated PET and independently modelled AET from the GCM of ECMWF. Rwasoka et al. (2011), on the other hand, estimated the land cover AET only for a few isolated days in the Upper Manyame Catchment in Zimbabwe and evaluated the modelled results against PET and estimates of AET calculated using the advection aridity equation. This study also differs from the work of Mohamed et al. (2010) in the approach used to upscale daily ET to monthly fluxes. In this study, monthly evaporative fluxes were derived from daily estimates of AET and the sunshine hours whereas Mohamed et al. (2010) determined monthly fluxes from daily estimates of AET and reference ET.

As reviewed in this chapter, few studies have attempted to quantify the spatial-temporal evaporative fluxes at a large scale taking into account temporal changes that are significant from a point of view of water resources management. Quantifying the variation of these fluxes over significant parts of the hydrological year, however, is important as it provides critical input data for closing the water budget and enhance water resources planning, monitoring and management in water-short regions. For this reason, this study applied the SEBS model to estimate the spatial and temporal variability of AET on warm-wet, cool-dry and hot-dry days and months in the semi-arid Barotse Sub-basin of South-Western Zambia. Such an approach is useful for assessing water availability in water stressed environments. This is because ET constitutes a dominant hydrologic flux in these areas. The lack of data in these areas on spatial-temporal variation of AET makes quantification of the limited water resources difficult, as is the case with the semi-arid Barotse Sub-basin (Kabika et al., 2010). This means that informed water resources management in such areas will depend on spatial modelling of evaporative fluxes at significant temporal scales which this study has investigated on.

CHAPTER 3: DESCRIPTION OF THE STUDY AREA

3.1 Location of the study area

The semi-arid Barotse Sub-basin is located in the South-Western part of Zambia (Figure 1). Geographically, it lies between Longitudes 23^{o} and 27^{o} East, and Latitudes 15^{o} and 18^{o} South. It sits on an average elevation of 900 metres above sea level and occupies an area of approximately 45,568Km^{2}. It covers mainly Sesheke and Kazungula Districts of Zambia, and some parts of Katima Mulilo of Namibia. This area is easily accessible by road from Livingstone and Katima Mulilo in Namibia on good tarred roads through to Botswana.

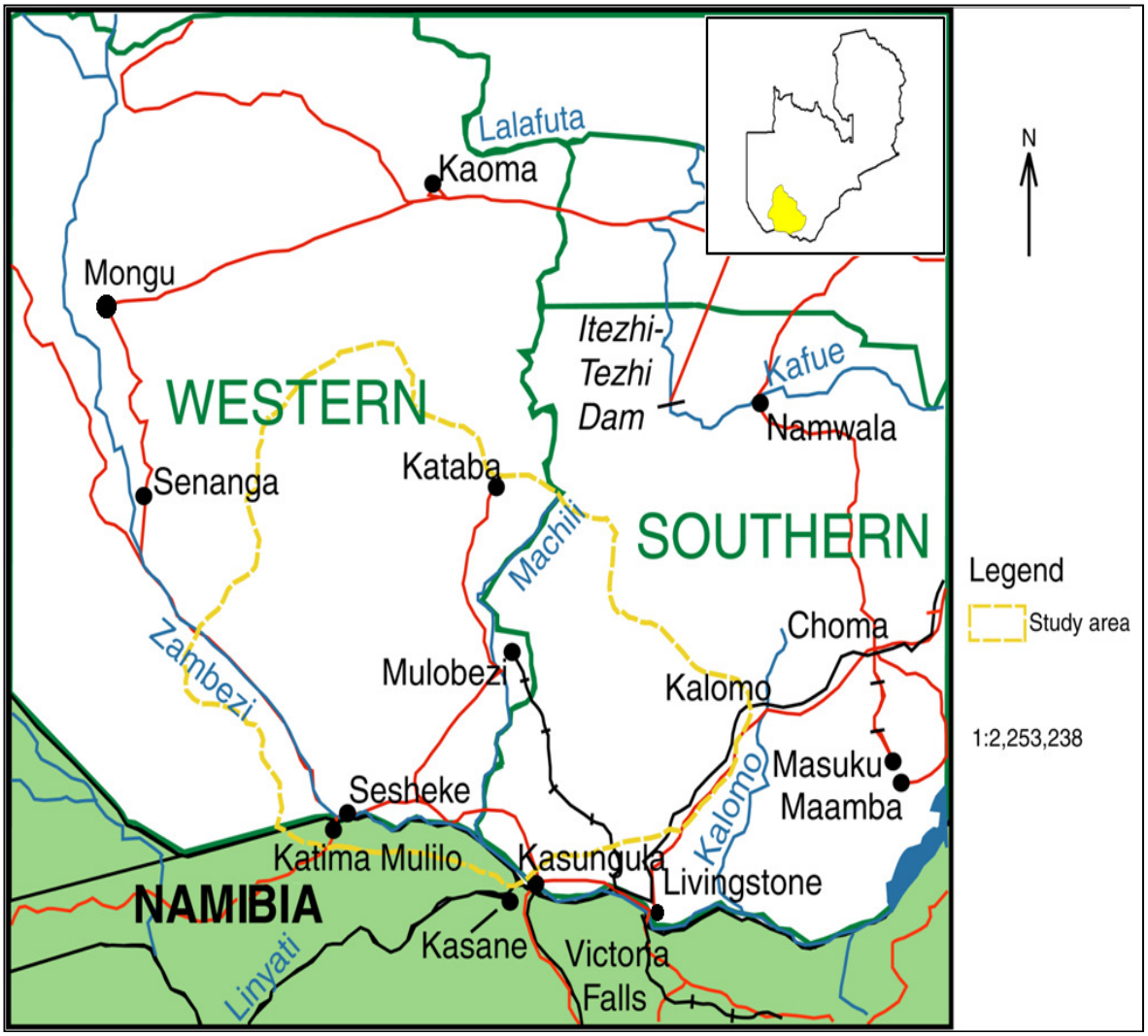

Figure 1: The location of the study area of the semi-arid Barotse Sub-basin, South-Western Zambia

3.1.1 Topography and Drainage

The land elevation over the study area ranges from 1,300 metres above sea level in the northern part to 850 metres in the south eastern part (Figure 2). The lower areas form part of the valley floors of the Zambezi River. This difference in elevation has some influences in climatic variations within the area. This means that even land cover type is also affected by these variations, especially between the northern and the southern parts of the basin.

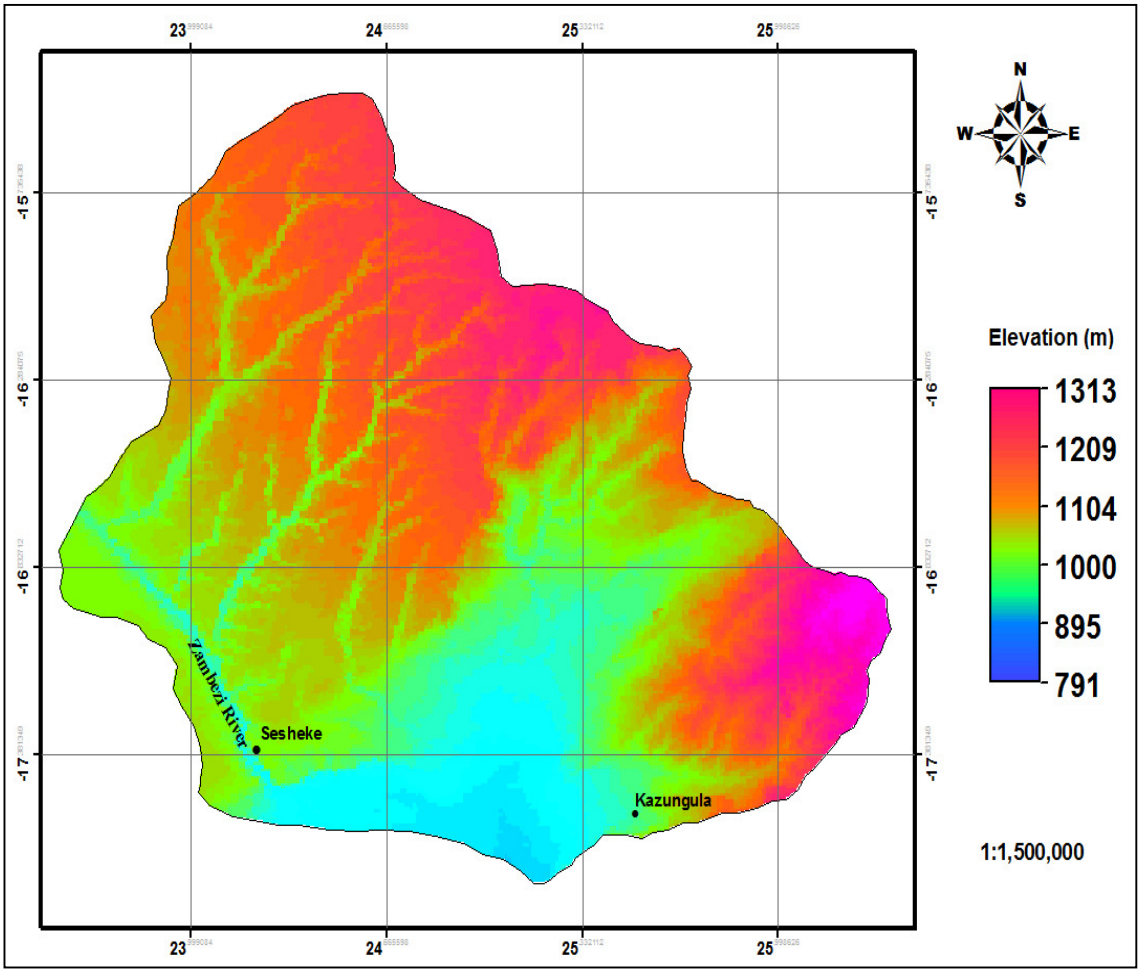

Figure 2: Digital Elevation Model over the semi-arid Barotse sub-basin, South-Western Zambia indicating high elevations in the northern and eastern parts and lower ones in the south.

The characteristic drainage pattern of the study area is trellis (Figure 3). All major streams in the area are tributaries of the Zambezi River and many are non perennial on account of high PET and percolation in the sandy river beds. The major streams include Lumbe, Njoko, Loanja, Ngwezi, Loazamba and Machili (Figure 3).

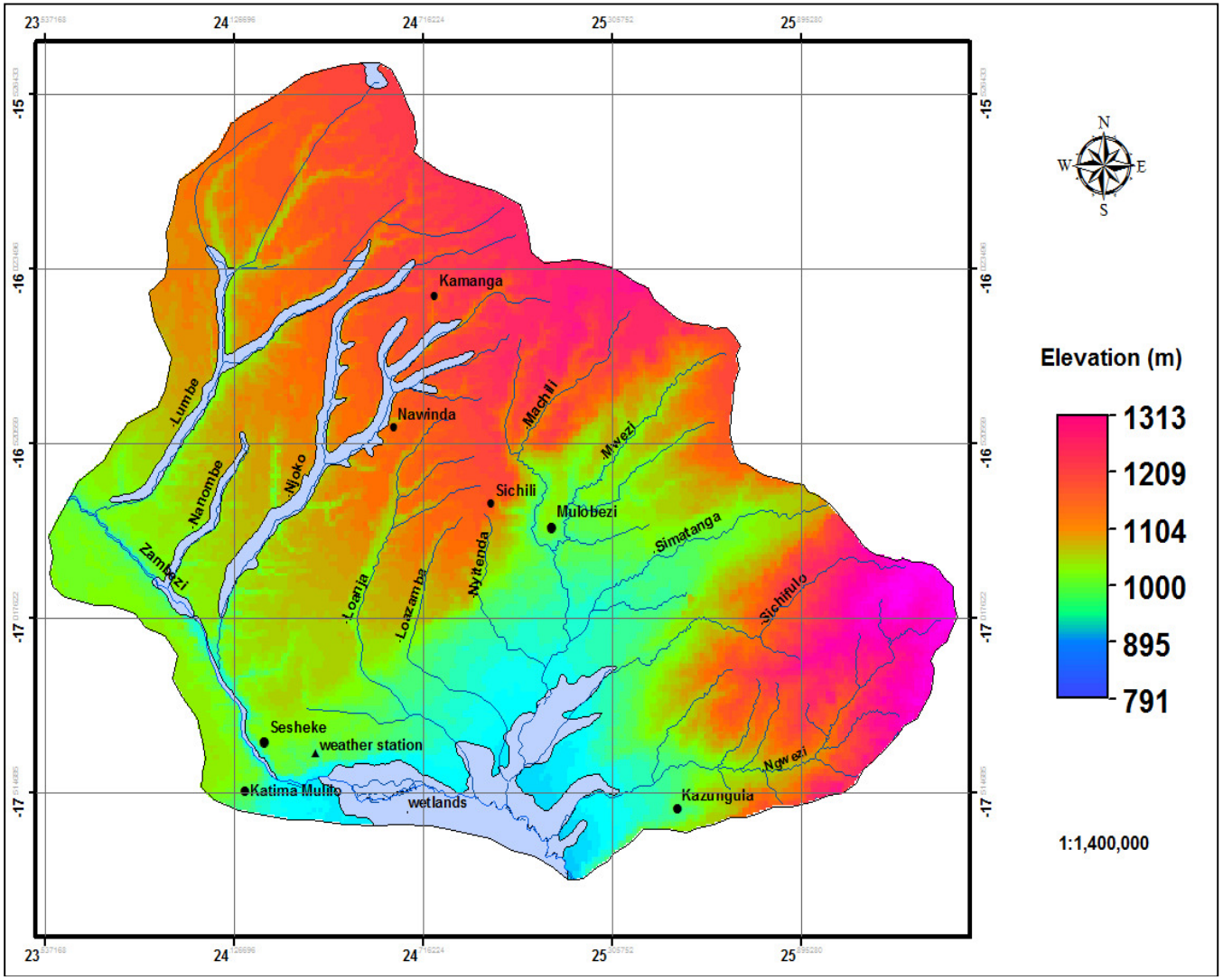

Figure 3: Trellis drainage system superimposed on a digital elevation model of the semi-arid Barotse Sub-basin, South-Western Zambia

3.1.2 Soils

The soil types which are found in the study area include arenosol, vertisol, gleysol, luvisol and acrisol as shown in Figure 4 (FAO and GRZ, 1986).

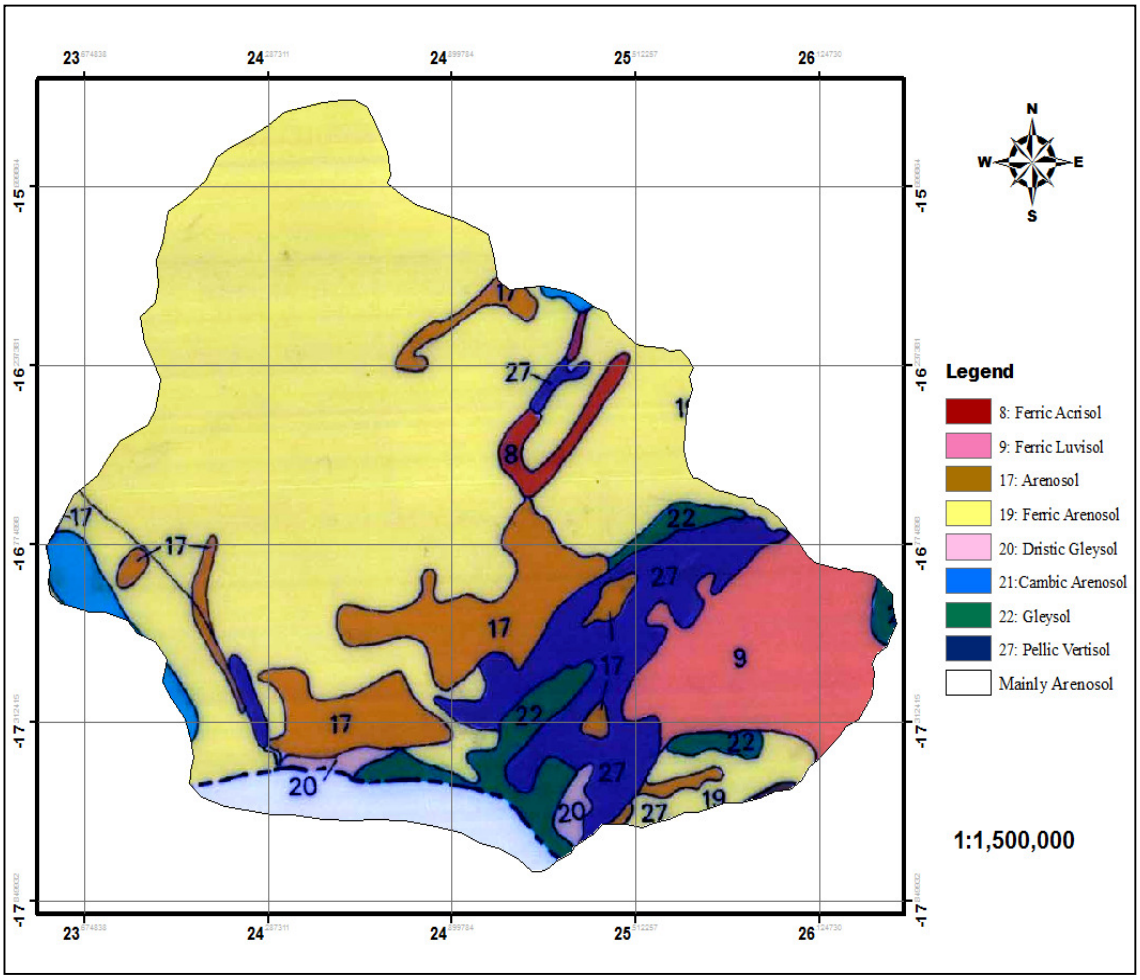

Figure 4: The soil types of the semi-arid Barotse Sub-basin, South-Western Zambia (modified from FAO and GRZ, 1986)

The major soil type in this area is arenosol, which is characterized by a sandy texture and lack of significant soil profile development. They exhibit only a partially formed surface horizon (uppermost layer) that is low in humus, and they are bereft of subsurface clay accumulation. Owing to their excessive permeability and low nutrient content, agricultural use of these soils in the study area is limited. The vertisol type is characterised by high content of expansive clay that forms deep cracks in drier seasons. These soils are well known for their high water holding capacity as they have heavy clayey proportions. The natural vegetation of the vertisol

is grassy woodland. This is because the heavy texture and unstable behaviour of this soil make it difficult for many tree species to grow, and thus forest is uncommon on this soil type. Gleysol is typically confined to the wetlands areas. Grass is a dominant vegetation cover on this soil. Luvisol is characterised by some nutrient content and good drainage making them suitable for farming. Generally, farming in the study area, is confined to the south-western part on Luvisol, Gleysol, vertisols and to some lesser extent on arenosols soil types (FAO and GRZ, 1986).

3.1.3 Vegetation and land use

The predominant land cover types over the semi-arid Barotse Sub-basin consist of mosaic grassland, mosaic vegetation/cropland, closed to open grassland and shrublands. The other types of land cover include water bodies, closed and open broadleaved deciduous forests (Figure 5) (Bicheron et al., 2008). Generally, the appearance of the vegetation type in this area is grassland interrupted in places by savannah and forest (Jeanes, 1991). The Savannah is characterized by open tree canopy with a tall grass understory. The forest is deciduous with the main species being Zambezi Teak (*Baikiaea plurijuga Harms*) locally known as Mukusi (Aregheore, 2006). The Mukusi tree is a valuable source of timber and is processed at Zambezi Saw Mills in Mulobezi. This timber is hard and strong and termite-resistant. It has been used for railway sleepers, parquet floors and door and window frames (Jeanes, 1991).

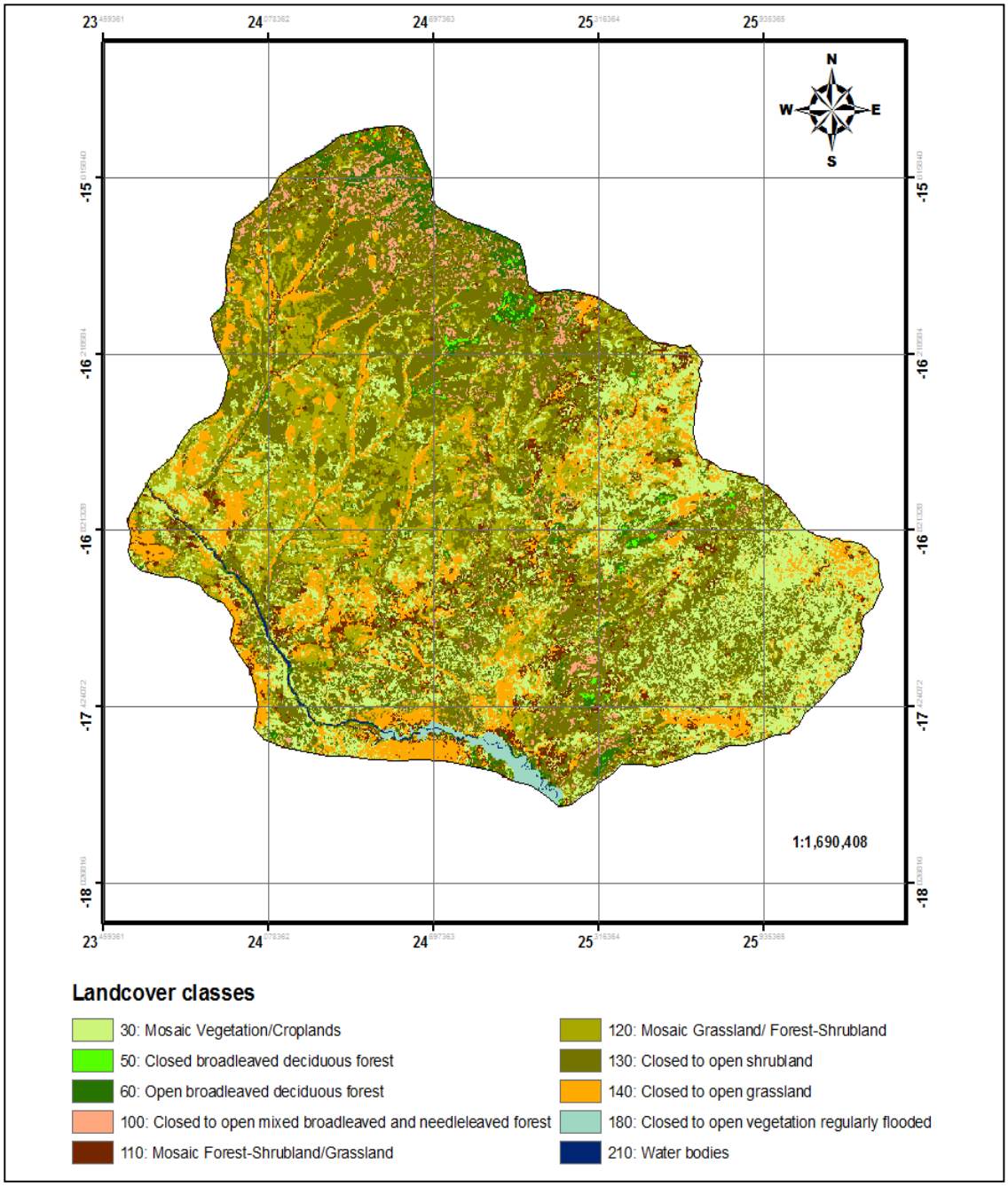

Figure 5: Land cover map of the semi-arid Barotse Sub-basin, South-Western Zambia (modified from Bicheron et al., 2008)

3.2 Climatic characteristics

The semi-arid Barotse Sub-basin experiences a tropical savanna climate with three distinct seasons: warm-wet, cool-dry and dry-hot seasons. The warm-wet period, which starts in November until the end of March, is characterised by rainfall and higher temperatures. The cool-dry season occurs between April and July while the dry-hot season is in phase between

August and October. The two seasons are marked by lower and very high temperatures respectively (ZDM, 1992).

3.2.1 Rainfall and evapotranspiration

Rainfall in the over the study area is influenced by the Inter-Tropical Convergence Zone (ITCZ) which moves over Zambia from the north between October and March. Being further south of the ITCZ, the semi-arid Barotse Sub-basin is one of the areas in Zambia which receives lower amounts of annual rainfall (ZDM, 1992). It lies in agro-ecological zone (Region I) that receives rainfall of between 600-800 mm year^{-1} (Figure 6). The agro-ecological zones II and III receive rainfall of between 800-1200 mm year^{-1} and above 1200 mm year^{-1}, respectively (Siacinji-Musiwa, 1999; Aregheore, 2006). Although rainfall totals and intra-season distribution vary greatly from year to year throughout Zambia, it is more pronounced in Region I (Sichingabula, 1998).

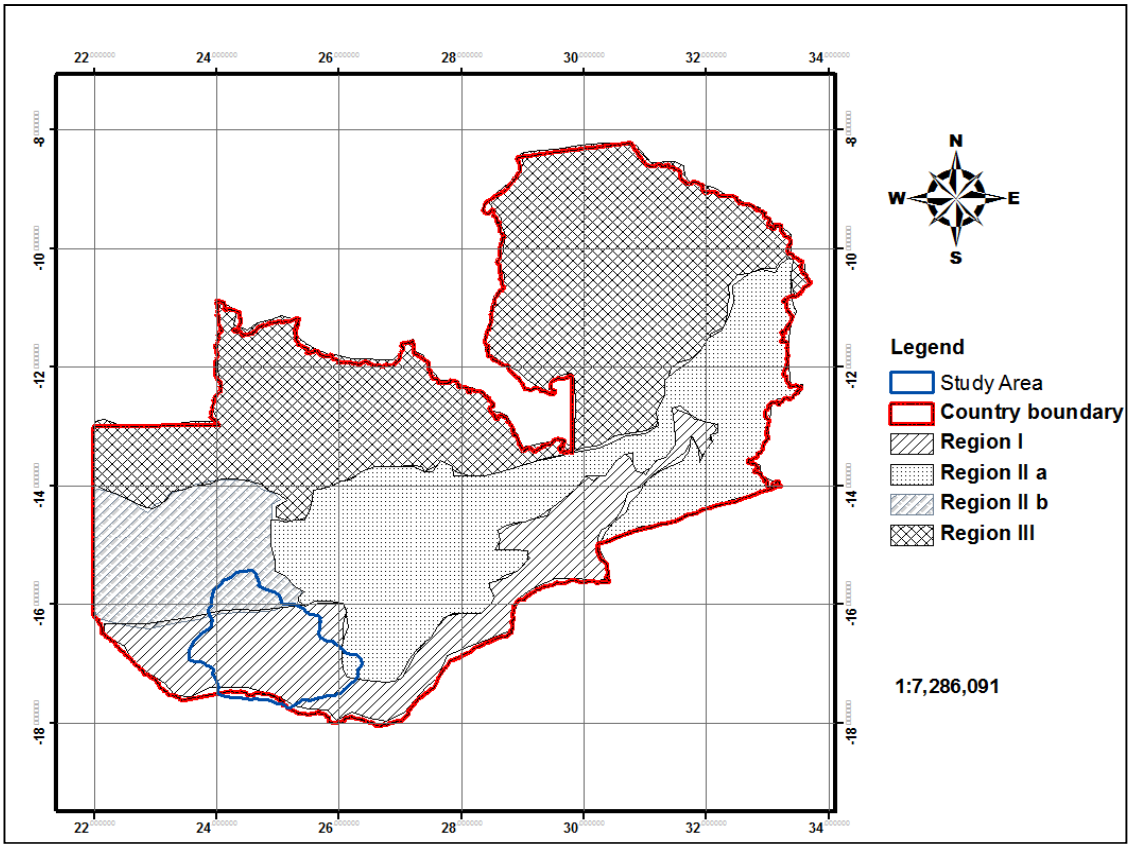

Figure 6: Location of the study area of semi-arid Barotse Sub-basin, South-Western Zambia within the context of agro-ecological regions of Zambia (modified from Aregheore, 2006)

Therefore, rainfall is markedly seasonal in the semi-arid Barotse Sub-basin, falling generally between October and April. The start and the ending of the rains are however extremely variable. The average annual rainfall is estimated at 657mm at Sesheke weather station (ZMD, 1992). The variability of annual rainfall between 1950 and 2004 at this station is shown in Figure 7. There was a long absence of data between 1977 and 1983 as measurements were not taken. From the available data, it is shown that annual rainfall totals frequently exceeded the 600 mm mark from 1950 to 1977 (Figure 7). However, from 1983 to 2005, rainfall patterns seem to have declined as the annual totals barely exceeded the same mark. It was during this same period (1983-2005), that the lowest annual rainfall totals (compared with the period from 1950-1977) of 363 and 358 mm year^{-1} were recorded in 1995 and 2002 respectively.

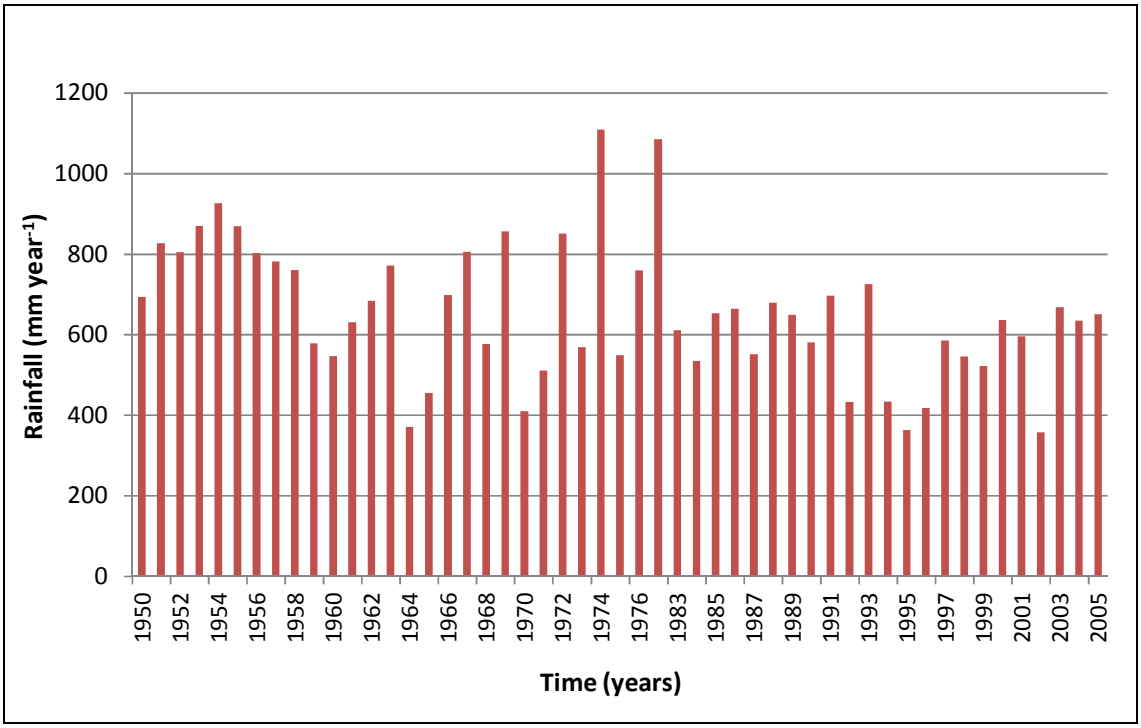

Figure 7: Annual rainfall measured at Sesheke Meteorological Station, semi-arid Barotse Sub-basin, South-Western Zambia (1950 and 2005)

The peak of the rain season in the semi arid Barotse Sub-basin normally occurs in January, after coming into phase between October and November. Effective rainfall is received until the end of March (ZMD, 1992; MEWD-JICA, 1995). Figure 8 shows the mean monthly rainfall at Sesheke weather station between 1983 and 2004.

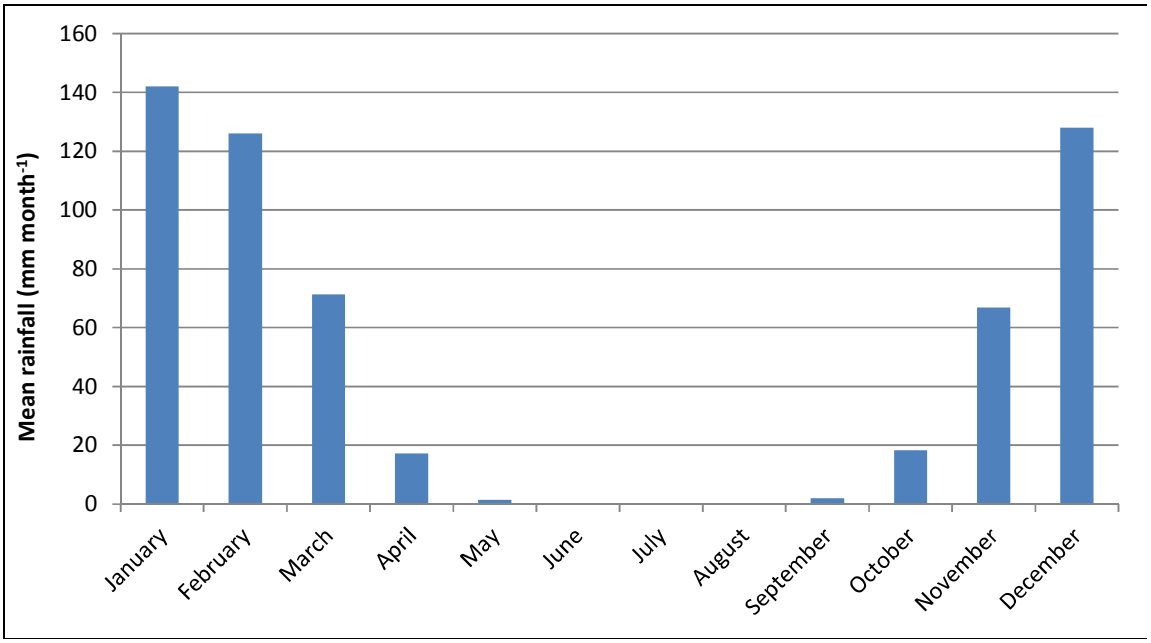

Figure 8: Mean monthly rainfall at Sesheke Meteorological Station, semi-arid Barotse Sub-basin, South-Western Zambia (1983-2005)

The annual pan evaporation is estimated at 2,215 mm whereas PET stands at 1,718 mm and is high from August to November (200-300 mm month^{-1}) and low from December to July (100-200 mm month^{-1}) around Sesheke Meteorological Station (ZDM, 1992). The actual annual ET at Sesheke Station is estimated at 616 mm against 657 mm of annual rainfall (ZDM, 1992). This implies that rainfall barely exceeds ET, especially in the southern part of the basin.

3.2.2 Temperature and relative humidity

Temperatures in the semi-arid Barotse Sub-basin begin to rise from the second half of August and reach the highest point in October. The average climate over the area is characterised by a maximum mean monthly temperature of 34.2^{o}C, which occurs in October, and a minimum mean temperature in July of 4.4^{o}C (ZDM, 1992). Cool temperatures prevail from April to the first half of August, with night-time temperatures approaching freezing point in July (ZDM, 1992). The mean monthly relative humidity varies between 75 % in January and 35% in September. Figure 9 shows the mean monthly temperatures (maximum mean, minimum mean and mean temperatures) and relative humidity measured at Sesheke weather station between 1983 and 2005.

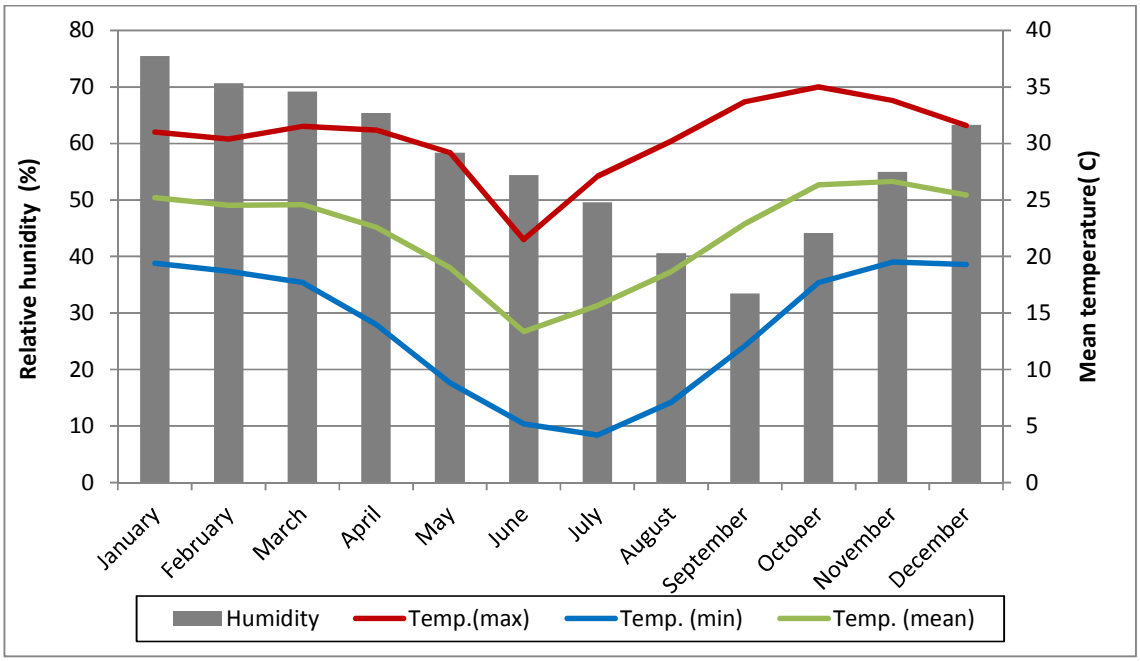

Figure 9: Mean monthly temperature and relative humidity (1983-2005) at Sesheke Meteorological Station, semi-arid Barotse Sub-basin, South-Western Zambia

3.3 Demographic characteristics

The population in the study area is approximately 192,904 with an estimated density of 5.0 persons per square kilometers (CSO, 2010). In the year 2000, the population in this area was estimated at 146,434 (CSO, 2010). This means that the population has been growing steadily in this area.

3.4 Social and economic activities

The major economic activity in the semi-arid Barotse Sub-basin is agriculture, although fishing and cross-border trade form part of the people's occupation. Crops are grown on the flood plains and along the margin of the flood plain. These include maize, rice, millet and vegetables. Other crops grown include groundnuts and cassava. Animal rearing is also an old tradition of the district. The major animals reared include cattle, goats, pigs and sheep (CSO, 2010).

Once a sleeping giant, Sesheke District is poised for a hive of activities after the completion of the M10 road commonly known as the Livingstone-Sesheke-Senanga Road and the Katima Mulilo Bridge. The 900 meters long bridge, which was completed in May 2004, spans the Zambezi River connecting the district with the Namibian town of Katima Mulilo also known

as Ngwezi. The paved road from Sesheke to Livingstone and the Victoria Falls 200 kilometres east has added economic value to Sesheke in terms of tourism. In particular the bridge and the roads have unlocked the potential for trade and transport, whilst opening up vital access to the Namibian port of Walvis Bay for central Africa. It is therefore not surprising that the recent boom in development has resulted in the growth of squatter camps near Sesheke and Katima Mulilo, cross-border smuggling and other social activities on both sides of the Zambia-Namibia border (CSO, 2010).

CHAPTER 4: METHODOLOGY

4.1 The approach to the study

Arising from the gap analysis in Chapter Two and the objectives outlined in Chapter One, the spatial-temporal AET on warm-wet, cool-dry, hot-dry days and months were estimated over the semi-arid Barotse Sub-basin using the SEBS model. Furthermore, point-based PET was determined at Sesheke Meteorological Station in Sesheke District of Zambia using the FAO Penman-Montieth method as given in Equation 1. The formulae applied to retrieve net radiation, which is an input in the FAO Penman-Montieth equation, are given in Appendix 1. Finally, the SEBS fluxes were evaluated against independently modelled AET from ECMWF and the calculated PET. The comparisons were made at a point scale at two reference points: (1) Sesheke Meteorological Station, which is in the southern part of the study area, and (2) Kamanga station in the northern part. The modelled fluxes at Kamanga station were compared with ECMWF estimates only. Potential ET was not calculated at this station because of the lack of meteorological data at satellite over pass time. In this study, it was assumed that the SEBS modelled fluxes at the two reference stations would be comparable to that from ECMWF and would not exceed PET on all the days.

The three approaches which were applied to estimate ET in this study are shown in the flow chart in Figure 10. The research processes that were followed in the remote sensing (SEBS) approach involved downloading MODIS satellite images, estimating input (biogeophysical) parameters, running the model and estimating monthly ET from sunshine and daily fluxes. The point-based approach (Penman-Montieth method) relies only on atmospheric variables whereas the SEBS model utilises both meteorological and remote sensing data. Thus, the available meteorological data (Table 2) corresponding to satellite overpass time were collected from Sesheke Meteorological Station and used to run the SEBS model and calculate PET. Some data which were not available at this station were obtained from the nearby one at Katima Mulilo of Namibia (Appendix 2). Ground truthing was also done during the same field work campaign. This involved identifying land cover types and collecting ground control points using the Global Positioning System (GPS). The third method used to quantify evaporative fluxes of the study area was by estimating it from an independent model (ECMWF). Both daily and monthly ET was estimated from this model. Finally, the modelled SEBS fluxes were evaluated against PET and ECMWF estimates (Figure 10).

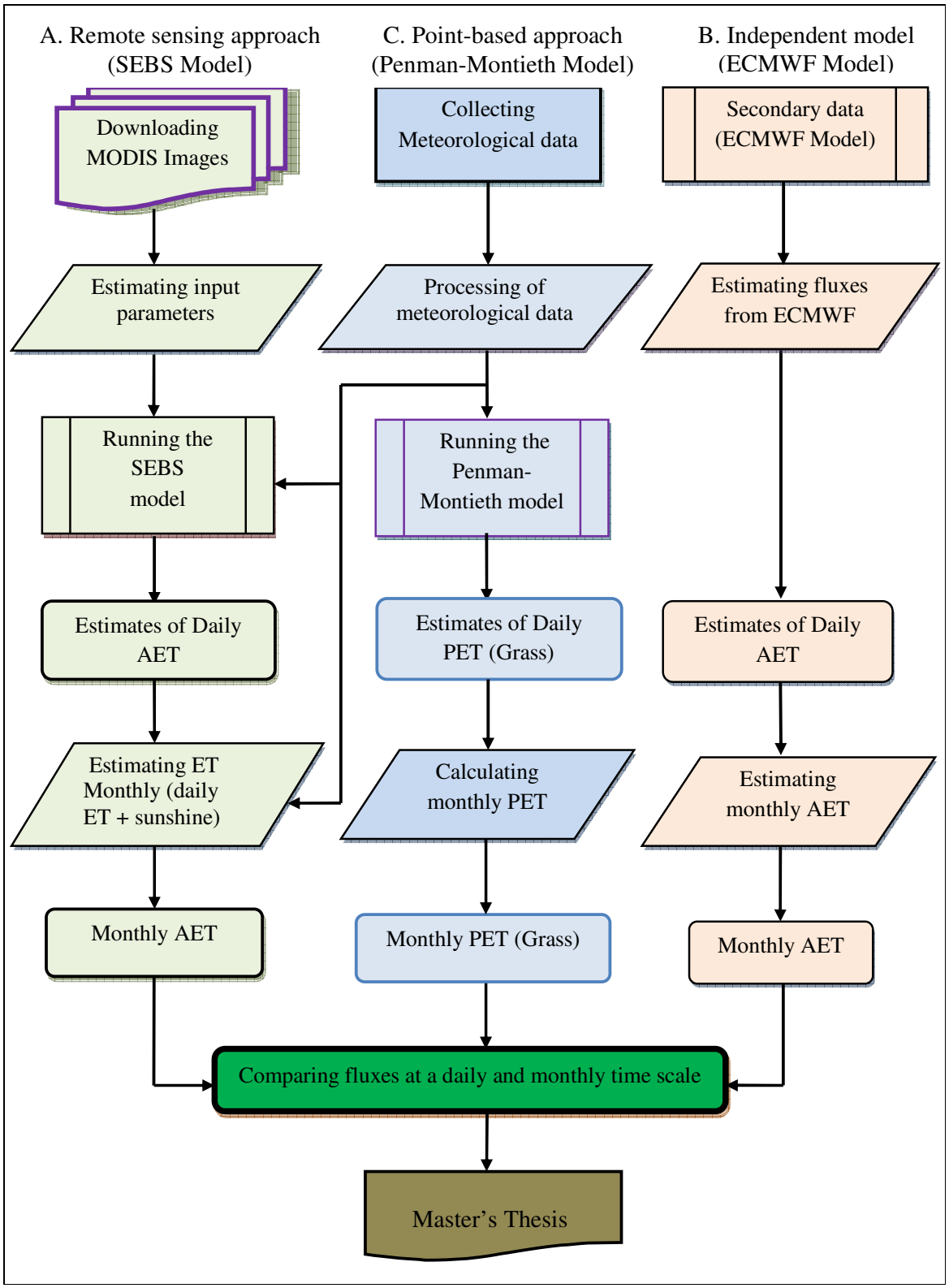

Figure 10: The study approach used to estimate evaporative fluxes and compare SEBS modelled actual evapotranspiration with European Centre for Medium-Range Weather Forecast (ECMWF) estimates and potential evapotranspiration in the semi-arid Barotse Sub-basin in Sesheke area

The details of the SEBS computational steps used in this study to estimate biogeophysical parameters, which are pre-requisite inputs needed to run the model, and evaporative fluxes in conjunction with meteorological data are shown in Figure 11.

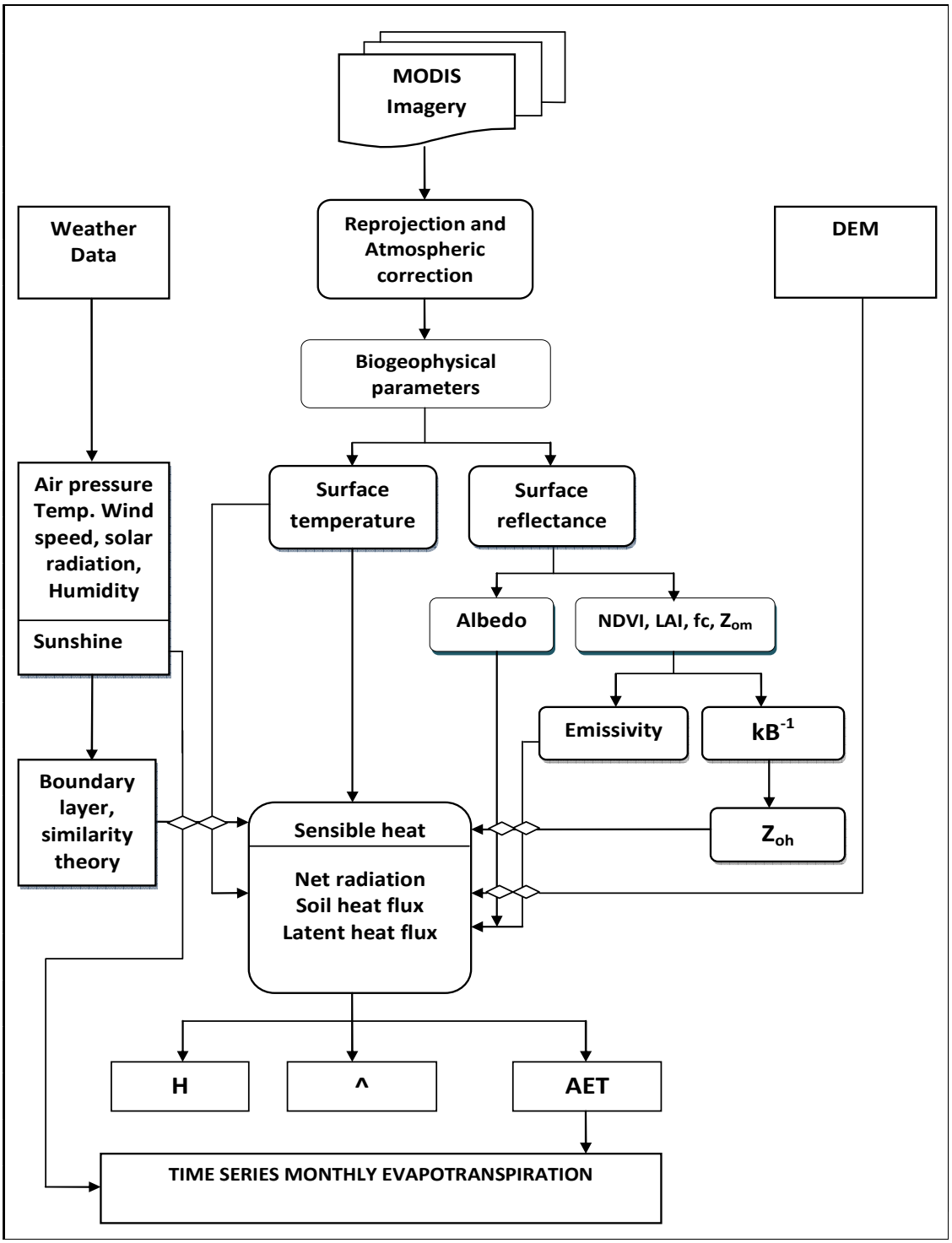

Figure 11: The flowchart of the SEBS computational steps used in this study to obtain daily and monthly fluxes (modified after Hailegorgis, 2006)

4.2 Description of meteorological input data used

Three sets of data were required to run the SEBS model: remotely sensed, solar radiation and meteorological data as shown in Figure 11. Solar radiation data included shortwave solar radiation and downwards longwave radiation. With respect to meteorological data, the SEBS model requires bright sunshine hours, average air temperature, specific humidity, wind speed, pressure at a reference and surface height. In this study, additional data on daily relative humidity, minimum air temperature and maximum air temperature, were required for the calculation of PET using the Penman-Montieth equation.

As anticipated, weather data accessed from the Meteorological Department of Zambia in Lusaka had gaps and was limited to a few atmospheric variables which included monthly temperature, rainfall, pressure and wind speed. Scanty data at a daily time-step were available at Sesheke Meteorological Station. Again these were limited to temperature, rainfall, pressure and wind speed. Radiation and bright sunshine hours data over satellite passing time were not available. At the time of data collection, the station had since stopped operating as it was in a state of disrepair. The gaps in weather data and the absence of radiation data were solved using a two-pronged approach: (1) calculating the missing variables from a few available ones using a number of formulae and (2) retrieving such data from GCMs as will be shown later in this thesis. The climatic data at Sesheke Meteorological Station over satellite passing time are shown in Table 2.

Table 2: Climatic data at satellite passing time at Sesheke Meteorological Station in the semi-arid Barotse Sub-basin, South-Western Zambia. RH= Relative humidity; Min. = Mininium; Max. = Maximum; Temp. = Temperature, e_s= Saturation vapour pressure; e_a= Actual vapour pressure; e_s-e_a= Vapour pressure deficit; q= Specific humidity of air; ρ_{air}= mean air density at constant pressure; Δ= Slope of saturation vapour curve. The asterisk * means that data was estimated from the European Centre for Medium-Range Weather Forecast

Latitude: -17.47, Longitude: 24.30, Elevation: 951 metres a.s.l																	
Date	Julian Day	Time Overpass	Temp. Min.	Temp. Max.	Temp. Mean	Air Temp.	RH	Wind Speed	Pressure*	Solar Radiation*	Bright Sunshine*	e_s	e_a	e_s-e_a	q	ρ_{air}	Δ
		(GMT)	**^oC**	**^oC**	**^oC**	**K**	**%**	**ms^{-1}**	**hpa**	**Wm^{-2}**	**hrs**	**Kpa**	**Kpa**	**Kpa**	**-**	**Kgm^{-3}**	**Kpa $^oC^{-1}$**
21/11/06	325	8:45	20.3	34.4	27.4	307.55	50	2.6	960	833.88	7.27	5.439	2.382	3.057	0.0015	1.147	0.302
30/11/06	334	8:40	20.2	33.8	27.0	306.95	61	2.5	905	846.48	7.09	5.260	2.367	2.893	0.0016	1.150	0.293
02/12/06	336	8:25	20.2	33.6	26.9	306.75	69	2.1	910	848.06	7.07	5.202	2.367	2.835	0.0016	1.150	0.290
04/12/06	338	8:15	20.4	33.5	27.0	306.65	65	1.9	890	849.62	7.05	5.173	2.397	2.776	0.0016	1.151	0.289
12/01/07	12	8:20	19.7	32.0	25.9	305.15	66	1.7	907	841.27	7.24	4.755	2.295	2.460	0.0015	1.156	0.269
14/01/07	14	8:10	19.7	32.0	25.9	305.15	76	1.6	905	841.59	7.23	4.755	2.295	2.460	0.0015	1.156	0.269
14/02/07	45	9:05	19.8	32.2	26.0	305.35	77	1.5	906	834.53	7.08	4.809	2.309	2.499	0.0015	1.156	0.271
18/02/07	49	8:40	19.8	28.7	24.3	301.85	73	1.2	901	826.93	7.14	3.937	2.309	1.627	0.0015	1.169	0.228
12/03/07	71	8:05	18.7	32.2	25.5	305.35	64	1.5	910	746.93	8.12	4.809	2.157	2.652	0.0014	1.156	0.271
15/03/07	74	8:35	18.5	32.3	25.4	305.45	71	1.6	1080	737.35	8.21	4.836	2.130	2.706	0.0012	1.155	0.273
16/04/07	106	8:35	14.6	31.8	23.2	304.95	61	2.0	903	620.71	9.43	4.701	1.662	3.039	0.0011	1.157	0.266
23/04/07	113	8:40	13.3	31.3	22.3	304.45	59	1.6	1080	600.37	9.51	4.570	1.527	3.042	0.0009	1.159	0.260
16/05/07	136	8:45	9.7	29.0	19.4	302.15	46	1.5	980	533.80	10.10	4.006	1.203	2.802	0.0007	1.168	0.231
23/05/07	143	8:50	8.2	27.7	18.0	300.85	54	1.4	920	521.31	10.08	3.714	1.087	2.627	0.0007	1.173	0.217
17/06/07	168	8:45	6.6	26.9	16.8	300.05	48	1.7	1120	505.88	9.53	3.544	0.975	2.570	0.0005	1.176	0.208
19/06/07	170	8:35	5.6	26.0	17.1	299.15	54	1.0	1020	507.55	9.42	3.361	0.910	2.452	0.0005	1.180	0.199
10/07/07	191	8:50	5.1	26.3	15.7	299.45	58	1.0	1410	517.46	9.42	3.422	0.878	2.543	0.0004	1.178	0.202
16/07/07	197	8:15	5.0	28.0	16.5	301.15	50	1.0	1410	524.44	9.45	3.780	0.872	2.908	0.0004	1.172	0.220
13/08/07	225	8:40	8.2	29.8	19.0	302.95	43	1.7	960	568.75	10.00	4.195	1.087	3.107	0.0007	1.165	0.241
20/08/07	232	8:45	9.4	30.7	24.2	303.85	48	2.0	980	584.49	10.06	4.416	1.179	3.237	0.0007	1.161	0.252
12/09/07	255	8:50	11.3	33.9	22.6	307.05	71	2.1	907	641.15	10.03	5.290	1.339	3.951	0.0009	1.149	0.295
14/09/07	257	8:46	11.7	34.2	23.0	307.35	69	2.1	904	645.45	10.04	5.379	1.375	4.004	0.0009	1.148	0.299
14/10/07	287	8:50	17.0	34.5	25.8	307.65	36	3.3	980	716.15	9.44	5.469	1.938	3.531	0.0012	1.147	0.303
19/10/07	292	9:10	17.2	34.4	25.8	307.55	34	3.4	930	729.15	9.22	5.439	1.962	3.476	0.0013	1.147	0.302

In this study, solar radiation, bright sunshine hours and surface pressure data were retrieved from the ECMWF website: http://www.ecmwf.int/. This website provides directly measured data as well as modelled parameter fields. The advantage of this data is that it is spatially distributed and one can mask out ones area of interest to retrieve it. This data is available free of charge after registration. The meteorological data obtained from this website was used to fill the gaps in the data collected from Sesheke Meteorological Station for the satellite passing time. Figure 12 illustrates the distribution of surface pressure at satellite passing time as modelled by ECMWF on the DOY 45 (14th February, 2007:09.00 GMT).

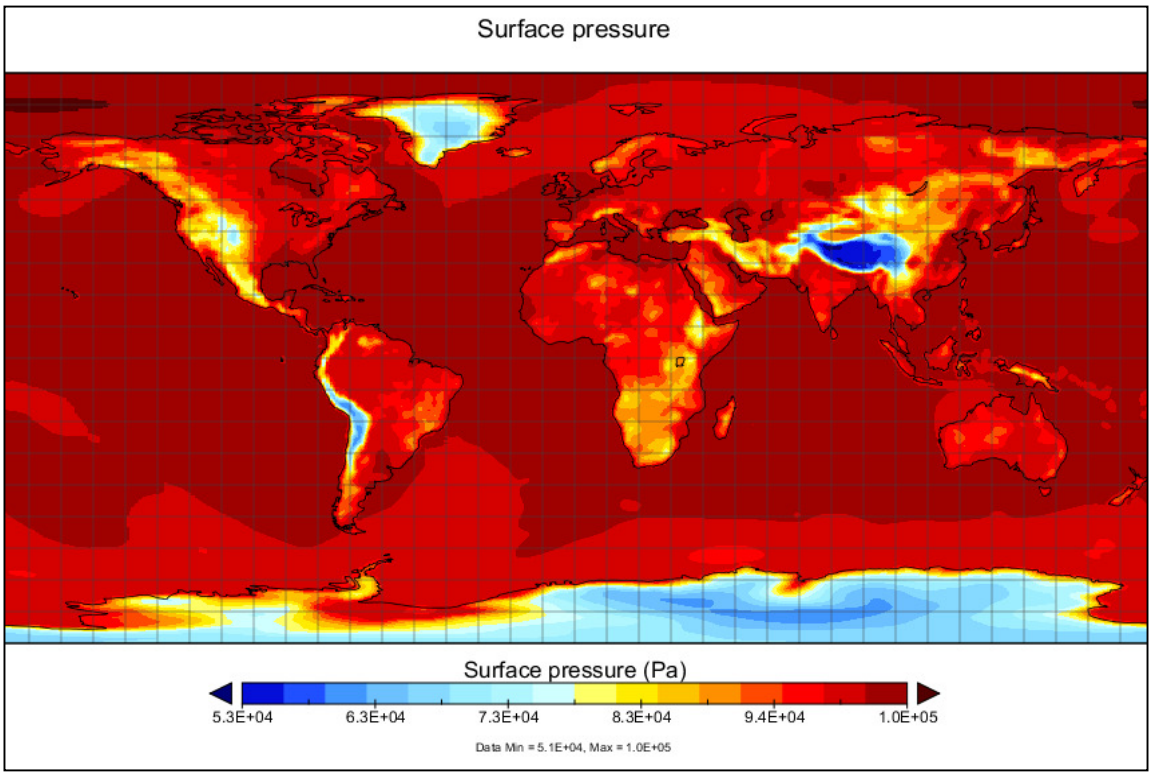

Figure 12: Surface pressure over satellite passing time: 14th February, 2007:09.00 GMT (http://www.ecmwf.int/)

4.3 Description of satellite (MODIS) images used

The Moderate-resolution Imaging Spectroradiometer (MODIS) is a payload scientific instrument launched into Earth orbit by NASA in 1999 on board the Terra (EOS AM) Satellite, and in 2002 on board the Aqua (EOS PM) satellite. They are designed to provide measurements in large-scale global dynamics including changes in Earth's cloud cover, radiation budget and processes occurring in the oceans, on land, and in the lower atmosphere.

The MODIS instrument provides high radiometric sensitivity (12) bits in 36 spectral bands (20 reflective solar and 16 thermal emissive bands) ranging in wavelength from 0.4μm to 14.4 μm. Two bands are imaged at a nominal resolution pixel of 250 m at nadir with five bands at 500 m, and the remaining 29 bands at 1 Km. A 2,330 Km (across track) by 10 Km (along track at nadir) swath and provides global coverage with a temporal resolution of one to two days (Kaufman et al., 1998). Thus, because of its high temporal resolution, satellite remote sensing data from MODIS sensors provide unprecedented information regarding vegetation and surface energy (Justice et al., 1998), which can be used to develop a remotely sensed ET model. The description of the spectral characteristics of the MODIS imagery used to run the SEBS model is shown in Table 3.

Table 3: Description of the spectral characteristics of MODIS satellite imagery used in this study

BAND	WAVELENGTH	SPECTRAL RANGE (μm)	RESOLUTION (m)
1.	Visible	0.62 – 0.67	250
2.	Visible	0.841 – 0.876	250
3.	Visible	0.459 – 0.479	500
4.	Visible	0.545 – 0.565	500
5.	Visible	1.230 – 1.250	500
6.	Visible	1.628 – 1.652	500
7.	Panchromatic	2.105 – 2.155	500
31.	Thermal Infrared Red	10.780 – 11.280	1000
32.	Thermal Infrared Red	11.770 – 12.270	1000

In this study, twenty-four (24) cloud free MODIS satellite images were pre-processed for the determination of various biogeophysical parameters which were needed to run the SEBS model. These images were carefully selected by considering the seasonal variations which typify the climatic pattern of the semi-arid Barotse sub-basin. Thus, the temporal resolution of these cloud free images represent typical warm-wet, cool-dry and hot-dry clear sky days which are dominant in the seasonal cycle and climatic pattern of the study area. In this study, by definition, warm-wet days start from November to March, the cool-dry days fall between April and July and the hot-dry days appear between August and October (ZDM, 1992;

Hutchinson, 1974; MEWD-JICA, 1995). In this regard, MODIS images were downloaded considering this time scale. The selected images which satisfied this criterion that were used in this study are shown in Table 4. These MODIS images were downloaded free of charge and are available on this web site: http://www.ladsweb.nascom.nasa.gov/browse image. For this study, however, some MODIS images were accessed courtesy of the Integrated Water Resources Management (IWRM) Centre of the University of Zambia (UNZA) which is undertaking research studies in the Zambezi Basin using remote sensing and geographical information system (GIS) techniques.

Table 4: Selected cloud-free MODIS satellite images used in this study

No.	DATE	YEAR	DAY OF THE YEAR	OVERPASS TIME (GMT)
	Warm-wet Days			
1.	21st November	2006	325	08:25
2.	30th November	2006	334	08:40
3.	02nd December	2006	336	08:25
4.	04th December	2006	338	08:15
5.	12th January	2007	12	08:20
6.	14th January	2007	14	08:10
7.	14th February	2007	45	09:05
8.	18th February	2007	49	08:40
9.	12th March	2007	71	08:05
10.	15th March	2007	74	08:35
	Cool-dry days			
11.	16th April	2007	106	08:35
12.	23rd April	2007	113	08:40
13.	16th May	2007	136	08:45
14.	23rd May	2007	143	08:50
15.	17th June	2007	168	08:45
16.	19th June	2007	170	08:35
17.	10th July	2007	191	08:50
18.	16th July	2007	197	08:15
	Hot-dry day			
19.	13th August	2007	225	08:40
20.	20th August	2007	232	08:45
21.	12th September	2007	255	08:50
22.	14th September	2007	257	08:46
23.	14th October	2007	287	08:50
24.	19th October	2007	292	09:10

4.4 Pre-processing of MODIS images

The pre-processing of MODIS images involved two main activities: re-projection and atmospheric correction of the visible bands (1 to 7). The details of how the two processes were carried out are described below.

4.4.1 Re-projecting MODIS imagery

The level 1 B MODIS images used in this study are in a map projection format called Integerised Sinusoidal (ISIN) projection and cannot be read by Integrated Land and Water Information System (ILWIS) and many other GIS software. In order to use the data in ILWIS, there was need to re-project the MODIS images and convert them to Geographical Tagged File Format (Geotiff). In this study, the MODIS Re-projection Tool (MRTSwath) software was used to covert MODIS images from their native format to Geotiff file format which is supported by ILWIS. The re-projection parameters used are as follows: resample method: nearest neighbour; output projection type: Geographic; output file type: Geotiff; and output pixel: 0.01 (1Km pixel size). The Geotiff files were imported into ILWIS via Geospatial Data Abstraction Library (GDAL).

4.4.2 Atmospheric correction of the visible bands with the SMAC algorithm

The correction for atmospheric absorption and attenuation is important for any approach concerned with the energy balance equation. It is known that the presence of gases, water vapour and aerosols in the atmosphere causes scattering and absorption of the electromagnetic spectrum with consequent effects on the energy measured by satellite sensors. For this reason, techniques which correct for the atmospheric effects have been developed to retrieve the actual surface radiance. According to Parodi (2006), atmospheric correction techniques can be broadly divided into two categories: relative atmospheric correction and absolute atmospheric correction. The former is based on known ground reflectance properties of objects while the latter is an atmospheric modelling approach.

The Simplified Method for Atmospheric Correction (SMAC) is a semi-empirical radiative transfer model which was developed by Rahman and Dedieu (1994). It is built on a set of equations with coefficients, which are determined depending on the spectral bands of the sensor and aerosol model. These parameters are retrieved by a best-fit against a full radiative transfer model like 5s and 6s codes (Raupach, 1994). Semi-empirical models like SMAC,

FLAASH and ATCOR are several hundred times faster than full radiative transfer models because they reduce the input requirements to some widely measured standard parameters. However, numerous coefficients have to be determined in advance from best-fits with a full numerical model. Further, if there is a change in the spectral band characteristics this would also require new coefficients.

The data which was required to run the SMAC algorithm include: optical thickness at 0.55µm, ozone concentration (gram.atm.cm), water vapour column (g cm^{-2}), surface pressure (hpa), MODIS coefficient files and satellite and solar angles. The various sources and methods used to estimate this input data in this study are described below.

Aerosol Optical Thickness (AOT) is a measure of the extinction of the solar beam by dust and haze (Iqbal, 1983). Therefore, AOT measures how much direct sunlight is prevented from reaching the ground by these aerosols particles. By definition, AOT is a dimensionless number (0.05-0.8) that is related to the amount of aerosol in the vertical column of the atmosphere over the observation location (Parodi, 2009). Although this data is retrievable from the website, http://aeronet.gsfc.nasa.gov/, there were no measurements which were done within the study area over satellite passing time. The nearest station on which AOT was evaluated was at Mongu, the provincial capital of Western Province, Zambia. Since AOT is extremely dynamic (Iqbal, 1983; Parodi, 2009), the Mongu values could not be imported into the study area. Thus, AOT in this study was estimated using empirical relationships. This involved converting hourly visibility observations obtained at Katima Mulilo Meteorological Station of Namibia shown in Appendix 2 to atmospheric turbidity following the procedure of MacClatchey and Selby (1972). The turbidity values were then multiplied with the appropriate wavelength to get AOT. The formulae used are given in Appendix 3.

Ozone concentration data in this study was retrieved from the OMI ozone monitoring project on this website: http://toms.gsfc.nasa.gov/ozone/ozone_v8.html. Daily ozone measurements were obtained for the point location of the reference station. Ozone content is measured in grams by atmosphere by centimetre (gram.atm.cm) and the value range is 0.0 to 0.7. It is also measured in Dobson Units (DU; 1000 DU= 1 g.atm.cm) (Parodi, 2006). An example of how ozone concentration is retrieved over satellite passing time from the OMI ozone monitoring website is shown in Figure 13 for the 14th day of September, 2007. Thus, on this day, ozone

concentration in the study area, and using Sesheke Meteorological Station as a reference point, was calculated as follows: 275 DU/1000 = 0.28 g.atm.cm.

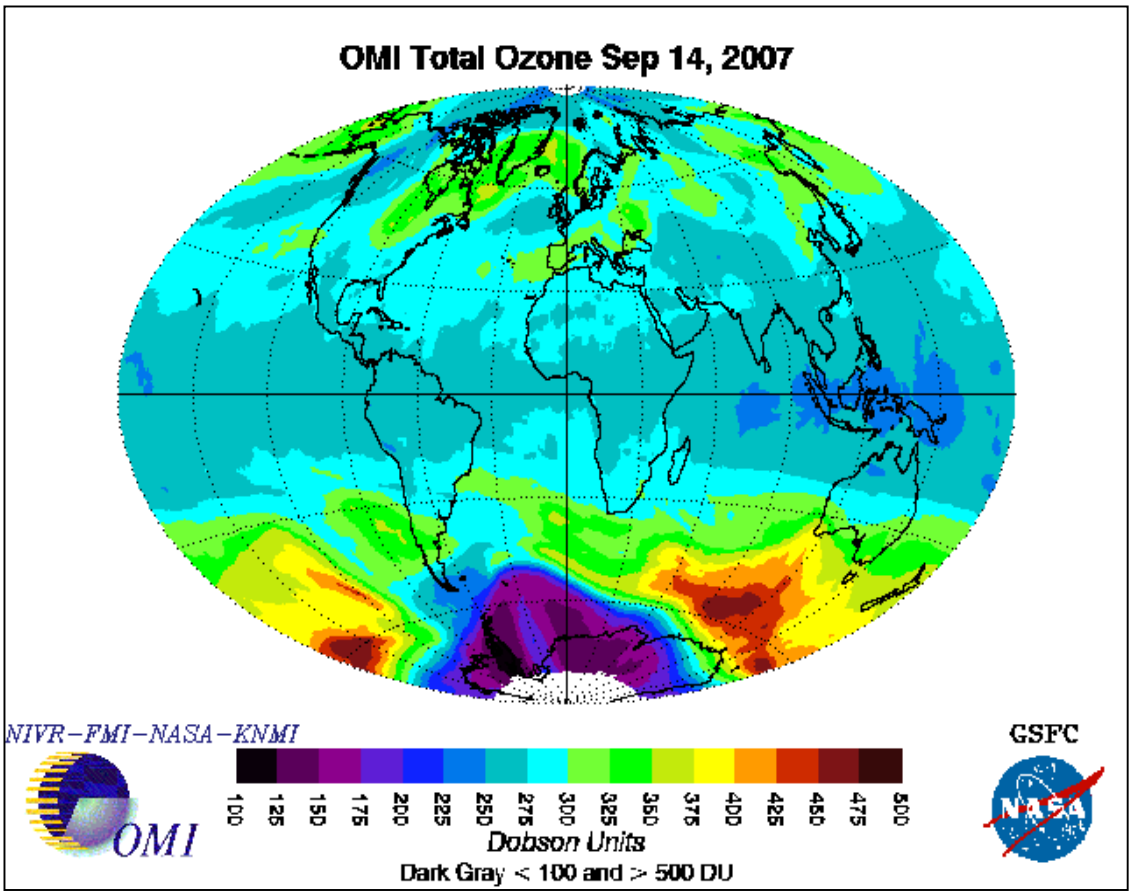

Figure 13: Global ozone concentration on 14th of September 2007 as modelled by OMI Ozone Monitoring Project: http://toms.gsfc.nasa.gov/ozone/ozone_v8.htm

The water vapour content (g cm^{-2}) defined from the perspective view of precipitable water (w') is the total amount of water vapour between the surface and top of the atmosphere (TOA) in a vertical column. It is also visualised as the thickness of the liquid water that would be formed if all the vapour in the zenith direction were condensed at the surface of a unit area (Iqbal, 1983). Water vapour content is retrievable from the aeronet website: (http://aeronet.gsfc.nasa.gov/).). For instance, the water vapour content on DOY 14 (14^{th} February, 2007) evaluated over the nearest meteorological station at Mongu is shown in Figure 14. Although Mongu is outside the study area, the data evaluated at that station was used to run the SMAC algorithm in this study because the precipitable water is less variable in time and space in comparison with AOT (Igbal, 1983; Parodi, 2009). The water vapour

content was estimated for the satellite over pass time. Thus, in the case of DOY 14 at 09:05 GMT, the value was approximately 2.1 cm (Figure 14).

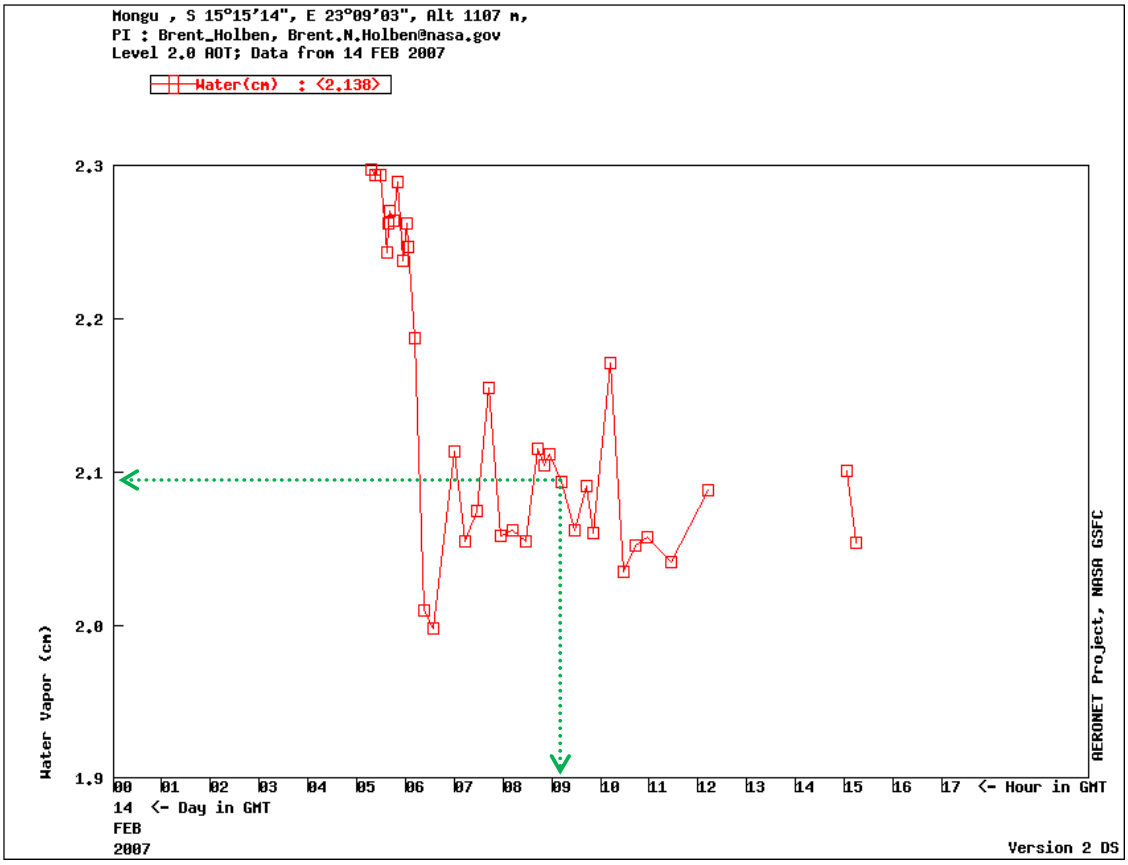

Figure 14: Water vapour content, Mongu, Zambia (From http://aeronet.gsfc.nasa.gov/)

The aerosol optical thickness, ozone concentration and water vapour content data inputs that were used to run the SMAC algorithm are shown in Table 5.

Table 5: Input data of aerosol optical thickness, ozone concentration and water vapour content for the SMAC algorithm used in this study.

No.	DATE	AEROSOL OPTICAL THICKNESS (-)	OZONE CONCENTRATION (gram.atm.cm)	WATER VAPOUR CONTENT (g cm^{-2})
1.	21-11-2006	0.47	0.27	2.1
2.	30-11-2006	0.45	0.27	2.0
3.	02-12-2006	0.44	0.27	2.0
4.	04-12-2006	0.43	0.26	2.0
5.	12-01-2007	0.43	0.25	1.8
6.	14-01-2007	0.44	0.25	2.0
7.	14-02-2007	0.45	0.26	2.1
8.	18-02-2007	0.46	0.25	1.8
9.	12-03-2007	0.44	0.25	1.7
10.	15-03-2007	0.44	0.25	2.0
11.	16-04-2007	0.47	0.26	1.9
12.	23-04-2007	0.47	0.25	1.8
13.	16-05-2007	0.46	0.26	1.2
14.	23-05-2007	0.47	0.25	1.9
15.	17-06-2007	0.48	0.25	1.8
16.	19-06-2007	0.48	0.25	1.4
17.	10-07-2007	0.48	0.25	1.6
18.	16-07-2007	0.48	0.26	1.5
19.	13-08-2007	0.48	0.26	1.8
20.	20-08-2007	0.48	0.26	1.2
21.	12-09-2007	0.48	0.28	1.6
22.	14-09-2007	0.48	0.28	1.5
23.	14-10-2007	0.47	0.28	1.4
24.	19-10-2007	0.45	0.28	1.6

4.5 Estimation of biogeophysical parameters

The land surface parameters that were determined from reflectance and radiance satellite data were as follows: albedo, Normalised Difference Vegetation Index (NDVI), emissivity, fractional vegetation cover, leaf area index, land surface temperature, vegetation height,

displacement height and surface roughness height for momentum and heat transport. The details of the methods used to estimate these parameters are described below.

4.5.1 Land surface albedo (r_o)

The surface reflection is an important physical parameter in determining the net radiation available on the earth`s surface. Surface reflectance (albedo) represents the shortwave surface reflectance in the range of 0.3–3 μm, and was calculated from band-wise surface reflectance using the formula by Liang (2001) which is given in equation (11).

$$\text{Albedo } (r_o) = 0.160*r1 + 0.291*r2 + 0.243*r3 + 0.116*r4 + 0.112*r5 + 0.018*r7 - 0.0015 \quad \text{Eq. 11}$$

Where, r1, r2, r3, r4, r5, r7 are the surface reflectance derived from MODIS atmospherically corrected bands 1, 2, 3, 4, 5 and 7

4.5.2 Normalized Difference Vegetation Index (NDVI)

NDVI is an indirect measurement of photosynthetic activity. It ranges between -1 for low and +1 for high photosynthetic activity. It uses the principle that for vegetated surface, red (RED) and near-infrared (NIR) are characterized by high and low absorption respectively. NDVI can therefore be used to monitor algae spread on the lake or presence of plants (e.g evasive species) on wetlands. The normalized vegetation index is important input in the calculation of the evaporation fraction, and on open water it is very small and normally negative. The NDVI algorithm used in this study is given in equation (12).

$$\text{NDVI} = \frac{\text{NIR}-\text{RED}}{\text{NIR}+\text{RED}} \quad \text{Eq. 12}$$

Where RED and NIR are atmospherically corrected ground reflectance in the red band (band 1) and near infrared band (band 2) respectively (Gupta, 2003).

4.5.3 Fractional Vegetation Cover (f_c)

The fractional vegetation cover defines the partition between vegetated and non vegetated surfaces. In the SEBS algorithm, this parameter is used to determine other biogeophysical parameters such as Leaf Area Index (LAI), the excessive resistance term (kB^{-1}), ground heat

flux and surface temperature (Su, 2002). In this study, the formula proposed by Sobrino et al. (2003) was applied to determine fractional vegetation cover and is given in equation (13).

$$f_c = \frac{(NDVI - NDVI_{min})^2}{(NDVI_{max} - NDVI_{min})^2} \quad \text{Eq. 13}$$

Where $NDVI_{max}$ is the value of full vegetation cover, $NDVI_{min}$ is the value of bare soil, and NDVI is the value of the current pixel (derived from NDVI map). The $NDVI_{min}$ and $NDVI_{max}$ are taken as 0.2 and 0.5 respectively (Sobrino et al., 2003)

4.5.4 Leaf Area Index (LAI)

Leaf Area Index (LAI) is defined as the one sided green leaf area per unit ground area in broadleaf canopies, or as the projected needle leaf area per unit ground area in needle canopies (Bolstad and Gower, 1990). The interaction between vegetation surface and the atmosphere such as radiation uptake, precipitation interception, momentum and gas exchange is substantially determined by the vegetation surface (Monteith and Unsworth, 1990). During vegetation period of deciduous trees, total vegetation surface itself is mainly composed of leaf area, by lesser part of twigs, branches and stem surface. During times of absent foliage (dry season in tropical areas) woody parts determine vegetation surface area. The annual course of LAI for deciduous trees peaks at the height of growing season, whereas LAI of coniferous stands vary far less over the year. Thus, determination of LAI for specific catchments is important in satellite based energy balance modelling. In this study, LAI was calculated using the formula given in equation (14) (Parodi, 2009).

$$LAI = \left[NDVI\left(\frac{1+NDVI}{1-NDVI}\right)\right]^{0.5} \quad \text{Eq. 14}$$

4.5.5 Land Surface Emissivity (Ɛ)

Land surface emissivity is a property of materials which controls the radiant energy flux. Emissivity (Ɛ) for a blackbody is unity. All natural materials have emissivity of less than 1, ranging generally from 0.7 and 0.95 (Gupta, 2003). Emissivity depends on two main factors: composition and surface geometry. It is intimately related to reflectance (spectral property) as governed by Kirchoff`s Law. Dark materials absorb more and thus emit more energy than light materials and thus spectral absorptivity is equal to spectral emissivity (Gupta, 2003).

In this study, land surface emissivity is computed using the visible (red) and near infrared (nir) bands following the method of Sobrino et al (2003), which considers three types of pixels depending on the NDVI value as follows:

For bare soil pixels, NDVI < 0.2

Emissivity **e** = 0.9832 – 0.058 * Bred

Emissivity difference **de** = 0.0018 – 0.06 * Bred

For mixed pixels 0.2 =< NDVI < = 0.5

Emissivity **e** = 0.971 + 0.018 * Pv

Emissivity difference **de** = 0.006 * (1 – Pv)

For vegetation pixels NDVI > 0.5

Emissivity **e** = 0.990 +de

Emissivity difference **de** = 0.005 .....Eq. 15

This method is restricted to land pixels. The emissivity for water pixels is extracted depending on the surface albedo value: For water area, albedo < 0.035, emissivity e = 0.995 (Sobrino et al., 2003).

4.5.6 Land Surface Temperature (LST)

Land surface temperature of clear-sky pixels in MODIS scenes was retrieved from brightness temperatures in bands 31 and 32 using the split window technique of Sobrino and Raissouni (2000) as given in equation (16).

LST = btm32 + (1.97 + 0.2 * W) *(btm32 – btm31) - (0.26 - 0.08 * W) * sqrt (btm32 – btm31) + (0.02 - 0.67 * W) + (64.5 - 7.35 * W) * (1 - e) - (119 - 20.4 * W) * de ..…... Eq. 16

Where LST is land surface temperature, btm31 is brightness temperature, btm32 is brightness temperature, W is water vapour content, e is surface emissivity, de is surface emissivity difference (Parodi, 2009).

4.5.7 Surface Roughness Height for Momentum Transport (Z_{om})

The roughness length for momentum transfer is assumed as the reference height for momentum flux calculations. It is defined as the height at which the logarithmic wind profile reaches zero (Lee et al., 2012). At a large scale, this parameter is well estimated using

spatially distributed vegetation height data or a detailed land use map tagged with literature values (Wieringa, 1993; Su, 2005). Given the difficulties in estimating spatially distributed vegetation heights from field measurements and the scarcity of remote sensing data on vegetation heights (LIDAR), the empirical relationship with NDVI by Su and Jacobs (2001) was used in this study to estimate surface roughness as given in equation (17).

$$z_{om} = 0.005 + 0.5\left(\frac{NDVI}{NDVI_{max}}\right)^{2.5} \quad \text{.....Eq. 17}$$

The land use map tagged with surface roughness estimates based on literature values was also used to calculate of ET. This was done in order to understand the effect of this parameter on evapotranspiration estimates in the study area.

4.5.8 Vegetation Height

Vegetation height was estimated inverting the equation used to derive surface roughness based on vegetation height by Brutsaert (1982) as given in equation (18). This parameter was used to derive displacement height.

$$h = \frac{z_{om}}{0.136} \quad \text{.....Eq. 18}$$

4.5.9 Displacement Height (d_o)

Displacement height (d_o), defined as the mean level where momentum is absorbed by a canopy (Allen et al., 1998), was estimated using empirical relationship with vegetation height as given in equation 19 (Brutsaert, 1982).

$$d_o = \frac{2}{3} h \quad \text{.....Eq. 19}$$

4.5.10 The Roughness Length for heat Transport (Z_{oh})

The roughness length for heat transfer was calculated as given in equation (20) (Su, 2002).

$$z_{oh} = \left(\frac{z_{om}}{\exp(kB^{-1})}\right) \quad \text{.....Eq. 20}$$

Where kB^{-1} is a parameter called excess resistance to heat transfer which is used to compare Z_{om} and Z_{oh} (Su, 2002). The physically based model of Su et al (2001) for the determination of kB^{-1} was used and is expressed as given in equation (21).

$$kB^{-1} = \frac{kC_d}{4C_t\frac{U^*}{U(h)}(1-e^{-nec/2})} f_c^2 + 2f_c f_s \frac{k.\frac{U_*}{U(h)}.Z_{om}/h}{C_t^*} + kB_s^{-1} f_s^2 \quad \text{.....Eq. 21}$$

Where f_c is fractional vegetation cover of the canopy and f_s is fraction of non-vegetated soil, C_t and C_t^* are the heat transfer coefficient of the leaf and soil respectively; C_d is the drag coefficient of the foliage, n_{ec} is the within canopy wind speed extinction coefficient and kB_s^{-1} is the term that applies for bare soils (Su, 2002).

4.6 Similarity Theory

The Monin-Obukhov Similarity (MOS) theory states that if various statistics of the atmospheric parameters at a height (Z) are normalised by proper powers of friction velocity and the Obukhov length (L), are universal functions of Z/L (Monin and Obukhov, 1954). This theory was applied in this study to derive the friction velocity (u_*), the sensible heat flux (H) and the stability length (L). The relationship for the mean wind and temperature profiles are written in integral form as given in equations (22) and (23) (Su, 2002).

$$u = \frac{u_*}{k}\left[In\left(\frac{Z-d_o}{Z_{om}}\right) - \Psi_m\left(\frac{Z-d_o}{L}\right) + \Psi_m\left(\frac{Z_{om}}{L}\right)\right] \quad \text{.....Eq. 22}$$

$$\theta_o - \theta_a = \frac{H}{ku_*\rho C_p}\left[In\left(\frac{Z-d_o}{Z_{oh}}\right) - \Psi_h\left(\frac{Z-d_o}{L}\right) + \Psi_h\left(\frac{Z_{oh}}{L}\right)\right] \quad \text{.....Eq. 23}$$

Where z is the reference height above the surface, u_* is the friction velocity, ρ is the density of air, k a von Karman's constant is 0.4, d_o is the zero displacement height, Z_{om} is the roughness height for momentum transfer, Z_{oh} is roughness length for heat transport, θ_o and θ_a are the potential temperature at the surface and the air, Ψ_m and Ψ_h are the stability correction functions for momentum and sensible heat transfer respectively, which were determined according to the formulation proposed for the Monin-Obukhov profile functions by Brutsaert (1999), and L is the Monin-Obukhov length, defined as the ratio between the energy produced by forced mechanical convection and energy produced by thermal convection (Monin and Obukhov, 1954), and was estimated as given in equation (24) (Su, 2002).

$$L = -\frac{\rho C_p u_*^3 \theta_v}{kgH} \quad \text{..... Eq. 24}$$

Where g is the acceleration due to gravity and θ_v is the potential virtual temperature near the surface (Su, 2002).

4.7 Additional Data for SEBS Algorithm

In addition to the remote sensing data, the following meteorological parameters were used to run the SEBS model and compute potential evapotranspiration: average wind speed, relative humidity, air temperature and air pressure at the reference height measured at Sesheke Meteorological Station. Since most of this data is not readily available at the reference station, it was estimated from the measured ones. These included the following:

4.7.1 Saturation Vapour Pressure (e_s)

According to Allen et al. (1998) since saturated vapour pressure is related to air temperature, it can be calculated from air temperature using the relationship expressed in equation (25).

$$e_s = 0.6108\exp\left(\frac{17.27T}{T+273.3}\right) \quad \text{Eq. 25}$$

Where e_s is saturation vapour pressure at the air temperature T (kPa) and T is air temperature (^oC) measured near surface layer (Allen et al., 1998).

4.7.2 Actual vapour Pressure (e_a)

Actual vapour pressure can be derived from dew point temperature or from the relative humidity (RH) data. In this study, actual vapour pressure was calculated using the relationship with relative humidity as given in equation (26) (Allen et al., 1998).

$$e_a = \frac{RH_{mean}}{100} . e_s \quad \text{Eq. 26}$$

Where mean relative humidity is the average between RH_{max} and RH_{min} (Allen et al., 1998).

4.7.3 The Slope of the Saturation Vapour Pressure Curve (Δ)

The slope of the relationship between saturation vapour pressure and temperature is calculated as given in equation (27) (Allen et al., 1998).

$$\Delta = \frac{4098\left[0.6108\exp\left(\frac{17.27T}{T+237.3}\right)\right]}{(T+237.3)^2} \quad \text{Eq. 27}$$

4.7.4 Specific Humidity

$$q = \left(\frac{R_d}{R_v}\right) * \frac{e_a}{p_s} \quad \text{.....Eq. 28}$$

Where R_d (278.04) and R_v (461.05) are the gas constants for the dry air and water vapour air (Alvarez, 2007).

4.7.5 Atmospheric Pressure

$$P = 101.3\left(\frac{293-0.0065Z}{293}\right)^{5.26} \quad \text{.....Eq. 29}$$

Where P is atmospheric pressure (kPa), z is elevation above sea level (m) (Allen et al., 1998).

4.7.6 Potential Temperature

$$\theta = T\left(\frac{p_o}{p}\right)^{0.286} \quad \text{.....Eq. 30}$$

Where, θ is the potential temperature (K), T is the near surface layer air temperature and surface temperature (K) and P is pressure in mbar (Hailegorgis, 2006).

4.7.7 Virtual Potential Temperature

Virtual potential temperature was calculated using the formula given in equation (31) (Hailegorgis, 2006).

$$\Theta_v = (1 + 0.61q)\Theta \quad \text{.....Eq. 31}$$

4.8 Parameterisation of land surface heat fluxes

The downward solar radiation at satellite passing time was calculated using methods described by Allen et al. (1998) whereas the outgoing long wave radiation was derived from satellite data with some parameterisation. The incoming longwave radiation was derived from air temperature. The net radiation was then calculated as the residual of all incoming and outgoing short wave and long wave radiation. The soil heat flux was derived from the empirical relationship with vegetation cover and net radiation.

4.8.1 Net radiation (R_n)

Net radiation is the difference between incoming solar radiation and outgoing terrestrial radiation at the Earth's surface. Net radiation is expressed as given in equation (32).

$$R_n = (1-\alpha)K\downarrow + \varepsilon . L\downarrow - L\uparrow \quad \text{.....Eq. 32}$$

Where Rn is net radiation, K ↓ is incoming shortwave radiation, L ↓ and L↑ are incoming and outgoing longwave radiation respectively, α is albedo and ε is surface emissivity (Su, 2002). The incoming longwave radiation (L ↓) is calculated using equation (33) (after Su, 2002).

$$L\downarrow = \sigma . \varepsilon_a T_a^4 \quad \text{……..……..……..…Eq. 33}$$

Where σ is the Stefan-Boltzman constant (5.67×10^{-8} Wm^{-2} K^{-4}), ε_a is the emissivity of air by Campbell and Norman (1998) which is given in equation (34).

$$\varepsilon_a = 9.2.10^{-6}. (T_a + 273.15)^2 \quad \text{……..……..……..…..Eq. 34}$$

Where T_a is the air temperature at reference height.

The outgoing long wave radiation (L↑) was determined as a function of surface temperature and emissivity as given in equation (35) (Su, 2002).

$$L\uparrow = \varepsilon_s . \sigma . T_s^4 \quad \text{……..……..……..……..Eq. 35}$$

Where ε_s and T_s are surface emissivity and temperature respectively.

4.8.2 The soil Heat Flux (G_o)

The equation for the soil heat flux was parameterized as given in equation (36) (Su, 2002).

$$G_o = R_n[\Gamma_c + (1-f_c)(\Gamma_s - \Gamma_c)] \quad \text{……..……..…...Eq. 36}$$

Where Γ_c is 0.05 for full vegetation canopy by Montieth cited in Su et al. (2001) and Γ_s is 0.315 for bare soil (Kustas and Daughtry, 1989).

4.8.3 The Sensible Heat Flux (H)

Sensible heat refers to energy transferred between the surface and air when there is difference in temperature between them. The surface temperature is usually much higher than the air

temperature during the day. Therefore the sensible heat flux is normally directed upwards during the day. During the night the situation may be reversed. Sensible heat transport takes place mostly by diffusive processes near the surface, but after a distance, surface turbulent transport becomes more vital. Sensible heat flux is calculated based on weather data (wind speed, humidity) and land/water surface temperature which is calculated from satellite data.
The actual sensible heat derived in equation (10) is constrained by the sensible heat flux at the wet limit (H_{wet}) and the sensible heat flux at the dry limit (H_{dry}) in SEBS (Su, 2002). Thus, from equation (10), the dry limit is given in equation (37) (Su, 2002).

$$ƛE_{dry} = R_n - G_0 - H_{dry} \equiv 0 \quad \text{or} \quad H_{dry} = R_n - G_o \quad \text{.....Eq. 37}$$

Equation (37) implies that latent heat evaporation becomes zero due to the limitation of soil moisture and sensible heat would be at its maximum. Under the wet limit, however, evaporation takes place at a potential rate and is limited by the available energy at the earth's surface. In this case sensible heat flux becomes as given in equation (38) (Su, 2002).

$$ƛE_{wet} = R_n - G_o - H_{wet} \quad \text{or} \quad H_{wet} = R_n - G_0 - ƛE_{wet} \text{.....Eq. 38}$$

The equation similar to the FAO Penman-Montieth (Allen et al., 1998) is combined with equation (38) to come up with sensible heat at the wet limit as given in equation (39).

$$H_{wet} = \left((R_n - G_o) - \frac{\rho c_p}{r_{ew}}.\frac{e_s - e_a}{\gamma}\right) / \left(1 + \frac{\Delta}{\gamma}\right) \text{ ..... Eq. 39}$$

Where e_a is actual vapour pressure , e_s is saturation vapour pressure, γ is the psychrometric constant, Δ is the rate of change of saturation vapour pressure with temperature and r_{ew} is the external resistance which is determined by equation (40) (Su, 2002).

$$r_{ew} = \frac{1}{ku_*}\left[In\left(\frac{Z-d}{Z_{oh}}\right) - \psi_h\left(\frac{Z-d}{L_w}\right) + \Psi_h\left(\frac{Z_{oh}}{L_w}\right)\right] \text{ .....Eq. 40}$$

The external resistance in equation (40) is dependent on the Obukhov length at the wet limit and is expressed as given in equation (41) (Su, 2002).

$$L_w = \frac{\rho u_*^3}{kg.0.61.(R_n - G_o)/\lambda} \text{ .....Eq. 41}$$

Where λ is the latent heat of vapourisation (2.45MJ kg^{-1}) (Allen et al., 1998).

4.9 Determination of evaporative fraction

From equations (10), (37) and (38) Su, (2002) arrives at the formula for determining the relative evaporation as given in equation (42).

$$\Lambda_r = \frac{\lambda E}{\lambda E_{wet}} = 1 - \frac{\lambda E_{wet} - \lambda E}{\lambda E_{wet}} = 1 - \frac{H - H_{wet}}{H_{dry} - H_{wet}} \quad \text{.....Eq. 42}$$

The evaporative fraction is finally expressed as given in equation (43) (Su, 2002).

$$\Lambda = \frac{\lambda E}{R_n - G} = \frac{\Lambda_r \lambda E_{wet}}{R_n - G} \quad \text{..... Eq. 43}$$

Daily ET was calculated based on the evaporative fraction, which is assumed to remain constant throughout the day (Sugita and Brutsaert, 1991; Crago and Brutsaert, 1996; Jia et al., 2009). In this way, evaporation which was in mm^{-s} for instantaneous satellite observation was upscaled to total daily ET using the expression given in equation (44) (Su, 2002).

$$AET = 8.64 \times 10^7 \times \frac{\Lambda \,.\, R_{ndaily} - G_{daily}}{\lambda \rho_w} \quad \text{.....Eq. 44}$$

Where, ρ_w is density of water (kgm^{-3}) and R_{n_day} is daily net radiation in (Wm^{-2}). The 24 hours net radiation is estimated as given in equation (45) (Hailegorgis, 2006).

$$R_{n\_day} = (1 - C_1.r_o).K{\downarrow}_{day} + L_{day} \quad \text{.....Eq. 45}$$

Where r_o is broad band surface albedo derived in equation (11), L_{day} is average daily net long wave radiation (Wm^{-2}), C_1 is conversion factor of instantaneous albedo to daily average (default =1.1), $K{\downarrow}_{day}$ is measured incoming solar radiation (Wm^{-2}) and L_{day} is estimated using the daily atmospheric transmittance as given in equation (46) (Hailegorgis, 2006).

$$L_{day} = 110\tau \quad \text{..... Eq. 46}$$

Where τ is determined from sunshine fraction using equation (47) (Hailegorgis, 2006).

$$\tau = \left(a_s + b_s.\frac{n}{N}\right) \quad \text{.....Eq. 47}$$

Where the default values a_s and b_s are 0.25 and 0.5 respectively (Allen et al., 1998).

4.10 Up-scaling daily fluxes to monthly actual evapotranspiration

In this study, daily ET calculations were integrated with meteorological data to upscale daily fluxes to monthly actual ET. Gokmen et al. (2012a) show that it is possible to upscale daily fluxes to monthly using the expression given in equation (48).

$$ET_{n\ daily} = ET_{daily} * (sunhours_{n\ daily}/sunhours_{daily}) \quad \text{Eq. 48}$$

Where $ET_{n\ daily}$ is ET for n days, ET_{daily} is ET calculation for a cloud free day, $sunhours_{n\ daily}$ is the cumulative sum of sunshine hours for n days, and $sunhours_{daily}$ is sunshine duration for a cloud free day. In equation (48), the sunshine term expresses the energy limiting factor whereas ET_{daily} represents the soil-moisture limiting factor because it is derived at limiting cases as given in equations 37 and 38. In this study, $ET_{n\text{-}daily}$ was for a 15-day period. However, to calculate $ET_{15\text{-}daily}$ is not mandatory as one can calculate $ET_{10\text{-}daily}$ or directly $ET_{monthly}$ depending on how often one has ET_{daily} calculations for cloud free days (Gokmen, 2011-personal communication).

Finally, monthly actual ET was calculated by summing up the 15 days ET as given in equation (49) (Gokmen et al., 2012a).

$$ET_{monthly} = ET_{15\ daily} + ET_{15\ daily} \quad \text{Eq. 49}$$

CHAPTER 5: RESULTS AND DISCUSSION

This chapter addresses the findings of this study by answering to the four objectives and the emerging sub-themes as outlined in Chapter 1**.**

5.1 The land cover types analysed for spatial-temporal consumptive water use

The land cover map of the semi-arid Barotse Sub-basin was derived from the European Space Agency (ESA) Globcover Project of 2006. According to Bicheron et al. (2008), the ESA Globcover map was generated from an automated processing chain using the 300m spatial resolution of Medium Resolution Imaging Spectrometer (MERIS). This product is accessible on http://www.esa.int/due/ionia/globcover together with the validation report. Results showed that there were ten (10) land cover types/uses in the semi-arid Barotse Sub-basin (Table 6). It was observed that closed to open shrubland covered the largest part of the study area (34.79%) whereas closed broadleaved deciduous forest occupied the smallest part (0.37 %).

Table 6: Land cover/use coverage by percentage in the semi-arid Barotse Sub-basin, South-Western Zambia (adapted from Bicheron et al., 2008)

Land cover code	Land cover type	Percentage of the sub-basin
30	Mosaic vegetation/ Cropland	20.78
50	Closed broadleaved deciduous forest	0.37
60	Open broadleaved deciduous forest	2.98
100	Closed to open mixed broadleaved and needleleaved forest	2.77
110	Mosaic forest-shrubland/Grassland	3.93
120	Mosaic grassland/Forest-shrubland	18.57
130	Closed to open shrubland	34.79
140	Closed to open grassland	14.56
180	Closed to open vegetation regularly flooded	0.77
210	Water bodies	0.48

In this study, the spatial and temporal consumptive water use by land cover type on warm-wet, cool-dry and hot-dry days were analysed based on the eight land cover types: mosaic vegetation/croplands (30), closed broadleaved deciduous forest (50), open broadleaved deciduous forest (60), mosaic grassland/forest-shrubland (120), closed to open shrubland (130), closed to open grassland (140), closed to open vegetation regularly flooded (180) and water bodies (210). This means that closed to open mixed broadleaved and needleleaved

forest (100) and mosaic forest-shrubland/grassland (110) were not considered. It was assumed that the evaporative fluxes over these could at least be inferred from the others with similar characteristics such as mosaic grassland/forest-shrubland and open broadleaved deciduous forest.

5.1.1 Accuracy assessment of the land cover map used

The extracted land cover map of the study area was validated against ground truth data that was collected during the field work campaign. Fifty-three field-points were collected in this campaign. Figure 15 shows some of the ground truth/validation points with their associated land cover type. Furthermore, sixty-five sample points were randomly selected over the study area for quality assessment. The true ground cover (reference data) for these points was obtained from a visual interpretation of very high resolution Google Earth images.

The results of the accuracy of the ESA landcover map over the semi-arid Barotse Sub-basin are shown in the contingency matrix in Table 7. The main diagonal (green) shows the number of correct points. An overall accuracy of 79.9% and kappa statistic of 74.4% were obtained. It was observed that errors were relatively higher on 'mixed' land cover. For instance, the omission and commission errors on closed to open grassland (140) were at 21.1% and 31.8% respectively. The former and latter (errors) were both at 28.6% on mosaic grassland/forest-shrubland (120). This was ascribed to fuzziness in the land cover. A fuzzy (mixed) land cover has a large spectral variability, which contributes to misclassification (Bicheron et al., 2008).

Table 7: Error matrix of the ESA Globcover-2006 land cover product over the semi-arid Barotse Sub-basin, South-Western Zambia

	Reference (field data and visually interpreted points from very high resolution Google Earth imagery)								Total No.	User`s accuracy (%)
ESA-2006 label	30	50	60	120	130	140	180	210		
30	17	0	0	0	2	2	0	0	21	81.0
50	0	7	1	0	0	0	0	0	8	87.5
60	0	1	11	0	2	0	0	0	12	91.7
120	2	0	0	10	0	0	0	0	14	71.4
130	2	0	1	2	14	1	0	0	20	70.0
140	2	0	0	2	0	15	1	2	22	68.2
180	0	0	0	0	0	1	9	1	11	81.8
210	0	0	0	0	0	0	1	9	10	90.0
Total No.	23	8	13	14	18	19	11	12	118	Accuracy: 79.9%
Producer`s accuracy	73.9	87.5	84.6	71.4	77.8	78.9	81.8	75.0		Kappa statistic: 74.4%

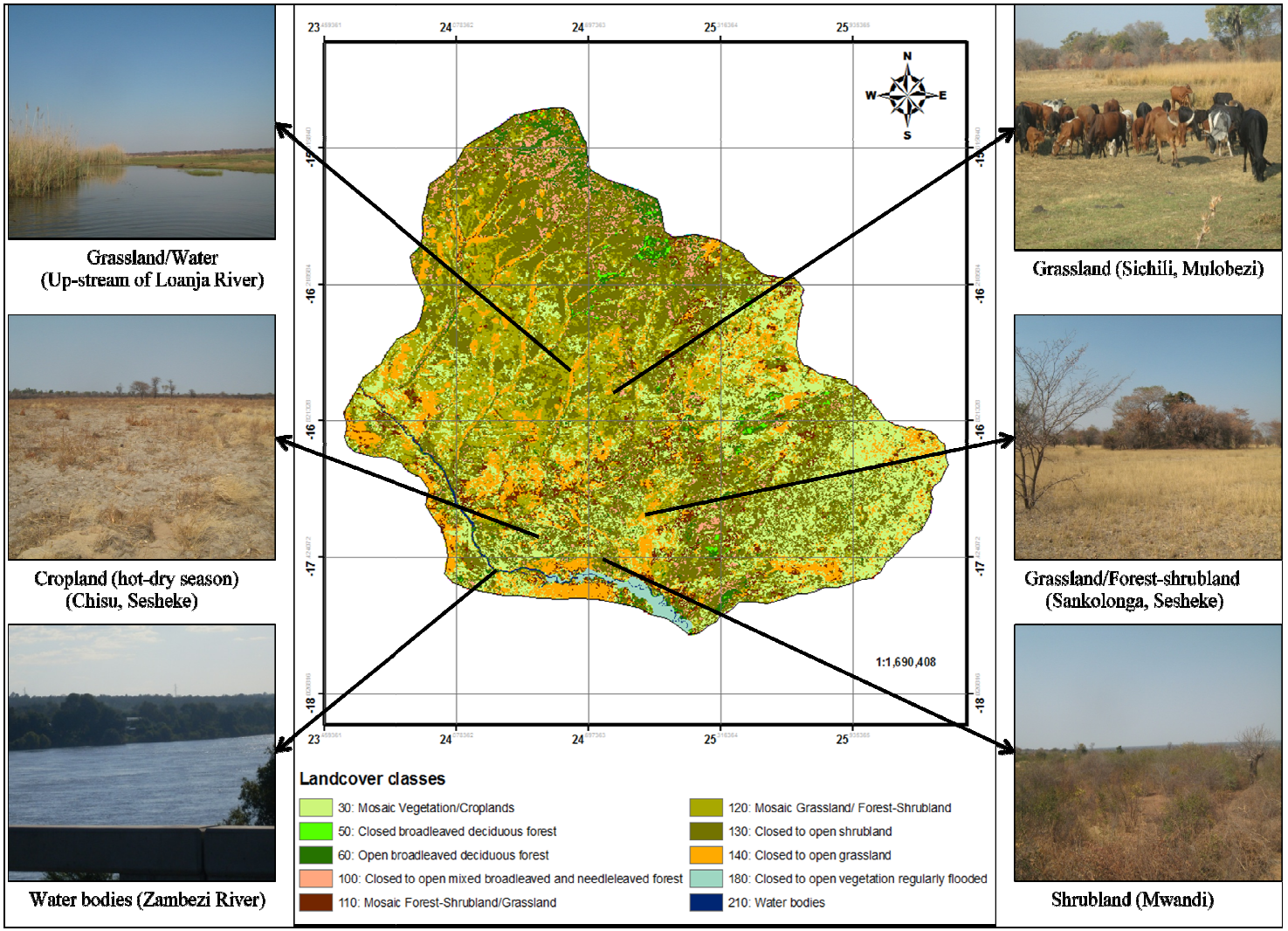

Figure 15: Land cover map showing some ground truth points in the study area (modified from Bicheron et al., 2008)

A kappa statistic of 74.4% indicated that there was good agreement between ground truth data and the ESA land cover map of the semi-arid Barotse Sub-basin. This is because it has a higher resolution (300m) compared to other coarser resolution land cover maps such as the Global Land Cover map (GLC) (2000), which has a resolution of 1 Km. This obscures certain land cover types such as the water bodies, particularly the Zambezi River (Figure 16).

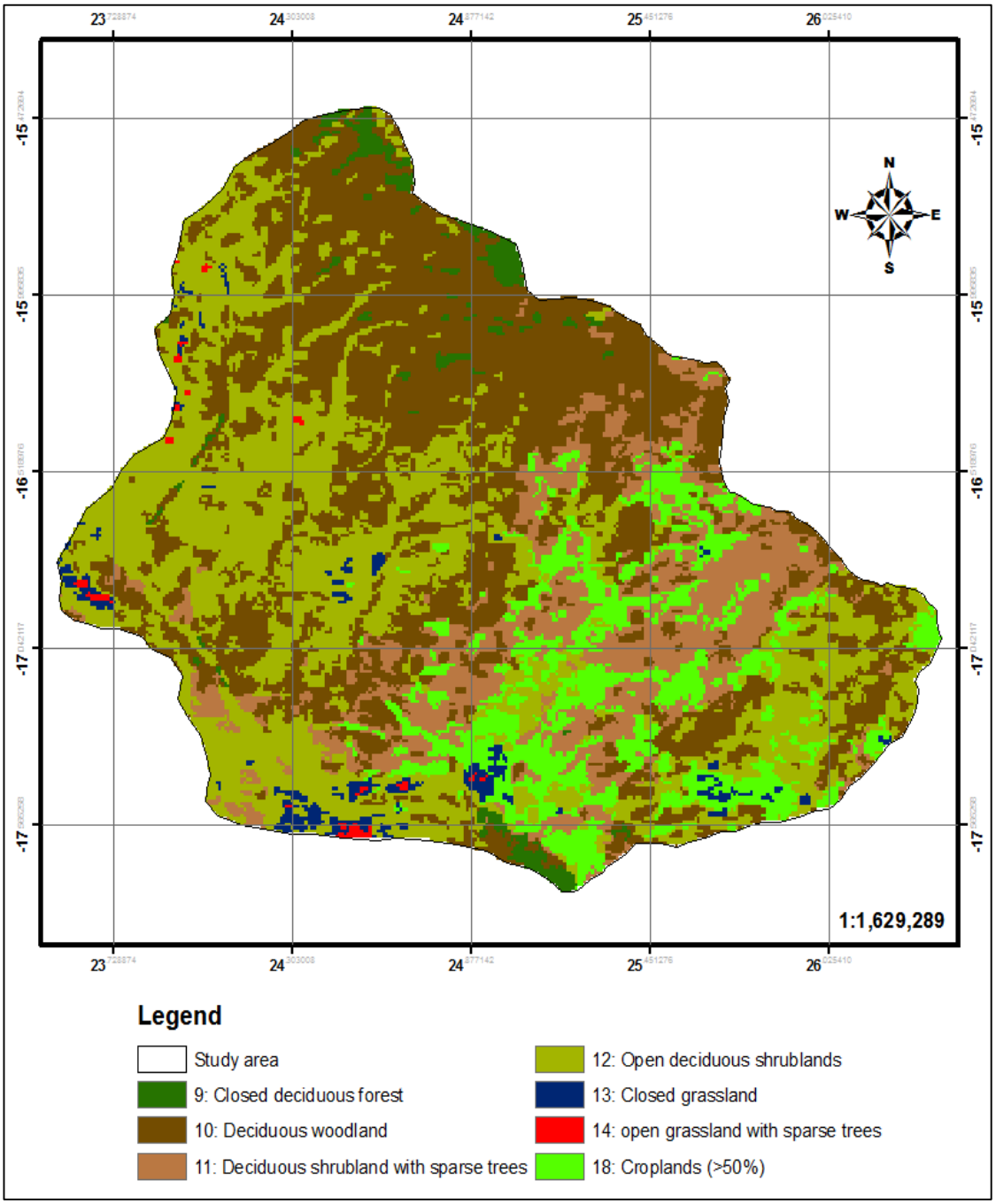

Figure 16: Land cover map of the semi-arid Barotse Sub-basin, South-Western Zambia (modified from GLC, 2000)

5.1.2 Discussion

The land cover distribution in the semi-arid Barotse Sub-basin was found to be varied (heterogeneous). This means that estimates of ET in this area cannot be accurately determined from point-based hydrometeorological equations such as the Penman (Penman, 1948), Priestly and Taylor (Priestly and Taylor, 1972) and FAO Penman-Montieth (Allen et al., 1998) or from the extremely localised lysimeters (Malone et al., 1999) as each land cover type has its own evaporative water use (Hughes, 2001; Hemakumara et al., 2003; Mu et al., 2007). Many studies, which have used remote sensing techniques of the SEBS model (Hailegorgis, 2006; Shan et al., 2007; Alvarez, 2007; Mohamed et al., 2010; Rwasoka et al., 2011) and other spatial modelling approaches such as SEBAL (Bastiaanssen et al., 1998a), S-SEBI (Roerink et al., 2000) and METRC (Allen et al., 2007), have demonstrated that different land cover types have different evaporative water use which vary over time. This is because of the differences in rooting depth, leaf area and canopy resistance which has an influence on how plants respond to the changes in environmental conditions such as water availability and temperature (Peilke, 1998; Allen et al., 1998; Boucher et al., 2004). Besides, the spatial variations in surface characteristics (topography and landcover) have a large influence on near-surface conditions such as air temperature and pressure, all of which affect the process of ET (Allen et al., 1998; Albertson et al., 2001; Su, 2002; Gibson et al., 2011). Thus, accurate estimation of ET in heterogeneous environments requires physically-based spatial modelling techniques (Su, 2002; Courault et al., 2005; Gibson et al., 2011). Given that the land cover distribution in the semi-arid Barotse Sub-basin is spatially varied, it was expected that the evaporative water use would vary over different land cover types and time.

5.2 Estimated surface fluxes by land cover type on warm-wet days

The average estimates of AET and surface parameters per land cover type on warm-wet days over the study area are shown in Table 8. Water bodies (210) and closed to open regularly flooded vegetation (180) had higher evaporative rates of ~6.9 and 5.9 mm day^{-1} respectively. This was due to the influence of lower albedo, which controls the net solar radiation available at the surface (cf. Alvarez, 2007). On the other hand, high rates of ET over closed broadleaved deciduous forest (50), open broadleaved deciduous forest (60) and other forested areas were associated with high photosynthetic activity and soil moisture as evidenced by the high NDVI values (cf. Pelke, 1998; Törnros, 2010). The overall histogram distribution of NDVI on different days over the semi-arid Barotse Sub-basin is shown in Appendix 4. Lower

evaporative fluxes occurred on mosaic vegetation/croplands (30) and closed to open grassland (140) due to the combined effect of high albedo and low NDVI values (Table 8) (cf. Boucher et al., 2004; Alvarez, 2007).

Table 8: Average estimates of evapotranspiration and surface parameters by land cover on warm-wet days in the semi-arid Barotse Sub-basin, South-Western Zambia

Land cover type (code)	Surface Albedo (-)	NDVI (-)	Z_{om} (m)	Net Radiation (Wm^{-2})	Surface Temp. (K)	Daily Actual ET ($mm\ day^{-1}$)
30	0.14	0.54	0.08	643	298	3.6
50	0.13	0.71	0.06	699	296	5.8
60	0.11	0.74	0.07	700	297	5.4
120	0.12	0.70	0.08	640	303	5.0
130	0.12	0.67	0.10	659	304	5.3
140	0.13	0.52	0.08	614	305	4.6
180	0.10	0.37	0.07	651	301	5.9
210	0.08	0.15	0.01	706	297	6.9

5.2.1 Scatter of mean AET per land cover class on warm-wet days

The scatter of mean AET per land cover type on warm-wet days is shown in Figure 17. Higher rates of ET occurred over water bodies (210) and closed to open regularly flooded vegetation (180). The maximum mean rates over these surfaces were 7.8 and 7.0 mm day^{-1} respectively. The flux rates over closed broadleaved deciduous forest (50), open broadleaved deciduous forest (60), mosaic grassland/forest-shrubland (120) and closed to open shrubland (130) were in the region of 3.7 to 6.7 mm day^{-1}. Lower mean values of between 1.2 and 5.8 mm day^{-1} occurred over mosaic vegetation/croplands (30) and closed to open grassland (140). It was observed that ET increased from DOY 325 (21st November) to DOY 14 (14th January) on most of the land surfaces. The highest rates of ET occurred on DOY 12 and DOY 14 (Figure 17). It is established that over 90 percent of rainfall in the study area falls between November and March and reach the peak in January (ZMD, 1992). Thus, the observed higher evaporative fluxes on warm-wet days appeared to occur contemporaneously with the increase in the occurrence of rainfall events over the semi-arid Barotse Sub-basin.

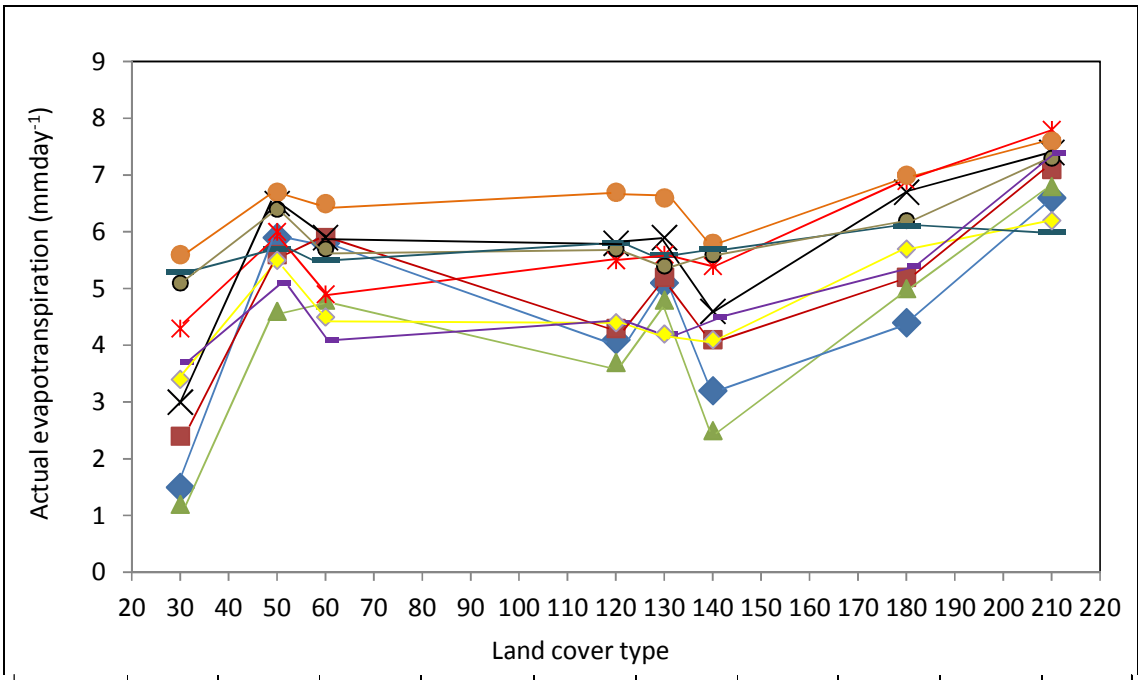

LAND COVER TYPE	DOY 325 2006	DOY 334 2006	DOY 336 2006	DOY 338 2006	DOY 12 2007	DOY 14 2007	DOY 45 2007	DOY 49 2007	DOY 71 2007	DOY 74 2007
30	1.5	2.4	1.2	3.0	4.3	5.6	5.1	3.7	5.3	3.4
50	5.9	5.6	4.6	6.5	6.0	6.7	6.4	5.1	5.7	5.5
60	5.8	5.9	4.8	5.9	4.9	6.5	5.7	4.1	5.5	4.5
120	4.1	4.3	3.7	5.8	5.5	6.7	5.7	4.4	5.8	4.4
130	5.1	5.2	4.8	5.9	5.6	6.6	5.4	4.2	5.6	4.2
140	3.2	4.1	2.5	4.6	5.4	5.8	5.6	4.5	5.7	4.1
180	4.4	5.2	5.0	6.7	6.9	7.0	6.2	5.4	6.1	5.7
210	6.6	7.1	6.8	7.4	7.8	7.6	7.3	7.4	6.0	6.2

Figure 17: Scatter of mean estimates of actual evapotranspiration per land cover type on warm-wet days over the semi-arid Barotse Sub-basin, South-Western Zambia

5.2.2 Discussion

The scatter of AET observed on warm-wet days (Figure 17) revealed salient evaporative water use by different land cover types over the semi-arid Barotse Sub-basin. Higher evaporative rates over water bodies, closed to open regularly flooded vegetation and forested areas were attributed to availability of moisture and increased energy at the surface (cf. Hailegorgis, 2006). It is shown in Table 8 that NDVI and net radiation values were very high on warm-wet days. The former (NDVI) is closely related to soil moisture availability in semi-arid environments (Knorr and Schulz, 2001; Ogunbadewa, 2010; Törnros, 2010). Furthermore, from the energy balance at limiting cases, it is known that high rates of ET are

physically possible when soil moisture is relatively high (Su, 2002). It is also known that ET is mainly limited by soil moisture availability rather than atmospheric demand in semi-arid regions (Gokmen et al., 2012b). This means that increased soil moisture content on warm-wet days coupled with high energy at the surface triggered the observed high rates of ET over the semi-arid Barotse Sub-basin.

The flux rate by land cover found in this study (Figure 17; Table 8) are comparable to the findings of Rwasoka et al. (2011) who carried out a similar study in the Upper Manyame catchment in Zimbabwe. They found the ET rates per land cover type on DOY 314-2003, which in the context of the present study is a warm-wet day, were as follows: water bodies (6.3 mm day^{-1}), closed broadleaved deciduous forest (6.0 mm day^{-1}), open broadleaved deciduous forest (5.7 mm day^{-1}), closed to open grassland (3.7 mm day^{-1}), mosaic grassland/forest-shrubland (4.6 mm day^{-1}), closed to open shrubland (4.7 mm day^{-1}), mosaic vegetation/cropland (4.2 mm day^{-1}). These findings are similar to the ones observed in this study. This was ascribed to similarity in climatic pattern as the semi-arid Barotse Sub-basin and Upper Manyame catchment are located within the Zambezi Basin in close proximity.

Kabo-bah et al. (2011), who studied hyper-temporal ET over the middle Zambezi using GEONETCAST and SEBS found high rates of ET on DOY11 and DOY 80. Although they were not studying any particular land cover evaporative behaviour, they found that the mean rates of ET on these two days were ~6.1 and 5.9 mm day^{-1} respectively. These values are similar to the ET rates observed on warm-wet days in this study. This was ascribed to the fact that the middle Zambezi Basin has a semi-arid climatic pattern that is similar to the semi-arid Barotse Sub-basin. Furthermore, Shan et al. (2007), who studied regional ET over the arid Heihe River Basin in North-West China also found that daily ET increased significantly in summer, a period almost similar to the warm-wet days. However, the comparison of ET rates to the ones found in this study is difficult to make because of the differences in environments.

The rate of ET observed over water bodies are similar to the findings of Alvarez (2007) who studied the effect of land cover changes on water balance of the Palo Verde wetland in Costa Rica, Central America. He found that evaporation over water was as high as 6.3 mm day^{-1} on DOY 75. This is very similar to the findings of this study, especially on DOY 71 and DOY 74 (Figure 17).

5.3 Estimated surface fluxes by land cover type on cool-dry days

The average estimates of AET and biogeophysical parameters by land cover type on cool-dry days are shown in Table 9. Water bodies (210) and closed broadleaved deciduous forest (50) had higher evaporative rates of ~5.0 and 4.8 mm day^{-1} respectively. The fluxes over open broadleaved deciduous forest (60), mosaic grassland/forest-shrubland (120) and closed to open regularly flooded vegetation (180) ranged from 4.0 to 4.4 mm day^{-1}. Lower rates occurred over closed to open grassland (140) and mosaic vegetation/croplands (30).

Table 9: Average estimates of evapotranspiration and surface parameters by land cover on cool-dry days in the semi-arid Barotse Sub-basin, South-Western Zambia

Land cover type (code)	Surface Albedo* (-)	NDVI* (-)	Z_{om}* (m)	Net Radiation (Wm^{-2})	Surface Temp. (K)	Daily Actual ET (mm day^{-1})
30	0.08	0.64	0.06	436	297	1.8
50	0.05	0.90	0.04	477	294	4.8
60	0.04	0.87	0.05	478	295	4.4
120	0.07	0.73	0.07	439	300	4.0
130	0.07	0.77	0.05	443	298	3.1
140	0.09	0.59	0.07	426	298	2.1
180	0.05	0.86	0.04	472	295	4.4
210	0.02	0.00	0.00	475	293	5.0

Asterisk* means the average exclude values for days in July

5.3.1The Scatter of mean AET per land cover type on cool-dry days

The scatter of mean AET per land cover type on cool-dry days is shown in Figure 18. The mean evaporative water use of mosaic grassland/forest-shrubland (120) and closed to open shrubland (130) varied from 1.2 to 5.9 mm day^{-1}. It was also observed that the mean fluxes over closed to open grassland (140) and mosaic vegetation/croplands (30) were varied, generally ranging from 0.3 to 4.6 mm day^{-1}. On the other hand, the mean evaporative rates over water bodies (210) and closed broadleaved deciduous forest (50) were higher. They ranged from 4.0 to 6.8 mm day^{-1}. High evaporative rates were also observed over open broadleaved deciduous forest (60) and closed to open regularly flooded vegetation (180).

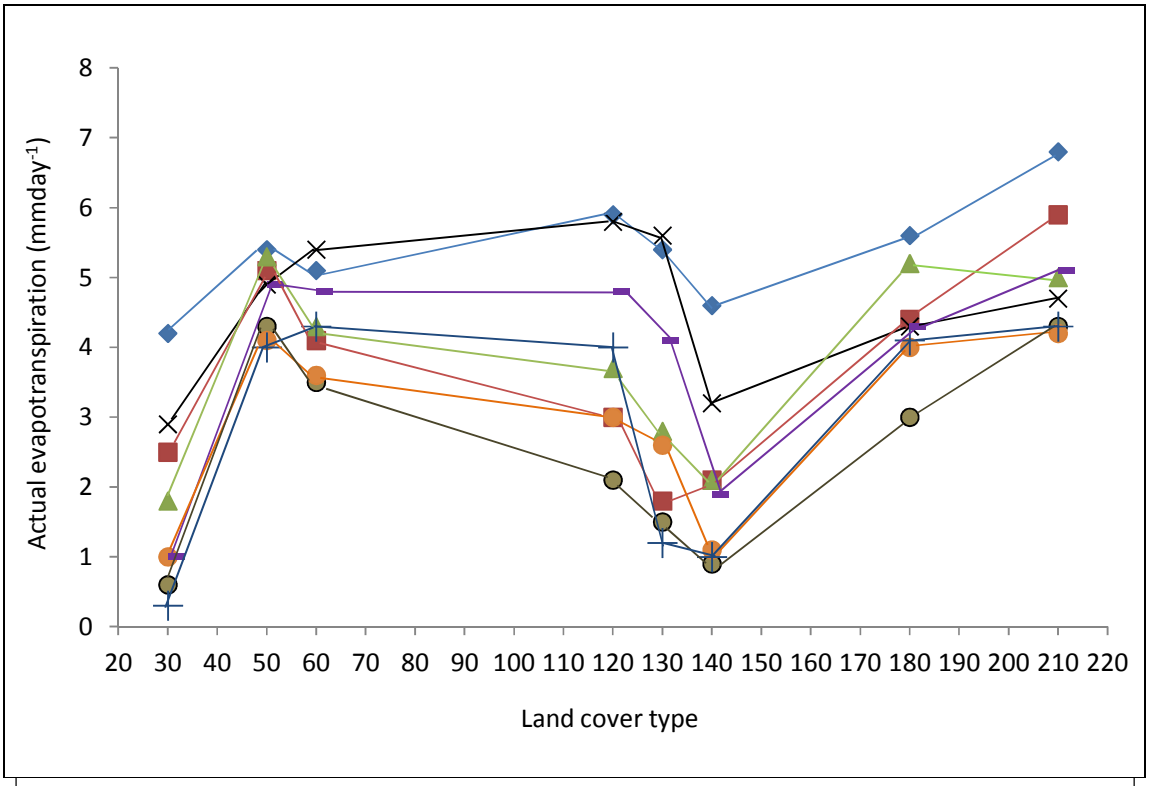

LAND COVER TYPE	DOY 106 2007	DOY 113 2007	DOY 136 2007	DOY 143 2007	DOY 168 2007	DOY 170 2007	DOY 191 2007	DOY 197 2007
30	4.2	2.5	1.8	2.9	0.6	1.0	0.3	1.0
50	5.4	5.1	5.3	4.9	4.3	4.1	4.0	4.9
60	5.1	4.1	4.3	5.4	3.5	3.6	4.3	4.8
120	5.9	3.0	3.7	5.8	2.1	3.0	4.0	4.8
130	5.4	1.8	2.8	5.6	1.5	2.6	1.2	4.1
140	4.6	2.1	2.1	3.2	0.9	1.1	1.0	1.9
180	5.6	4.4	5.2	4.3	3.0	4.0	4.1	4.3
210	6.8	5.9	5.0	4.7	4.3	4.2	4.3	5.1

Figure 18: Scatter of mean estimates of actual evapotranspiration per land type class on cool-dry days over the semi-arid Barotse Sub-basin, South-Western Zambia

5.3.2 Discussion

The general evaporative behaviour by land cover type on cool-dry days (Figure 18) indicated that ET decreased between DOY 106 and DOY 197. This was ascribed to declining soil water and reduction of energy at the surface. The major soils in the semi-arid Barotse Sub-basin are the arenosols (FAO and GRZ, 1986). These arid soils are characterised by a sandy texture and excessive drainage (MEWD-JICA, 1995). Consequently, soil water decreases soon after the rain season because of deep percolation over such areas. This was partly responsible for

the declining trend in evaporative fluxes over the land (cf. Suleiman and Richie, 2003). The reduction in the energy available at the surface is associated with the cold season (cf. Allen et al., 1998). It was found that higher fluxes remained over water bodies and closed to open regularly flooded vegetation due to the availability of moisture. Lower evaporative rates over closed to open grassland and mosaic vegetation/cropland were due to declining soil moisture. Furthermore**,** lower rates of ET over cropland were also ascribed to the harvesting of rain-fed crops. Actual ET, particularly transpiration, is expected to be lower over cropland after the harvest unless the soil contains moisture to support evaporation. These findings are supported by Shan et al. (2007) who found that ET over cropland was distinctly lower after the harvest.

The average evaporative rates found on cool-dry days in this study (Table 9) are comparable to the findings of Kabo-bah et al. (2011). In their study, they found that the average flux rate on DOY 165 was ~4.6 mm day^{-1}. Although this value is not associated with the evaporative water use of a specific land cover, it compares well with the ET rates of some of the land cover types observed in this study (Table 9, Figure 18).

5.4 Estimated surface fluxes by land cover type on hot-dry days

The average estimates of AET and land surface parameters on hot-dry days are shown in Table 10. It was observed that the rate of ET over mosaic vegetation/croplands (30) and closed to open grasslands (140) was very low due to the influence of drier conditions. This was evident from the lower NDVI (Table 10) and higher surface temperatures (cf. Alvarez, 2007). On the other hand, the average evaporative rates were higher over water bodies (210) and closed to open regularly flooded vegetation (180) due to the availability of moisture. The surface temperatures on these surfaces were lower. It was found that the average fluxes over forested areas such as broadleaved deciduous forest (50) and open broadleaved deciduous forest (60) ranged from moderate to high. Over these forested surfaces, ET fluxes tended to be high with the increase in the NDVI value (Table 10) and at variance with surface temperatures (cf. Jackson et al., 1977; Moran et al., 1994; Carlson et al., 1995).

Table 10: Average estimates of evapotranspiration and surface parameters by land cover on hot-dry days in the semi-arid Barotse Sub-basin, South-Western Zambia

Land cover Type	Surface Albedo (-)	NDVI (-)	Z_{om} (m)	Net Radiation (Wm^{-2})	Surface Temp. (K)	Daily Actual ET ($mmday^{-1}$)
30	0.12	0.35	0.09	465	308	1.1
50	0.08	0.73	0.06	524	301	3.9
60	0.07	0.70	0.06	551	300	3.6
120	0.13	0.48	0.09	458	310	3.5
130	0.11	0.56	0.08	454	309	3.0
140	0.11	0.41	0.09	455	310	1.3
180	0.09	0.66	0.07	493	305	4.6
210	0.04	0.12	0.00	550	300	6.7

5.4.1The scatter of mean AET per land cover type on hot-dry days

The scatter of evaporative fluxes on hot-dry days per land cover type is shown in Figure 19. It was observed that closed to open grasslands (140) and mosaic vegetation/croplands (30) had lower mean values of ET which ranged from 0.8 to 2.2 mm day^{-1}. On the other hand, higher mean values were observed over water bodies (210) and open regularly flooded vegetation (180). The mean maximum values on these surfaces were 7.7 and 5.6 mm day^{-1} respectively. The mean flux rates over closed broadleaved deciduous forest (50), open broadleaved deciduous forest (60), mosaic grassland/ forest-shrubland (120) and closed to open shrubland (130) varied in the region of 2.4 to 4.7 mm day^{-1}.

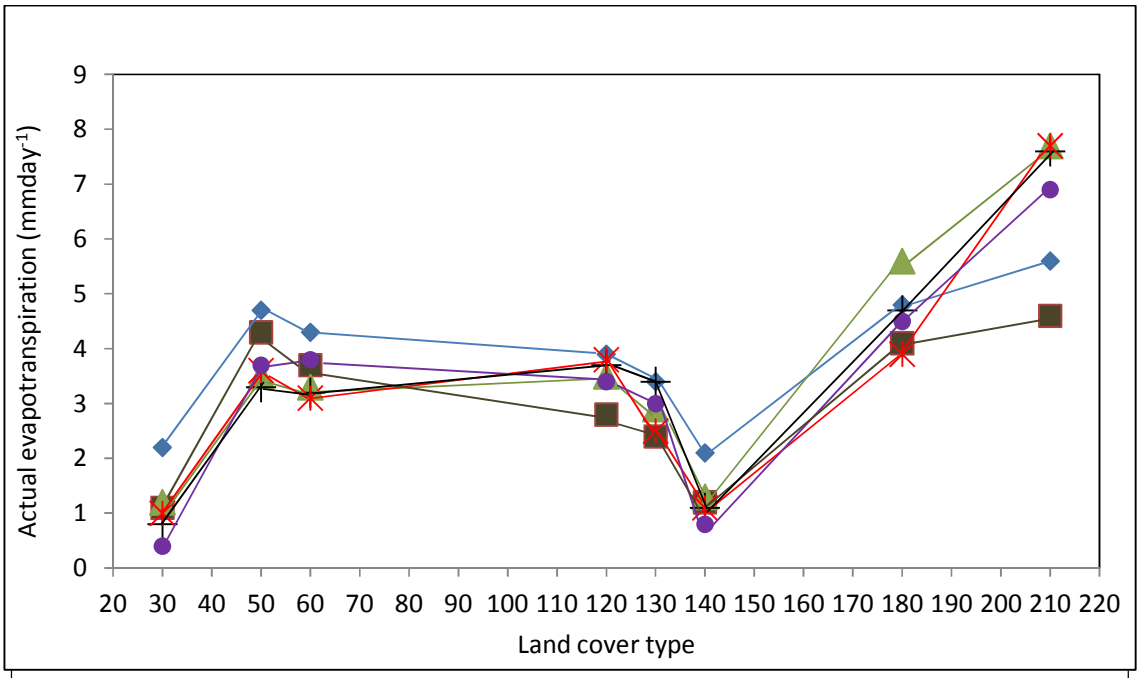

LAND COVER TYPE	DOY 225 2007	DOY 232 2007	DOY 255 2007	DOY 257 2007	DOY 287 2007	DOY 292 2007
30	2.2	1.1	1.2	0.8	1.0	0.4
50	4.7	4.3	3.5	3.3	3.6	3.7
60	4.3	3.7	3.3	3.2	3.1	3.8
120	3.9	2.8	3.5	3.7	3.8	3.4
130	3.4	2.4	2.9	3.4	2.5	3.0
140	2.1	1.2	1.3	1.1	1.1	0.8
180	4.8	4.1	5.6	4.7	3.9	4.5
210	5.6	4.6	7.7	7.6	7.7	6.9

Figure 19: Scatter of mean estimates of actual evapotranspiration per land cover type on hot-dry days over the semi-arid Barotse Sub-basin, South-Western Zambia

5.4.2 Discussion

The distribution of mean evaporative fluxes on hot-dry days (Figure 19) indicated that they were strongly influenced by land cover heterogeneity and spatial variability of soil moisture over the semi-arid Barotse Sub-basin (cf. Suleiman and Richie, 2003). For this reason, it was observed that evaporative rates were higher over water bodies (210) as moisture is readily available on these surfaces. On the other hand, ET was very low over mosaic vegetation/cropland (30) and closed to open grassland (140) because of the restrictions imposed by soil moisture in the dry season. As already noted, the major soil type in the study

area is the arenosols. Therefore, lower moisture conditions in the dry season are characteristic in semi-arid Barotse Sub-basin because of the poor retention capacity of the soils. This means that plant species with shallow roots such as closed to open grassland and rainfed crops dry out or transpire at a reduced rate in the dry season. Moreover, grassland and shrubland areas are laid bare as a result of bush-burning in the dry season, usually between August and October. This is a common practice in the Savanna-Miombo Woodlands (Archer, 1971; Hutchinson, 1974; Scholes et al., 1996; Aregheore, 2006; Desanker et al., 2007). Thus, ET is expected to be very low over grassland and cropland during this time. These findings are supported by Mohamed et al. (2010) who found that burnt areas in the Mkindo Catchment in Tanzania had low evaporative rates.

The evaporative fluxes found in this study (Table 10, Figure 19) are also similar to the study by Rwasoka et al. (2011), whose findings on DOY 285-2005, which in the context of present study is a hot-dry day, were as follows: water bodies (4.7 mm day^{-1}), closed broadleaved deciduous forest (3.2 mm day^{-1}), open broadleaved deciduous forest (2.4 mm day^{-1}), mosaic grassland/forest-shrubland (1.5 mm day^{-1}), closed to open shrubland (1.4 mmday^{-1}), closed to open grassland (1.3 mm day^{-1}), and mosaic vegetation/cropland (1.4 mm day^{-1}). The rate of ET over closed to open grassland and mosaic vegetation/cropland are very similar to this study. However, there are small differences in the rate of ET over water bodies and forested land areas. This was ascribed to uncertainties associated with surface parametrisation and input data as discussed in section 5.12

5.5 Evaporative fluxes by land cover type between warm-wet and cool-dry days

The average evaporative fluxes per land cover type between warm-wet and cool-dry days is shown in Figure 20. The percentage decrease in evaporative rate per land cover type between these days is indicated by a downward facing arrow and vice versa. It was observed that the average evaporative water use by land cover type had reduced by 12 to 54.3% between warm-wet and cool-dry days (Figure 20). The rate of ET over mosaic grassland/forest-shrubland (120) and closed broadleaved deciduous forest (50) declined minimally by 12.0 and 17.2% respectively. Over open broadleaved deciduous forest (60), closed to open regularly flooded vegetation (180) and water bodies (210), the rate of ET declined moderately by 18.5, 23.7 and 27.5% respectively. On the other hand, the evaporative rates over mosaic

vegetation/croplands (30) and closed to open grassland (140) declined substantially by 50.0 and 54.3% respectively (Figure 20).

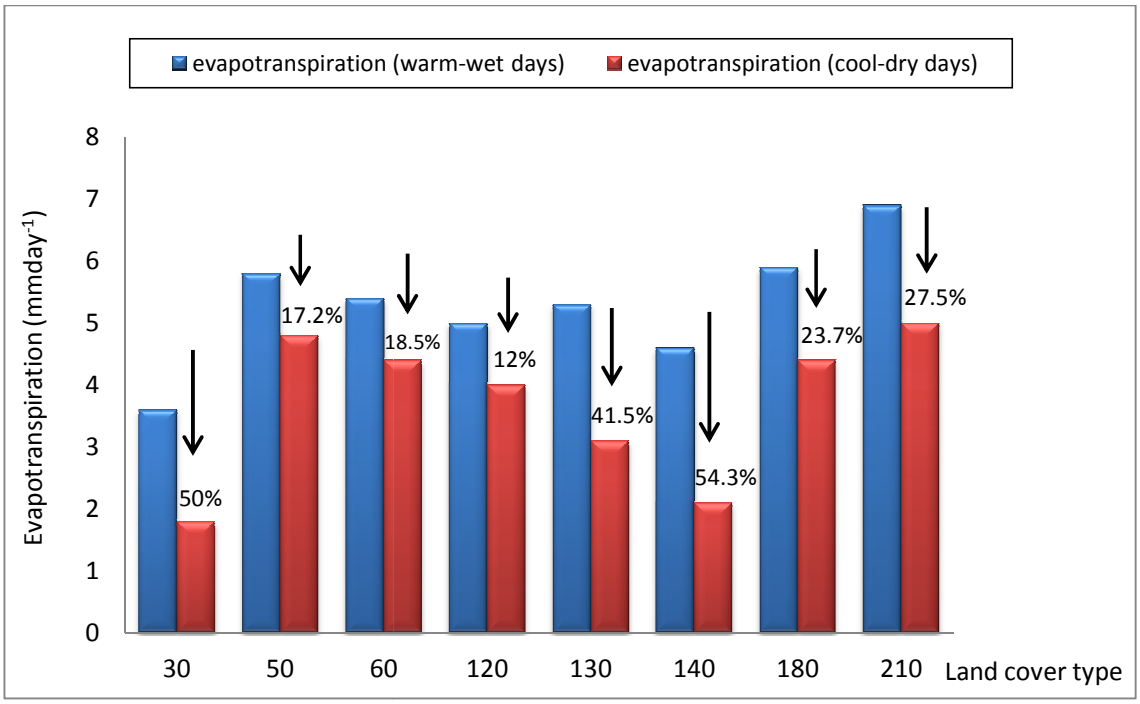

Figure 20: Variation of actual evapotranspiration by land cover type between warm-wet and cool-dry days in the semi-arid Barotse Sub-basin, South-Western Zambia

The evaporative fluxes per land cover type between warm-wet and cool-dry days over the semi-arid Barotse sub-basin, which are shown in Figure 20 above, are inferred from the distribution of ET on some representative days. To begin with, the distribution of AET for a warm-wet day (DOY 74; 15th March, 2007) is presented in Figure 21. On this day, ET ranged from 1.9 to 7.1 mm day^{-1}. The values were very high over water bodies and wetter surfaces (5.0 - 7.1 mm day^{-1}). Higher rates also occurred over forests (3.0 to 6.0 mm day^{-1}). Closed to open grassland and mosaic vegetation/cropland had lower rates (1.9 - 3.9 mm day^{-1}). On the other hand, Figure 22 shows AET on a cool-dry day (DOY 170; 19th June, 2007). The ET values on this day were generally lower (0.8-4.8 mm day^{-1}) than those on DOY 74 shown in Figure 21. This was attributed to reduced energy and declining soil moisture at the surface, which is associated with cool-dry seasons. The effect of declining soil moisture was inferred from the changes in ET over croplands, which are located in the south-western part of the study area.

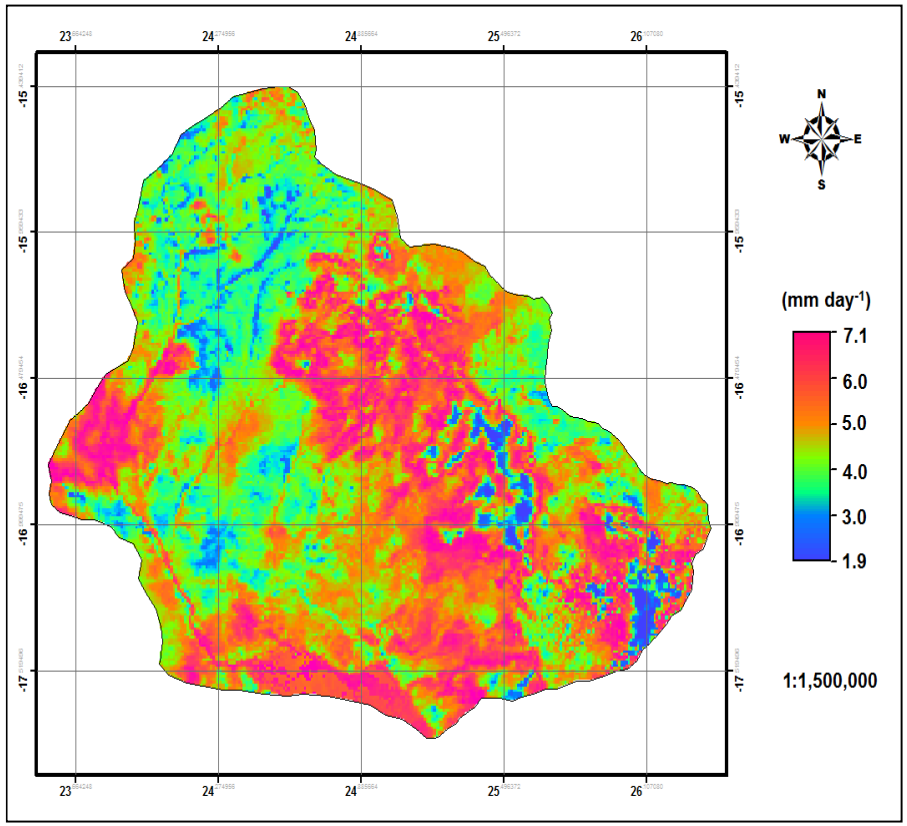

Figure 21: The spatial distribution of SEBS modelled actual evapotranspiration on a warm-wet day (DOY 74) over the semi-arid Barotse Sub-basin, South-Western Zambia

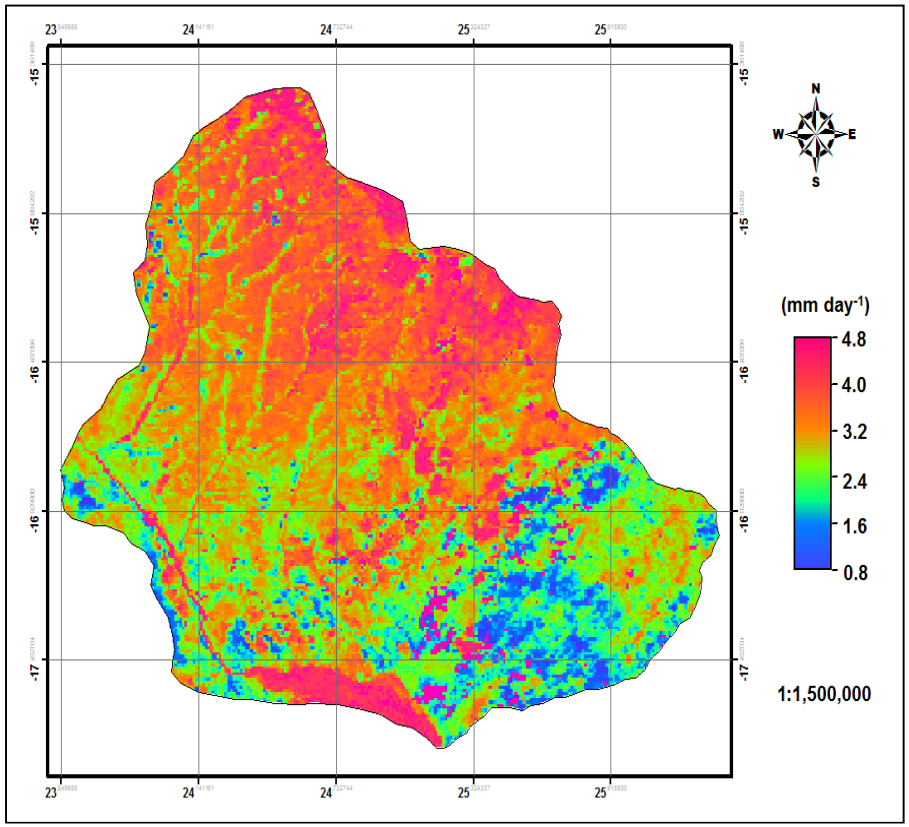

Figure 22: The spatial distribution of SEBS modelled actual evapotranspiration on a cool-dry day (DOY 170) over the semi-arid Barotse Sub-basin, South-Western Zambia

These areas (mosaic vegetation/croplands) were expected to have lower rates of ET as the rain-fed crops, such as maize, would have been harvested by June and the ground exposed to atmospheric forces which basically dries out the soil. The dominant process on such areas is expected to be evaporation than transpiration (cf. Shuttleworth and Wallace, 1985; Shan et al., 2007). If soil moisture is limited, however, evaporation occurs at a very low rate over such places. This is why the rate of ET over these surfaces was lower than that over water bodies and forested areas.

The spatial-temporal changes in the evaporative water use per land cover type between warm-wet and cool-dry days, which are depicted in Figure 20, represent the differences by which these land cover types in the semi-arid Barotse Sub-basin respond to the changing factors controlling ET, especially soil moisture, atmospheric condition and net solar radiation. In this regard, physiological features such as rooting depth, leaf area and stomata resistance play an important role in determining how plant species respond to these factors (Brutsaert, 1982; Peilke, 1998; Allen et al., 1998).

Thus, it was observed that the evaporative water use over closed broadleaved deciduous forests (50), mosaic grassland/forest-shrubland (120) and open broadleaved deciduous forest (60) decreased marginally between warm-wet and cool-dry days. It was, however, expected that these plant species would have a significant reduction in the rate of ET because of the declining soil moisture. This was ascribed to the ability of these plants to tap water at some depth compared to other species such as grass and maize (cf. Aregheore, 2006). It is known that latent heat fluxes (predominantly evaporative fluxes) are usually larger over forests than on short vegetation due to deeper rooting, greater transpiring leaf area, and increased roughness (Peilke, 1998). In other words, forests have a greater latent heat flux relative to sensible heat flux (lower Bowen ratio) than grasslands (Boucher et al., 2004). However, Suleiman and Richie (2003) and Boucher et al. (2004) note that cropland can also have higher latent flux relative to sensible heat flux due to irrigation of crops. Irrigation schemes are non-existent in the semi-arid Barotse Sub-basin. This was why the variation of ET over closed to open grassland and mosaic vegetation/cropland was higher between the warm-wet and cool-dry days.

The decrease in the rate of ET over water bodies (210) and closed to open regularly flooded vegetation (180) was ascribed to reduced energy at the surface. These surfaces experienced a

decline in the rate of ET despite having readily available moisture between warm-wet and cool-dry days. This implied that the available energy at the surface was reduced in response to the low peak in solar radiation in the cold season (cf. Vogt and Niemeyer, 2001).

5.6 Evaporative fluxes by land cover type between warm-wet and hot-dry days

The variation in the consumptive water use per land cover type between warm-wet and hot-dry days is shown in Figure 23. It was observed that the spatial-temporal variation in the evaporative water use by land cover type between warm-wet and hot-dry days was high over mosaic vegetation/cropland (30) and closed to open grassland (140). The average evaporative flux rate of the former was found to have declined by 69.4 % whereas that of the latter was lowered by 71.7 % between warm-wet and hot-dry days. The decline in rate of ET over forested areas ranged from 30 to 43.4% over these days. On the other hand, evaporative fluxes over water bodies (210) and closed to open regularly flooded vegetation (180) declined marginally by 2.9 and 22.0% respectively (Figure 23).

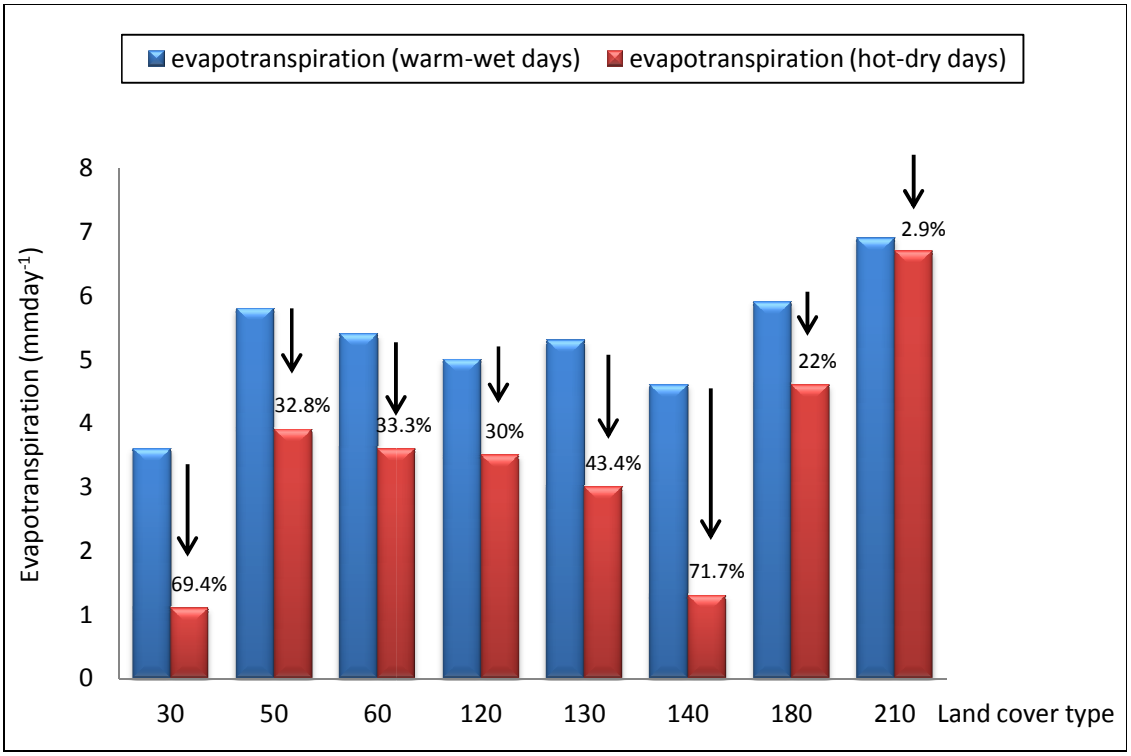

Figure 23: Variation of actual evapotranspiration by land cover type between warm-wet and hot-dry days in the semi-arid Barotse Sub-basin, South-Western Zambia

The fluxes in the consumptive water use by land cover type between warm-wet and hot-dry days shown in Figure 23 are depicted by the spatial and temporal variation of AET on some representative days (Figure 24 and 25). The distribution of AET on a warm-wet day (DOY 49; 18th February, 2007) is presented in Figure 24. On this day ET was high over the larger part of the basin. This was ascribed to increased soil moisture as it was in the rain season. The middle and southern parts of the study area had higher rates of ET ranging from 4.5 to 6.7 mm day^{-1}. These areas are covered by a mosaic forests, water bodies and wetter surfaces. Lower rates ET rates were observed in the upper north and south-eastern parts of study area (Figure 24). The distribution of AET on a hot-dry day (DOY 287; 14th October, 2007), on the other hand, is presented in Figure 25. On this day, places in the south and south eastern parts of the basin had lower evaporative rates. These areas are predominantly covered by mosaic vegetation/croplands and closed to open grasslands. Thus, the major flux areas were found to be over forests in the northern parts and water bodies in the south to south-western parts of the basin. The ET rates were very high over water bodies. This was attributed to high energy at the surface during the hot season. The relatively high energy intensified ET over water bodies so that the rates were in the region of 4.6 to 7.7 mm day^{-1}.

The spatial-temporal variations in the consumptive water use between warm-wet and hot-dry days (e.g Figures 24 and 25) and by land cover type (Figures 23) indicated the adaptive mechanism by which different plant species respond to fluctuations in soil water content. For this reason, evaporative fluxes over water bodies did not vary significantly as moisture and energy was readily available over these surfaces between warm-wet and hot-dry days (cf. Suleiman and Richie, 2003). On the other hand, the high variation in ET over mosaic vegetation/croplands and closed to open grassland was attributed to declined soil moisture. The decline in ET over these surfaces was very high as grasses and rainfed crops are less adapted to tap water from significant depths compared to plant species such as closed broadleaved deciduous forest, open broadleaved deciduous forests and closed to open shrubland forests when soil moisture declines in the dry season (cf. Jeanes, 1991; Peilke, 1998; Rwasoka et al., 2011). Furthermore, as already noted, the effect of bush burning between August and October contributes to dryness over shrublands, grasslands and croplands. This explains why evaporative fluxes over these surfaces were very variable between warm-wet and hot-dry days compared to forested areas.

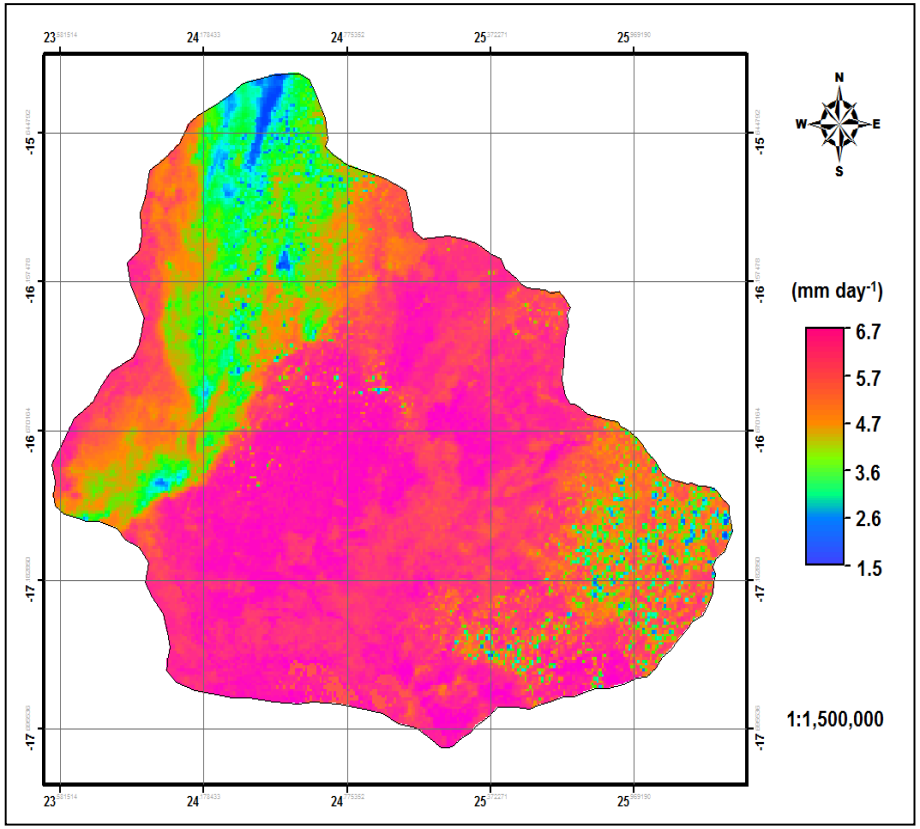

Figure 24: The spatial distribution of SEBS modelled actual evapotranspiration on a warm-wet day (DOY 49) over the semi-arid Barotse Sub-basin, South-Western Zambia

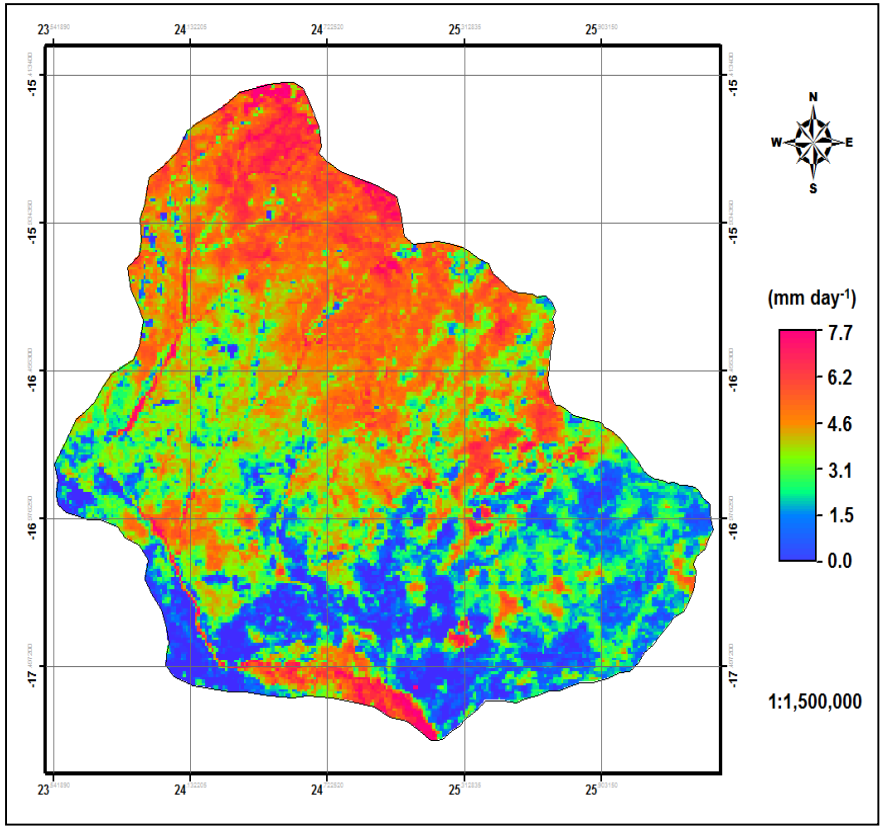

Figure 25: The spatial distribution of SEBS modelled actual evapotranspiration on a hot-dry day (DOY 287) over the semi-arid Barotse Sub-basin, South-Western Zambia

5.7 Evaporative fluxes by land cover type between cool-dry and hot-dry days

Figure 26 shows the variation of AET per land cover type between cool-dry and hot-dry days in the semi-arid Barotse Sub-basin. The average rates of ET on hot-dry days were ~2.2 and 34.0% greater than that observed on cool-dry days over closed to open regularly flooded vegetation (180) and water bodies (210) respectively (Figure 26). On the other hand, it was observed that the evaporative rates decreased by 38.9 and 38.1% over mosaic vegetation/cropland (30) and closed to open grassland (140) respectively. The flux rates over closed to open shrubland (130), open broadleaved deciduous forest (60) and closed broadleaved deciduous forest (50) declined minimally by 3.2, 18.2 and 18.8% respectively.

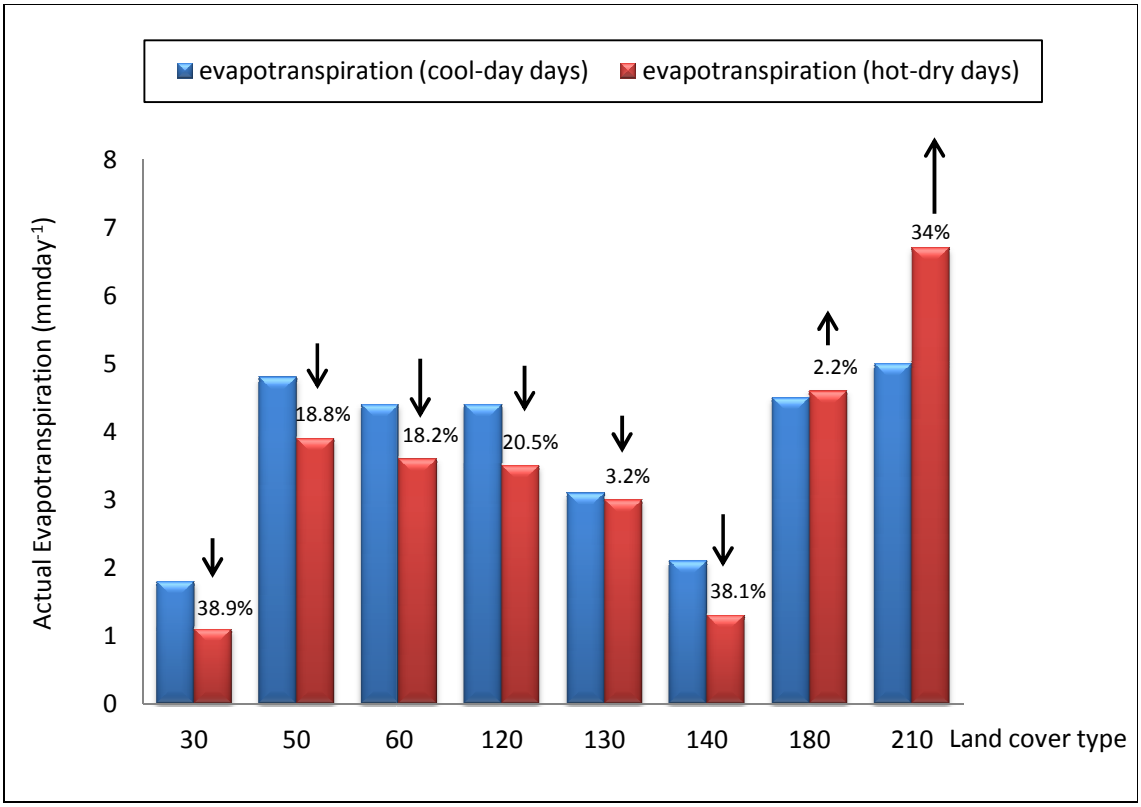

Figure 26: Variation of actual evapotranspiration by land cover type between cool-dry and hot-dry days in the semi-arid Barotse Sub-basin, South-Western Zambia

The spatial-temporal variation in the consumptive water use by land cover type on cool-dry days is distinguished from that of hot-dry days by some representative days (Figure 27 and 28). The distribution of AET on a cool-dry day (DOY 136; 16th May, 2007) is presented in Figure 27. It was observed that AET ranged from 1.3 to 5.9 mm day^{-1}. The major sources of

high fluxes on this day were over water bodies and wetter areas in the southern part of the basin, and over forested areas in the northern parts. Given that this day was not far from the end of rain season, soil moisture was still available to support the rain-fed crops. Thus, the south eastern part of the basin which holds a greater share of cropland had relatively high rate of ET. On the hand, the distribution of AET on a typical hot-dry day (DOY 257; 14th September, 2007) is presented in Figure 28. It was observed that AET was in the range of 1.1 to 8.2 mm day^{-1}. The major sources of high fluxes were confined to water bodies and closed to open regularly flooded surfaces in the southern part of the basin and the forested areas in the north. It appeared that the relatively high energy associated with the hot season intensified the rate of ET over these surfaces so that the fluxes increased to 5.4 and 8.2 mm day^{-1}. By contrast, the areas located in the south-eastern part of the basin experienced the lowest rates of ET. This was attributed to decreased soil water considering that these areas are covered mainly by croplands and grasslands which by this date (hot-dry season) would be bare or dry. Consequently, the estimated evaporative flux over these areas was very low.

The temporal variations in the consumptive water use by land cover type between cool-dry and hot-dry days (Figure 26) showed that water bodies and closed to open regularly flooded vegetation experienced an increase in the rate of evaporation. This was ascribed to increased energy at the surface between cool-dry and hot-dry season (cf. Vogt and Niemeyer, 2001). This accelerated the rate of ET over these surfaces as they possess readily available moisture. On the other hand, the rate of ET decreased over plant species in response to declining soil water. The lowest reduction in AET occurred over forests. This was ascribed to plant physiology. Trees are capable of drawing water from some depth during the transition from cool-dry to hot-dry seasons (cf. Jeanes, 1991) resulting in higher latent heat fluxes (cf. Boucher et al., 2004). Cropland and grassland areas had the highest reduction in ET as soil water declined far below the plant`s root system in the dry season (cf. Rwasoka et al., 2011). The changes in the evaporative rates over these different land cover types are depicted in Figure 27 and 28.

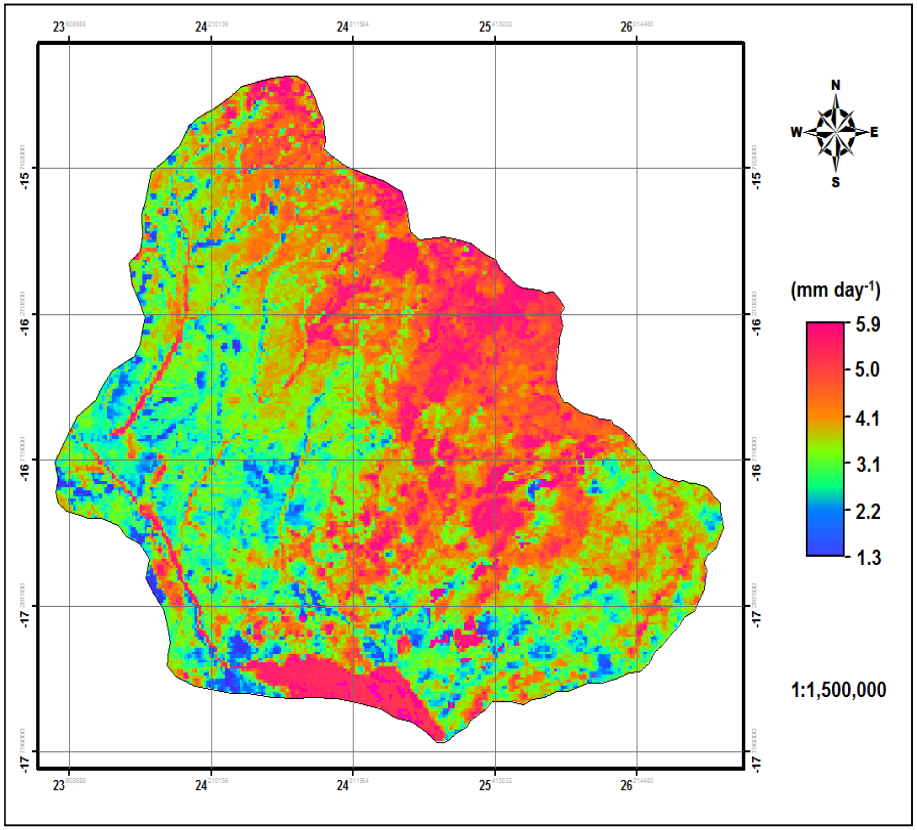

Figure 27: The spatial distribution of SEBS modelled actual evapotranspiration on a cool-dry day (DOY 136) over the semi-arid Barotse Sub-basin, South-Western Zambia

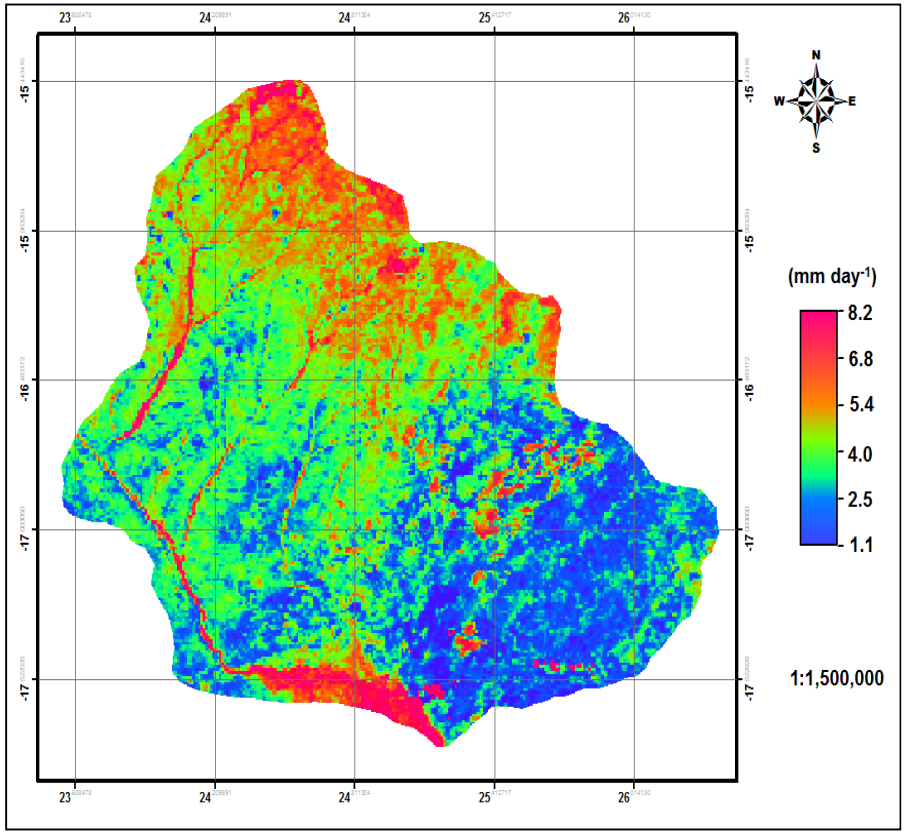

Figure 28: The spatial distribution of SEBS modelled actual evapotranspiration on a hot-dry day (DOY 257) over the semi-arid Barotse Sub-basin, South-Western Zambia

5.8 Estimated monthly actual evapotranspiration from daily fluxes and sunshine data

The modelled monthly AET over the study area for the year 2006/07 is shown in Table 11. The mean fluxes ranged from 45 to 232 mm month^{-1}. Maximum rates varied from 129 to 356 mm month^{-1}whereas the minimum ranged from Zero to 84.4 mm month^{-1}. The highest mean rate occurred in January and was also high in the other warm-wet months. In the cool-dry months (April-July), the fluxes ranged from 45 to 145 mm month^{-1}. The lowest rates occurred in the hot-dry months (August to October) and were between 56 and 78 mm month^{-1}.

Table 11: The modelled monthly actual evapotranspiration for the period 2006/07 over the semi-arid Barotse Sub-basin, South-Western Zambia

mm month^{-1}	November	December	January	February	March	April
Minimum	0.4	10.4	84.4	50.3	60.2	61.2
Maximum	276	275	304	231	272	242
Mean	137	145	232	155	126	145
	May	June	July	August	September	October
Minimum	2.6	0.0	0.0	0.0	0.0	0.0
Maximum	206	129	140	192	356	354
Mean	130	45	109	56	69	78

Distributed AET is presented for some months to illustrate its variability at a monthly time step. To begin with, AET for November is shown in Figure 29. The fluxes were higher in the northern and north-eastern areas than in the south-western parts. This distribution reflects the differences in evaporative water use by different land cover types and variability of soil moisture. The northern part receives relatively higher rainfall than areas to the south and is mainly covered by forests. The southern-western part is occupied by mosaic grassland/forest-shrubland and closed to open grassland which tends to transpire less than broadleaved and open broadleaved deciduous forest because of physiological differences such as rooting depth (cf. Boucher et al., 2004). Figure 30, on the other hand, depicts the distribution of AET in January, which is the peak period of the rain season in the study area. The fluxes were very high over the larger part of basin. This was ascribed to increased soil moisture and blooming of many plant species, which is characteristic of semi-arid areas in the rain season (Jeanes, 1991). Consequently, ET increased even in areas (eg. closed to open grasslands) that showed low values in the month of November. The highest rates (200-300 mm month^{-1}), however, were observed over water bodies, regularly flooded vegetation and other wet surfaces.

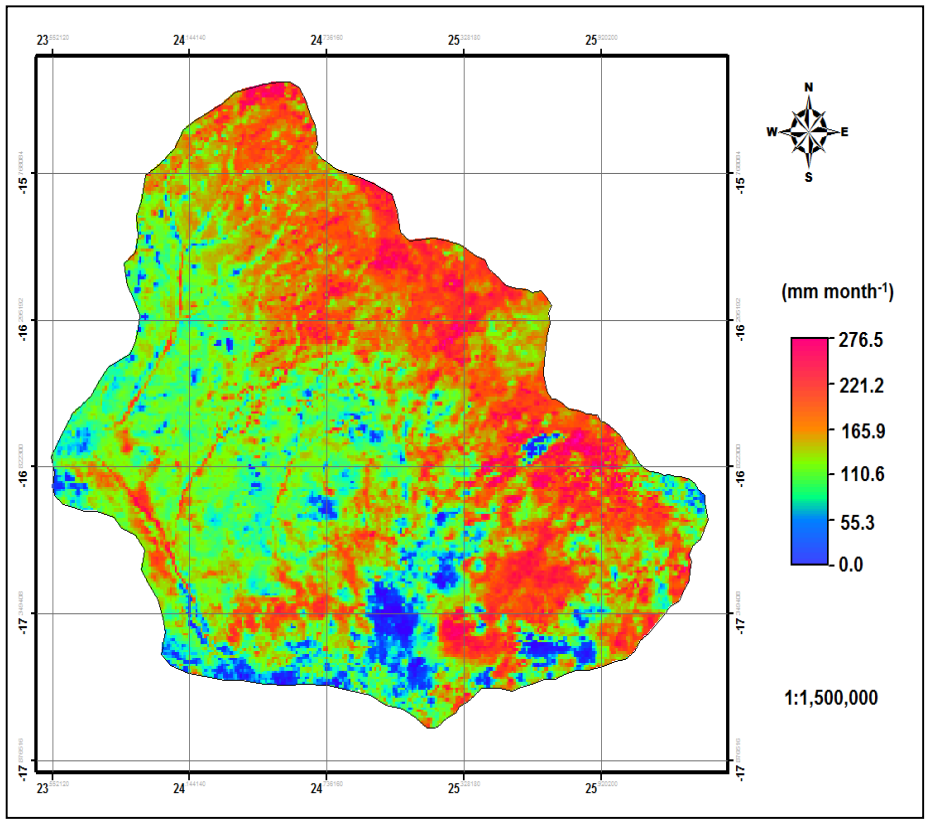

Figure 29: Estimated actual evapotranspiration for November, 2006 over the semi-arid Barotse Sub-basin, South-Western Zambia

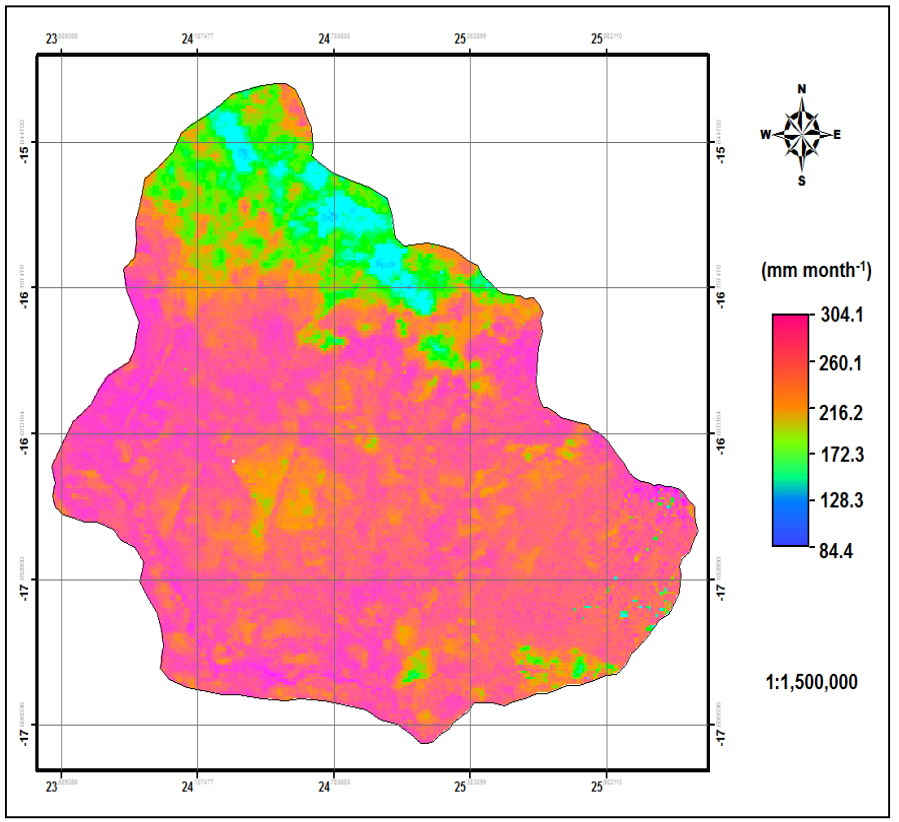

Figure 30: Estimated actual evapotranspiration for January, 2007 over the semi-arid Barotse Sub-basin, South-Western Zambia

The modelled spatially distributed AET for March, 2007 is shown in Figure 31. March is usually the last month in which effective rainfall is received in the semi-arid Barotse Sub-basin (MEWD-JICA, 1995). In this month, AET was relatively lower than that observed in January and February. The mean ET in March was ~126 mm month^{-1}. The general decline in the rate of ET was ascribed to the reduction in the number of rainfall events. The sources of high fluxes were in the southern (along the water bodies regularly flooded vegetation and parts of the forested area) and south eastern parts (over mosaic vegetation and cropland) of the basin. The lower rate of ET in the northern parts (forested areas) was attributed more to the amount of energy available at the surface and atmospheric condition than to the decline in soil moisture content. This is because the rain season was just coming to the end and tree species can use their long roots to tap water at some depth although much of the north and south western parts of the basin sit on the arenosol soils. This soil has a sandy structure and excessive drainage. This means that exposed areas with this type of soil would exhibit lower rate of ET shortly after the rain season (FAO and GRZ, 1986).

The spatial distribution of AET in the month of June, 2007, on the other hand, is presented in Figure 32. The estimated AET in this month was lower and ranged from nearly zero to 131 mm month^{-1}. The mean flux rate was ~45 mm month^{-1}. The reduction in the rate of ET is attributed to the limitation of soil moisture and reduced energy at the surface. The temperature in Sesheke District can be as low as 5.0 ^{0}C in the month of June and become even colder in July (ZDM, 1992). This affects the rate of ET besides other atmospheric factors like wind speed and humidity. The main source areas of high fluxes were over forested areas in the in northern part of the basin. Evaporation was also very high in the southern part of the basin on water bodies and other wetter surfaces. The high rates of ET observed in isolated areas in the southern part of the basin were attributed to the wetter vertisols. These heavy clayey soils have a high retention capacity and remain relatively wet long after the rain season. These soils are characterised by high evaporative rates relative to other soils because of their high water holding capacity (cf. Suleiman and Richie, 2003).

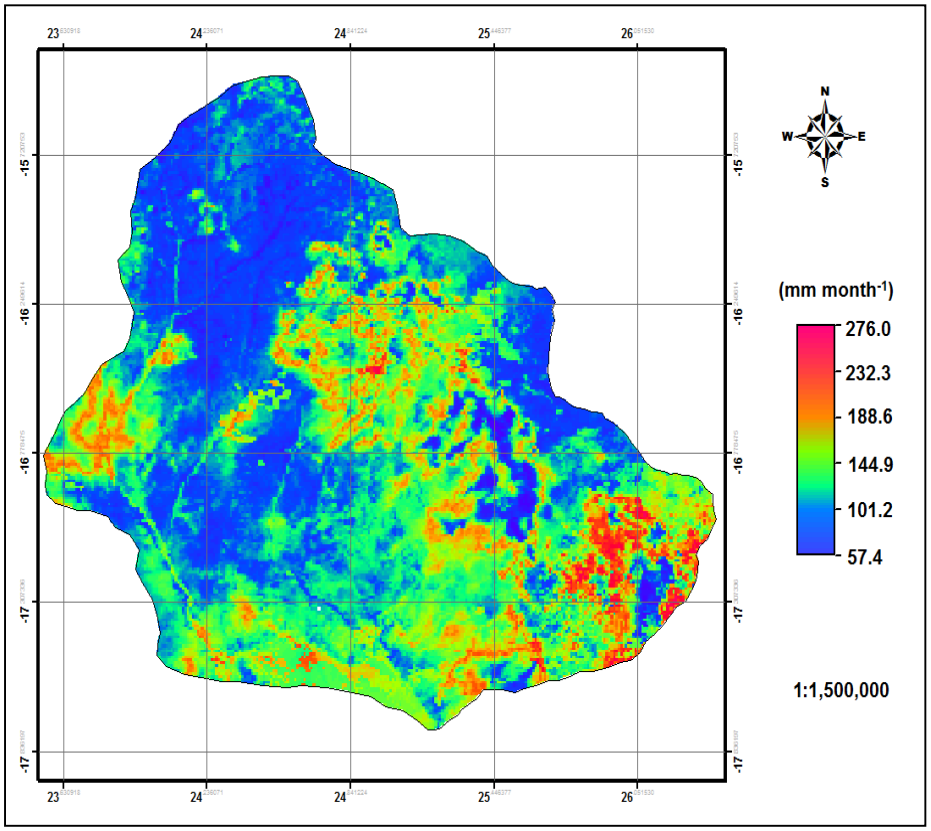

Figure 31: Estimated actual evapotranspiration for March, 2007 over the semi-arid Barotse Sub-basin, South-Western Zambia

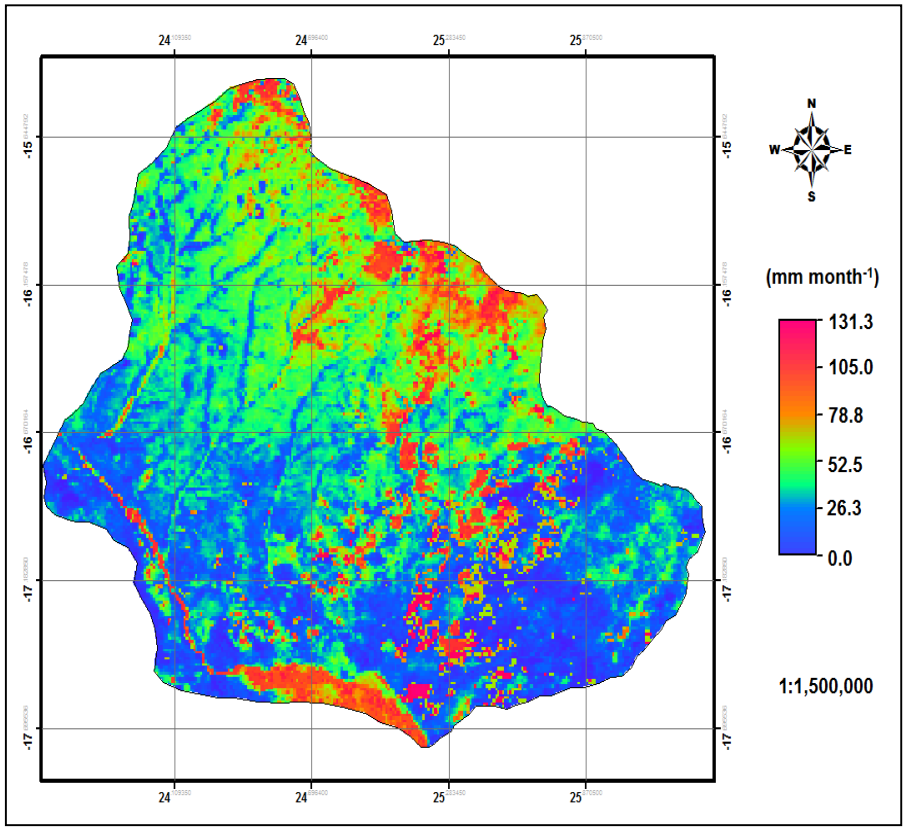

Figure 32: Estimated actual evapotranspiration for June, 2007 over the semi-arid Barotse Sub-basin, South-Western Zambia

The spatial distribution of AET in the month of August, which usually marks the beginning of the hot dry season, is shown in Figure 33. It was observed that the southern part of the basin, except on water bodies, regularly flooded vegetation and wetter vertisols, experienced lower rates of ET compared with the northern areas where forests are located. The lower rate of ET over the areas in the south-eastern and south-western parts of the basin is attributed to a combination of plant physiology and limitation of soil moisture. These areas are essentially covered with mosaic vegetation/cropland shrublands and open to closed grasslands all of which have shallower roots compared with tree species in the northern part. Furthermore, rainfall in the semi-arid Barotse Sub-basin reduces from north to south as it is related to movement of ITCZ (ZDM, 1992; MEWD-JICA, 1995).The general effect is that soil moisture is usually limited over areas in the southern parts, especially in the dry season.
Thus, AET was very low in the southern parts in this month due to the intensification of heat which dried up the soils. On the other hand, the relatively high solar radiation increased the rate of evaporation over water bodies and regularly flooded areas in the southern part of the study area.

Figure 34 shows the spatial distribution of AET in October. It is observed that there was a further reduction of ET over much of the semi-arid Barotse Sub-basin. The mean monthly AET in this month was ~78 mm month^{-1}. High evaporative fluxes were confined to forested areas, regularly flooded vegetation and water bodies due to the presence of relatively high moisture content over these surfaces. On the other hand, the rest of the study area experienced very low rates of ET because of the loss of soil moisture via deep percolation and high rate of ET, which is a characteristic feature of the semi-arid Barotse Sub-basin (ZDM, 1992). Therefore, this means the lower rates of ET over vegetated surfaces indicated the adaptive mechanism which plant species employ to survive the dry conditions. Most of the plant species in the study area are deciduous (Jeans, 1991; Aregheore, 2006). These shade their leaves in the dry season to reduce transpiration. This explains why the evaporative fluxes were lower over plant species such as open shrublands and mosaic vegetation in the southern part of the study area in this dry month.

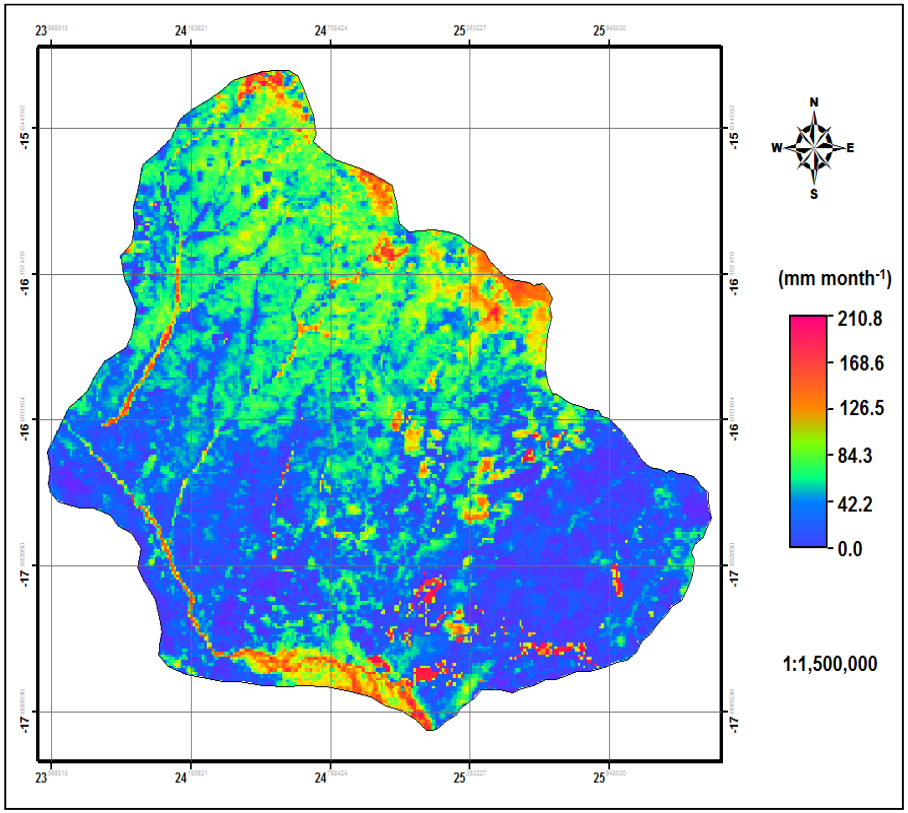

Figure 33: Estimated actual evapotranspiration for August, 2007 over the semi-arid Barotse Sub-basin, South-Western Zambia

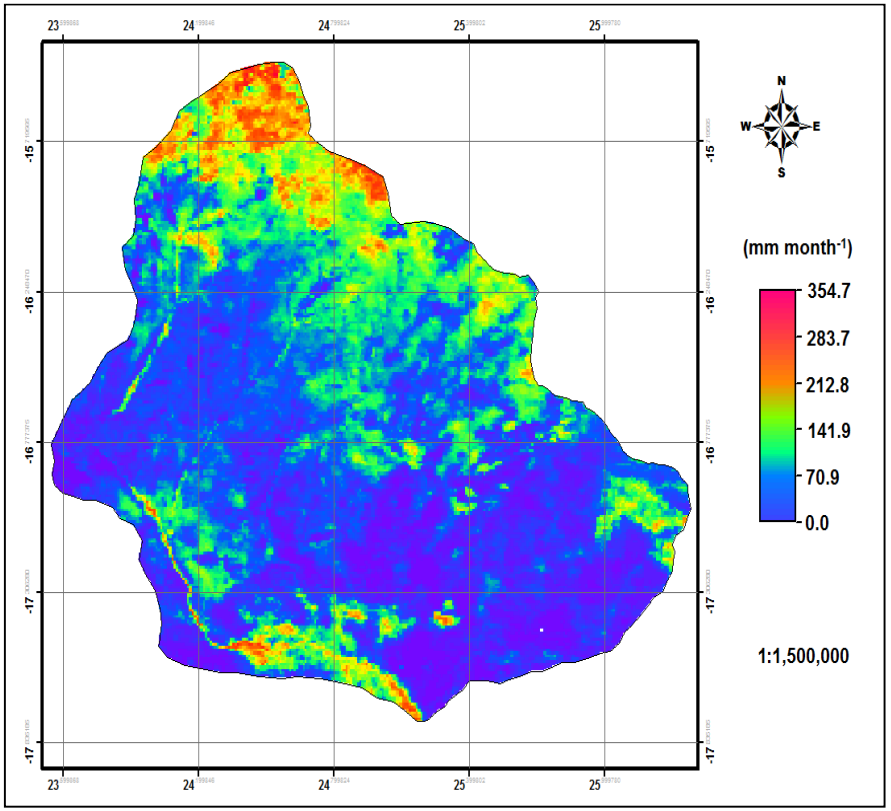

Figure 34: Estimated actual evapotranspiration for October, 2007 over the semi-arid Barotse Sub-basin, South-Western Zambia

The mean monthly evaporative rates over the semi-arid Barotse Sub-basin were highest in the warm-wet season, relatively high in the cool-dry season and lowest in the hot-dry season (Table 11). The higher evaporative rates observed in the warm-wet season (November-March) were expected as the semi-arid Barotse Sub-basin receives high rainfall during this period. Similarly, lower fluxes in the hot-dry season (August to October) were expected as the semi-arid Barotse Sub-basin is one of the areas in Zambia which experience very high temperatures in the hot-dry season (ZDM, 1992; Hutchinson, 1974; MEWD-JICA, 1995). Therefore, the evaporative demand of the atmosphere is usually very high during this period (cf. FAO, 2002). This means that the soils, especially the sandy soils (arenosols), become drier as a consequence of high rate of ET and deep percolation resulting in a scarcity of surface water over much of the semi arid Barotse Sub-basin (cf. MEWD-JICA, 1995). Under these conditions, ET becomes lower over land surfaces. Thus, the high energy (R_n- G) at the surface during this time contributes more to sensible heat (H) flux than to latent heat flux because of the lack of soil moisture over the area (cf. Su, 2002; Gibson et al., 2011).

Mohamed et al. (2010) found that monthly actual ET in June was in the range of 34 to 98 mm and declined in September to between 6 and 43 mm in the Mkindo Catchment, Tanzania. Although these ET trends are similar to the ones found in the present study, the values are different. This was ascribed to differences in climatic patterns. Mkindo Catchment receives higher amount of rainfall of ~1000 to 1800 mm year^{-1} (Mohamed et al., 2010) and is thus in a humid region. In such regions, ET tends to be lower on account of high humidity which saturates the air faster than in arid and semi-arid areas (Allen et al., 1998). In addition, the difference in land cover types and size between the two areas accounted for the differences in evaporative fluxes. The semi-arid Barotse Sub-basin (45,568Km^2) is bigger and more spatially varied than Mkindo Catchment (1,006 Km^2). The land cover types in the semi-arid Barotse sub-basin range from big water bodies such as the Zambezi River to forested land.

5.9 Calculated potential evapotranspiration (PET) over satellite passing time

It was observed that the calculated PET varied with the days considered in this study. It was found that on hot-dry days (DOY 225 to 292) PET was very high and ranged from 4.3 to 6.3 mm day^{-1}. On the other hand, the evaporative demand of the atmosphere on cool-dry days (DOY106 to 197) was lower, and was in the range of 3.2 to 4.9 mm day^{-1}. On warm-wet days (DOY 325 to 74) PET ranged from 3.8 to 5.7 mm day^{-1} (Table 12).

Table 12: Calculated potential evapotranspiration of the reference grass surface using FAO Penman-Montieth formula at satellite passing time over Sesheke Meteorological Station, semi-arid Barotse Sub-basin, South-Western Zambia

DATE	JD	Δ (Kpa)	Rn (MJ m^{-2} d^{-1})	G (MJ m^{-2} d^{-1})	ϒ (Kpa $^oC^{-1}$)	T(^{o}C)	U_2 (m s^{-1})	e_s-e_a (kpa)	PET (mm day^{-1})
21/11/06	325	0.30	12.14	0	0.06	34.4	3.0	3.06	5.3
30/11/06	334	0.29	12.09	0	0.06	33.8	3.5	2.89	5.7
02/12/06	336	0.29	12.10	0	0.06	33.6	2.1	2.83	4.1
04/12/06	338	0.29	12.14	0	0.06	33.5	3.4	2.78	5.4
12/01/07	12	0.27	12.22	0	0.06	32.0	2.7	2.46	4.4
14/01/07	14	0.27	12.20	0	0.06	32.0	2.8	2.46	4.5
14/02/07	45	0.27	11.70	0	0.06	32.2	2.7	2.50	4.4
18/02/07	49	0.23	11.78	0	0.06	28.7	3.3	1.63	3.8
12/03/07	71	0.27	11.12	0	0.06	32.2	3.2	2.65	5.0
15/03/07	74	0.27	10.96	0	0.06	32.3	3.4	2.71	5.3
16/04/07	106	0.27	8.36	0	0.06	31.8	2.8	3.04	4.9
23/04/07	113	0.26	7.54	0	0.06	31.3	2.7	3.04	4.7
16/05/07	136	0.23	5.31	0	0.06	29.0	2.5	2.80	4.2
23/05/07	143	0.22	4.68	0	0.06	27.7	2.5	2.63	4.0
17/06/07	168	0.21	3.61	0	0.06	26.9	2.0	2.57	3.3
19/06/07	170	0.20	3.50	0	0.06	26.0	2.0	2.45	3.2
10/07/07	191	0.20	3.69	0	0.06	26.3	2.1	2.54	3.5
16/07/07	197	0.22	3.74	0	0.06	28.0	2.0	2.91	3.6
13/08/07	225	0.24	5.98	0	0.06	29.8	2.3	3.11	4.3
20/08/07	232	0.25	6.71	0	0.06	30.7	2.5	3.24	4.7
12/09/07	255	0.29	8.69	0	0.06	33.9	2.8	3.95	5.8
14/09/07	257	0.30	8.91	0	0.06	34.2	2.9	4.00	6.0
14/10/07	287	0.30	11.75	0	0.06	34.5	3.3	3.53	6.2
19/10/07	292	0.30	11.89	0	0.06	34.4	3.4	3.48	6.3

Where Δ = Slope of temperature of pressure curve, JD= Julian Day, Rn= Net radiation, G= Ground heat flux, ϒ = Psychrometric constant, e_s-e_a= Pressure deficit, T= Temperature, U_2= Wind speed , PET= Potential Evapotranspiration

The estimates of PET found in this study (Table 12) compared well with long term averages computed by the FAO LocClim estimator (FAO, 2002). The FAO LocClim estimator also uses the FAO Penman-Montieth equation to estimate PET over selected stations around the globe (FAO, 2002). The reference point used in this study is less than ten kilometres from Katima Mulilo Meteorological Station of Namibia for which FAO LocClim data were available. Therefore, the climatic factors affecting PET between the two stations are the same given that the area is not mountainous (cf. Allen et al., 1998). The FAO LocClim estimates of daily evaporative demand over satellite passing time were as follows: hot-dry days (5 to 7.2 mm day^{-1}), warm-wet days (4.5 to 6.3 mm day^{-1}) and cool-dry days (3.9 to 4.5 mm day^{-1}).

Results of the calculated PET indicated that it varied with the seasons. This was expected because the major factors which affect the FAO Penman-Montieth PET of the reference grass surface are climatic parameters (cf. Feddes and Lenselink, 1994; Allen et al., 1998). It therefore expresses the atmospheric evaporative energy available to remove water from a grass surface and assumes that soil water is not limited (Allen et al., 1998). In this case, it considers meteorological parameters such as net radiation, air temperature, vapour pressure deficit and wind speed while holding surface conditions constant. This is why the PET rates were higher on the hot-dry days because of higher temperatures and net radiation associated with these days. Conversely, the calculated PET rates were lower on cool-dry days because of lower temperatures and radiation on these days (cf. Vogt and Niemeyer, 2001).

5.10 Effects of aerodynamic surface roughness on evapotranspiration estimates

The ET fluxes estimated using NDVI and landuse-based aerodynamic roughness values were compared on DOY 12 (January, 2007). The effect of NDVI and landuse-based surface roughness on ET per land cover type over the semi-arid Barotse Sub-basin is shown in Figure 35. It was observed that the evaporative fluxes based on landuse roughness were considerably lower than those based on NDVI roughness values especially over deciduous and ‘mixed’ forested areas. The highest reduction in ET of up to 25% occurred on closed to broadleaved deciduous forest whereas the lowest (a reduction of 6.5%) was on water bodies (Figure 35).

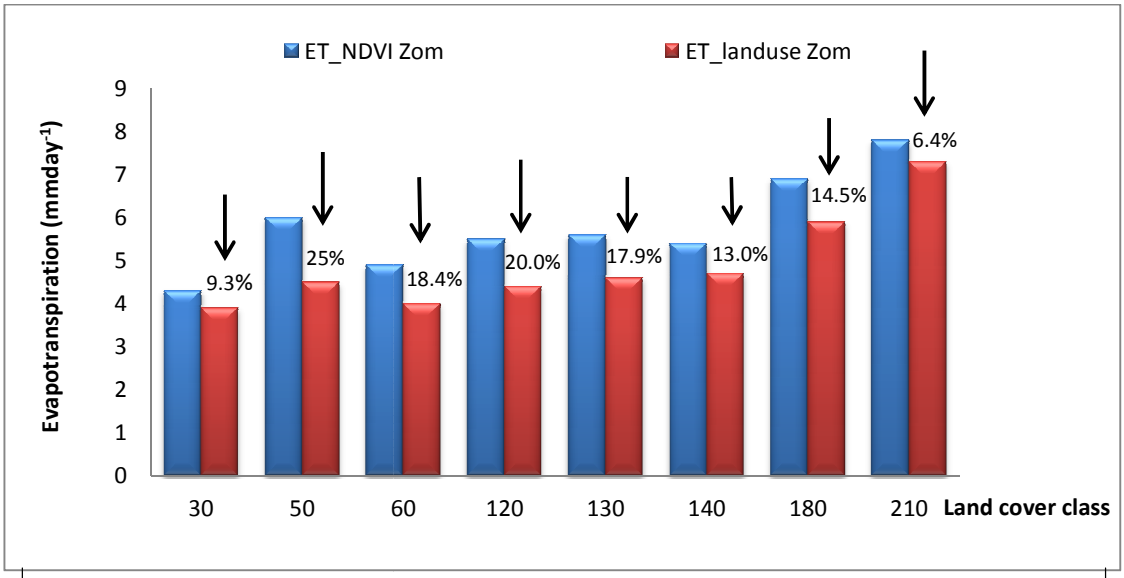

Land cover type	ET_NDVI Zom (mm day^{-1})	ET_landuse Zom (mm day^{-1})	% Change
30	4.3	3.9	-9.3
50	6.0	4.5	-25.0
60	4.9	4.0	-18.4
120	5.5	4.4	-20.0
130	5.6	4.6	-17.9
140	5.4	4.7	-13.0
180	6.9	5.9	-14.5
210	7.8	7.3	-6.4

Figure 35: Effect of NDVI vs. landuse-based surface roughness on the estimated fluxes on DOY 12 in the semi-arid Barotse Sub-basin, South-Western Zambia

Thus, the effect of roughness on ET was very high over deciduous and 'mixed' forested areas when the latter approximated the known literature values (cf. Alvarez, 2007; Hailegorgis, 2006). This was because the maximum roughness value that can be obtained from NDVI is very low over forests (Rauwerda et al., 2002; Su, 2005), which is around 0.5 when NDVI is greater than 0.7 (Alvarez, 2007). Thus, the use of NDVI to estimate roughness in higher canopy areas of the study area resulted in the underestimation of this parameter. The use of more accurate roughness values can considerably improve the estimates ET over the study area. Detailed surface roughness values associated with the landcover types of the study area were not available at the time of this study, as no measurement and validation have been done on these surfaces. The landuse roughness map (Figure 36) applied in this study was derived from literature values (Appendix 5) many of which were associated with generic landcover types in the study area. Accurate roughness values maps based on spatially distributed

vegetation height data (e.g. LIDAR), however, are difficult to acquire as this data is scarce and very expensive (Alvarez, 2007).

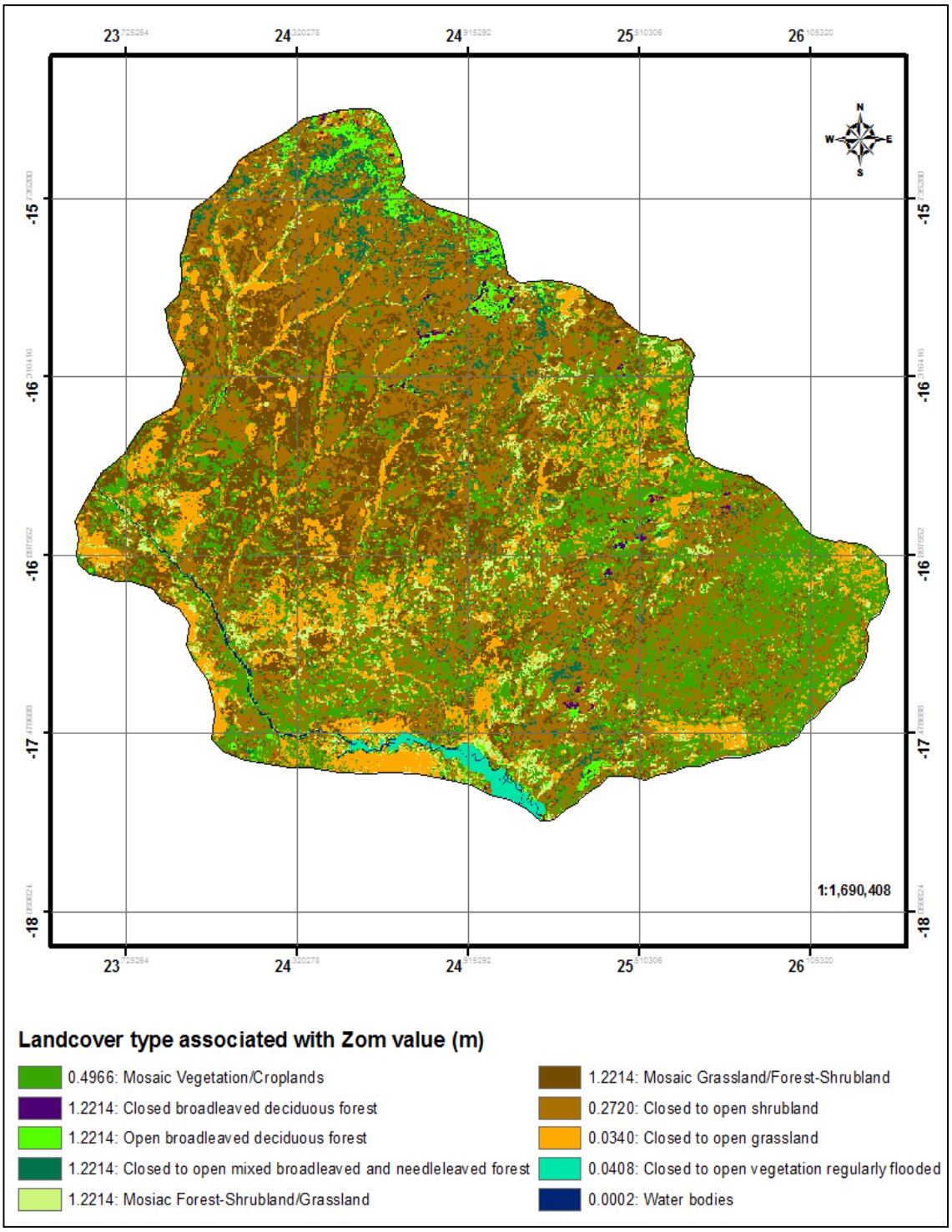

Figure 36: Estimated surface roughness based on landuse type and literature values over the semi-arid Barotse Sub-basin, South-Western Zambia

5.11 Sensitivity of actual evapotranspiration estimates to temperature gradients

The sensitivity of the evaporative flux estimates to the input data of near surface temperature was analysed in relation to the gradient temperature between the surface (T_0) and the air (T_a), [Δ (T_0-T_a)], by adjusting T_a up to 8 K around the estimated T_a value while holding T_0 constant (cf. Gibson et al., 2011). The results in Figure 37 shows that at Sesheke Station where the estimated T_0 was 310 K and T_a was 303 K, thus T_0-T_a was equal to7 K, the daily fluxes varied up to 3.0 mm day^{-1}. The value of ET at T_0-T_a = 7 K (red intersecting lines) was ~4.2 mm day^{-1}. Starting at this point, it is shown that when the (T_0-T_a) increases as a result of a decrease in T_a, ET reduces and the reverse happens when (T_0-T_a) reduces as a result of an increase in T_a.

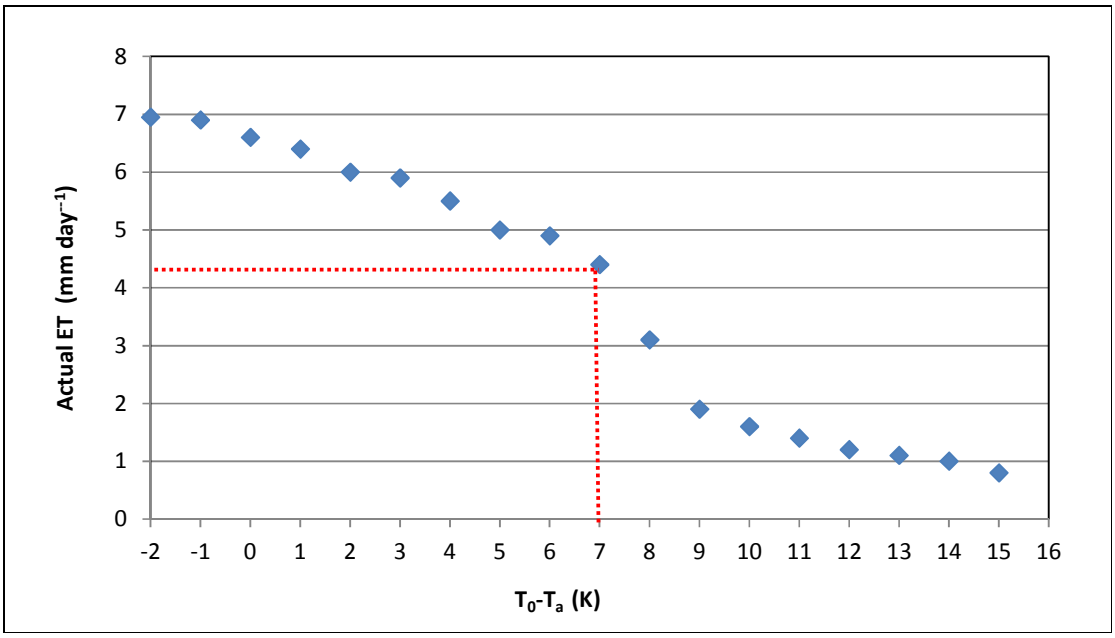

Figure 37: Sensitivity of evaporative fluxes to variation in air temperature in the $\Delta(T_0 - T_a)$ at Sesheke station, semi-arid Barotse Sub-basin South-Western Zambia

The high sensitive of the SEBS evaporative fluxes to the variation of air temperature (T_a) in the Δ (T_0-T_a) comes about because SEBS model estimates ET by setting a wet limit, at which equation 39 applies, and a dry limit when the combination of equations 22, 23 and 24 take effect (Su, 2002; Gibson et al., 2011). This means that accurate estimation of surface temperature and air temperature is required. The use of average air temperature in an environment that has diverse land uses (heterogeneous) can contribute to inaccurate results.

5.12 Evaluation of SEBS daily AET against PET and ECMWF estimates

The comparison of SEBS daily AET with PET and ECMWF estimates on warm-wet days at Sesheke Meteorological Station is shown in Figure 38. On average, the SEBS evaporative fluxes were ~104.2% of PET estimates. This means that the modelled fluxes were not in good physical agreement with PET on all the days as they exceeded the potential limit by 4.2%. It is shown that AET was physically consistent (below PET) on four occasions (DOY 325, 334, 336 and 74) out of the ten warm-wet days (Figure 38). In comparison with ECMWF estimates, the SEBS fluxes were ~142% of the former. It shown that modelled results were only comparable to ECMWF estimates on the same days they were observed to be physically consistent with PET. In general, it was observed that the SEBS evaporative fluxes were mainly greater than PET and ECMWF estimates between DOY 338 and DOY 71, a period associated with high rainfall events in the semi-arid Barotse Sub-basin. As such there was high moisture content available for evapotranspiration. This period spans from December to March. Furthermore, the comparison with grass evaporative rates indicated that the SEBS fluxes were physically consistent with PET on a number of days (DOY 325,334,336,338 and 74) and comparable to ECMWF estimates only on DOY 325, 334 and 74 (Figure 38).

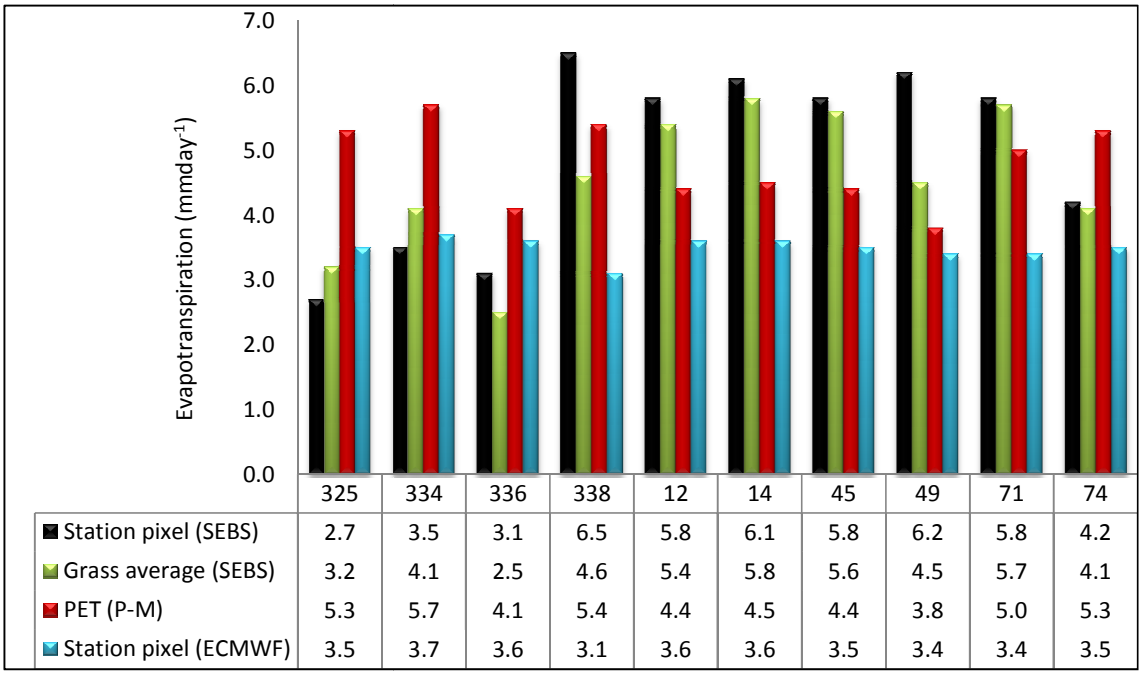

	325	334	336	338	12	14	45	49	71	74
Station pixel (SEBS)	2.7	3.5	3.1	6.5	5.8	6.1	5.8	6.2	5.8	4.2
Grass average (SEBS)	3.2	4.1	2.5	4.6	5.4	5.8	5.6	4.5	5.7	4.1
PET (P-M)	5.3	5.7	4.1	5.4	4.4	4.5	4.4	3.8	5.0	5.3
Station pixel (ECMWF)	3.5	3.7	3.6	3.1	3.6	3.6	3.5	3.4	3.4	3.5

Figure 38: Comparison of the SEBS evaporative fluxes with potential evapotranspiration and ECMWF actual evapotranspiration on warm-wet days (DOY 325-74) at Sesheke station, semi-arid Barotse Sub-basin, South-Western Zambia

The comparison of SEBS evaporative fluxes with PET and ECMWF estimates on cool-dry days at Sesheke Meteorological Station is shown in Figure 39. It was observed that modelled evaporative fluxes were less than PET on almost all the days (except for DOY 106) and compared well with ECMWF estimates only on DOY 136, 168 and 191. On the average, SEBS modelled fluxes were ~64.3% of PET and 138% of ECMWF estimates. This means that the SEBS modelled fluxes were largely physically consistent with PET on cool dry days and not good agreement with ECMWF estimates on all days. However, it was observed that the evaporative rates over grass were not only lower than PET (physically consistent) but also comparable to ECMWF estimates on many days, especially on DOY 113,136, 170 and 191 (Figure 39).

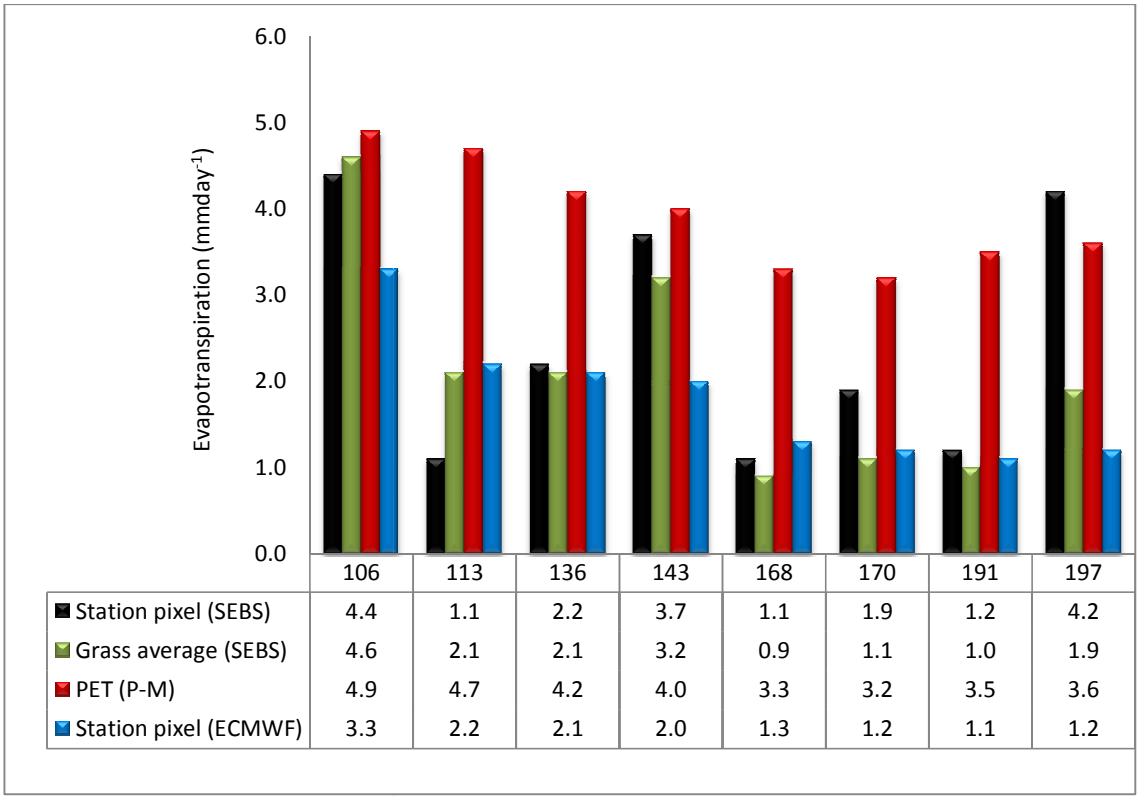

	106	113	136	143	168	170	191	197
Station pixel (SEBS)	4.4	1.1	2.2	3.7	1.1	1.9	1.2	4.2
Grass average (SEBS)	4.6	2.1	2.1	3.2	0.9	1.1	1.0	1.9
PET (P-M)	4.9	4.7	4.2	4.0	3.3	3.2	3.5	3.6
Station pixel (ECMWF)	3.3	2.2	2.1	2.0	1.3	1.2	1.1	1.2

Figure 39: Comparison of the SEBS evaporative fluxes with potential evapotranspiration and ECMWF actual evapotranspiration on cool-dry days (DOY 106-197) at Sesheke station, semi-arid Barotse Sub-basin, South-Western Zambia

The comparison of SEBS evaporative fluxes with PET and ECMWF estimates on hot-dry days at Sesheke station is shown in Figure 40. It was found that SEBS fluxes (station pixel) were in physical agreement with PET on all the days. These fluxes were also comparable to

ECMWF estimates. Over these days, the SEBS evaporative fluxes were ~29.4% of PET and 110% of ECMWF estimates. In comparison to PET, the SEBS actual evaporative fluxes clearly show that they had significantly declined on hot-dry days because of the limitation of soil moisture (cf. Rwasoka et al., 2011). Furthermore, it was observed that the evaporative fluxes over grass were lower than PET on all days and were almost of the same magnitude as ECMWF estimates on a number of days, especially on DOY 232, 255 and 257.

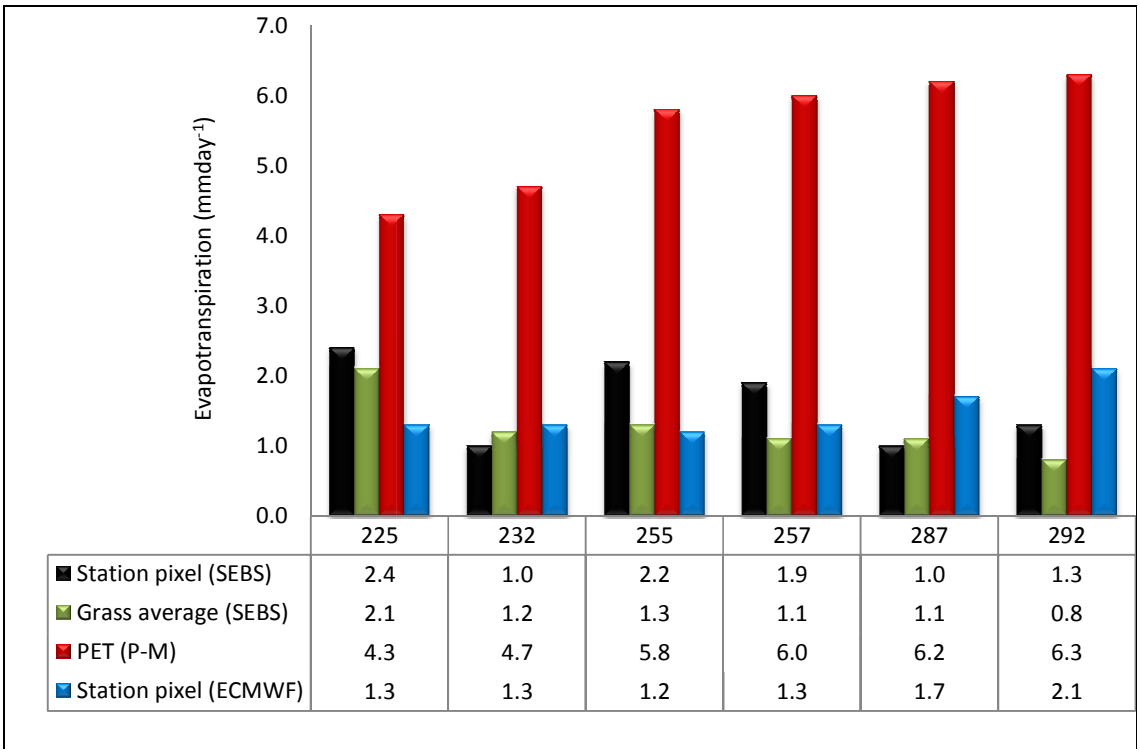

	225	232	255	257	287	292
Station pixel (SEBS)	2.4	1.0	2.2	1.9	1.0	1.3
Grass average (SEBS)	2.1	1.2	1.3	1.1	1.1	0.8
PET (P-M)	4.3	4.7	5.8	6.0	6.2	6.3
Station pixel (ECMWF)	1.3	1.3	1.2	1.3	1.7	2.1

Figure 40: Comparison of the SEBS evaporative fluxes with potential evapotranspiration and ECMWF actual evapotranspiration on hot-dry days (DOY 225-292) at Sesheke station, semi-arid Barotse Sub-basin, South-Western Zambia

On the overall, it was observed that the SEBS daily evaporative fluxes (station pixel and grass) were more variable than ECMWF estimates (Figure 41). The general trend, however, indicated that both models produced higher estimates of actual evaporative fluxes on warm-wet days and lower ones on hot-dry days. This implies that the two models are sensitive to the effect of soil moisture variation on ET. On the other hand, the FAO Penman-Montieth PET was higher on most of the days, declining significantly only on cool-dry days. This implies that this model is mainly very sensitive to energy inputs. It was observed that SEBS modelled evaporative fluxes were above PET on warm-wet days which are in the months

between December and March. The reasons behind this phenomenon are given at the end of this section.

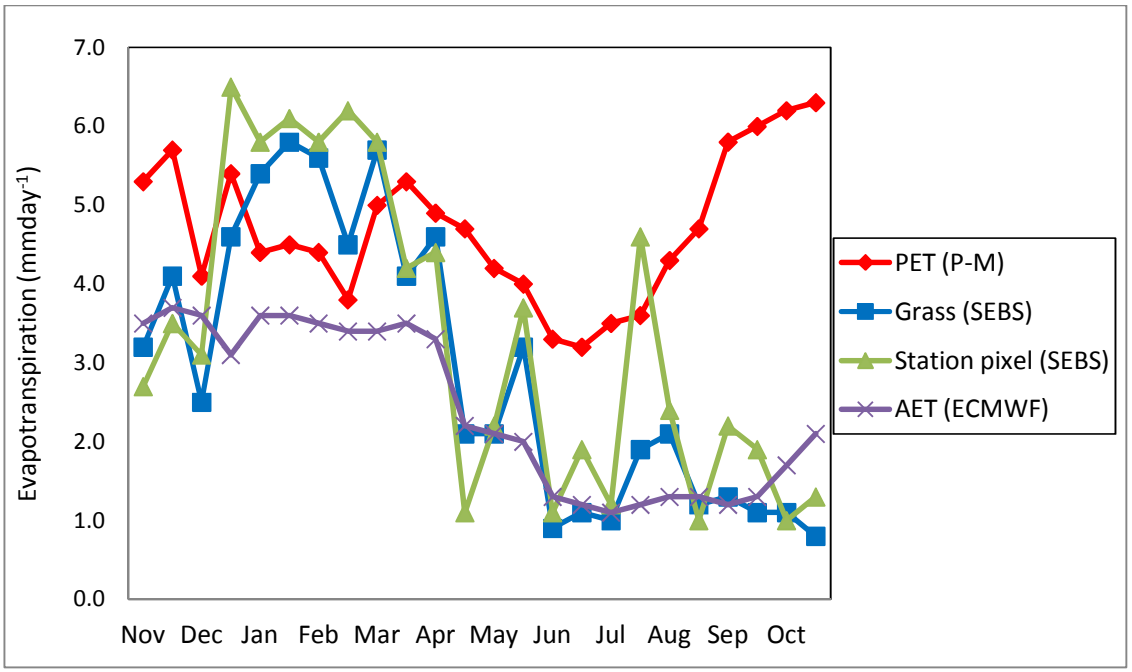

Figure 41: The variability of SEBS daily evaporative fluxes compared with PET and ECMWF estimates at Sesheke Meteorological Station, semi-arid Barotse Sub-basin, South-Western Zambia

An attempt was also made to evaluate the SEBS actual evaporative fluxes at a second reference point at Kamanga station, which is located in the northern part of the study area (Figure 3). This was done to check if the results would be similar to those observed at Sesheke Meteorological Station. Unfortunately, the modelled evaporative fluxes at Kamanga station were compared with the ECMWF estimates only due to the lack of meteorological data needed for the computation of the Penman-Montieth PET at satellite passing time.

The comparison of SEBS evaporative fluxes with ECMWF estimates on warm-wet days at Kamanga station is shown in Figure 42. Results indicated that the SEBS modelled fluxes were higher than ECMWF estimates on all the days except for DOY 336. On the average, SEBS fluxes were ~159% of ECMWF estimates. This implied that the modelled evaporative fluxes were not in good agreement with ECMWF estimates on many days around Kamanga station. This also indicated that the SEBS evaporative fluxes were higher in the northern parts of the semi-arid Barotse Sub-basin than those in the southern parts, as observed at Sesheke

Meteorological Station. It was observed, however, that the evaporative fluxes modelled by ECMWF were less variably or dynamic compared to those estimated by the SEBS model. The reasons behind this are related to the differences in the spatial resolution at which the two models were implemented. A full explanation about this is provided at the end of this section.

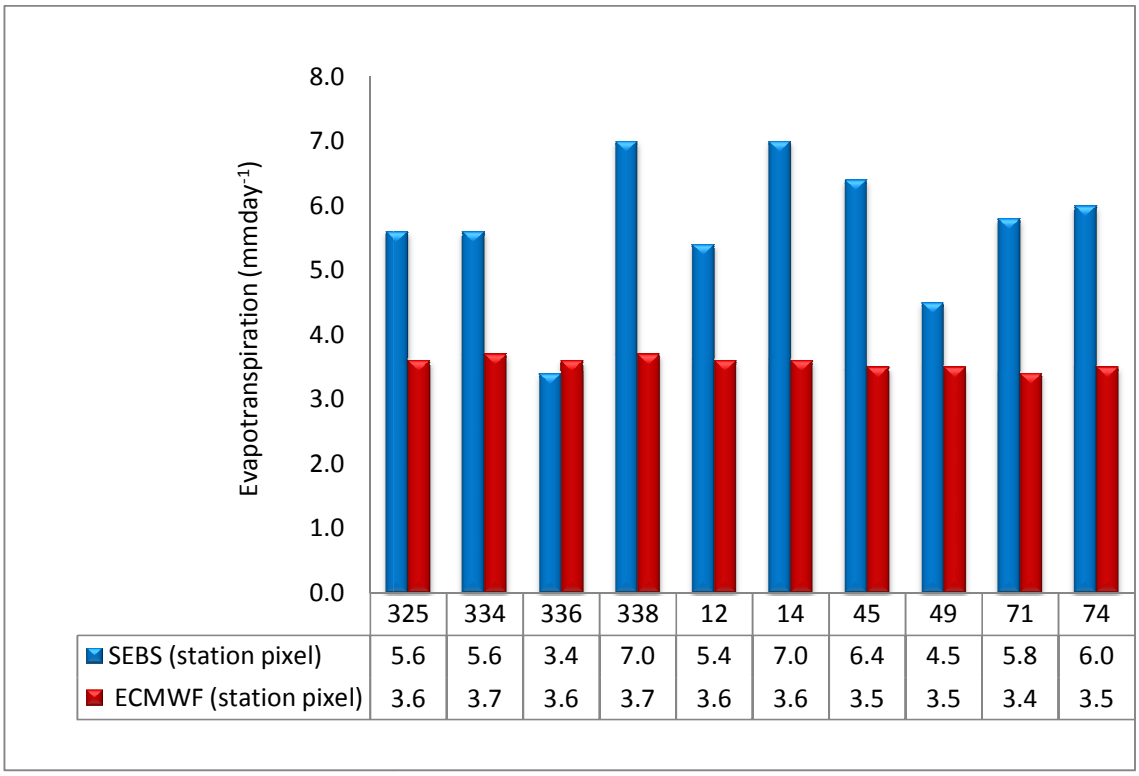

	325	334	336	338	12	14	45	49	71	74
SEBS (station pixel)	5.6	5.6	3.4	7.0	5.4	7.0	6.4	4.5	5.8	6.0
ECMWF (station pixel)	3.6	3.7	3.6	3.7	3.6	3.6	3.5	3.5	3.4	3.5

Figure 42: Comparison of the SEBS actual evaporative fluxes with ECMWF estimates of actual evapotranspiration on warm-wet days (DOY 325-74) at Kamanga station, semi-arid Barotse Sub-basin, South-Western Zambia

The differences between the SEBS actual evaporative fluxes and ECMWF estimates on cool-dry days at Kamanga station are shown in Figure 43. It was found that the SEBS fluxes were also higher than ECMWF estimates on all cool-dry days except for one (DOY 113). On the average, results indicated that these fluxes were ~171% of ECMWF estimates. This means that the SEBS estimates at Kamanga station were much higher than those found at Sesheke Meteorological Station and not in good agreement with ECMWF estimates on many of the cool-dry days.

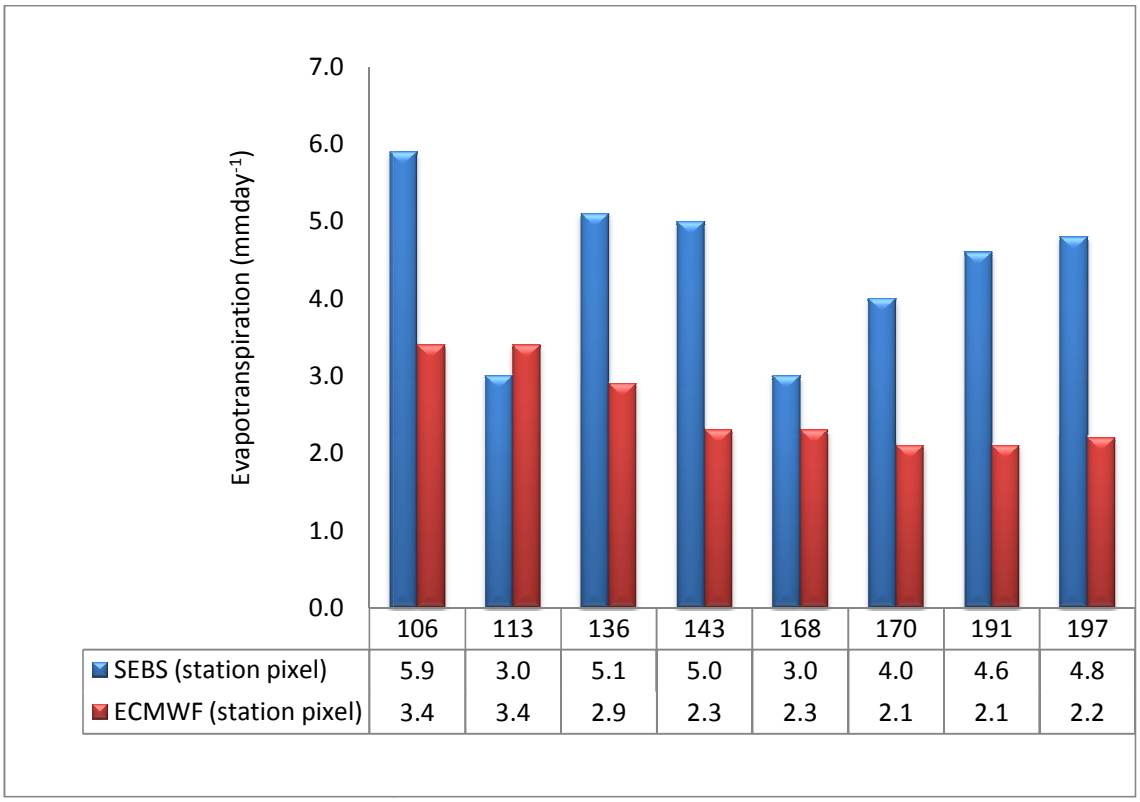

	106	113	136	143	168	170	191	197
SEBS (station pixel)	5.9	3.0	5.1	5.0	3.0	4.0	4.6	4.8
ECMWF (station pixel)	3.4	3.4	2.9	2.3	2.3	2.1	2.1	2.2

Figure 43: Comparison of the SEBS evaporative fluxes with ECMWF estimates of actual evapotranspiration on cool-dry days (DOY 106-197) at Kamanga station, semi-arid Barotse Sub-basin, South-Western Zambia

The comparison of the SEBS actual evaporative fluxes with ECMWF estimates of AET on hot-dry days at Kamanga station indicated that the former were consistently higher than the latter (Figure 44). On the average, the evaporative flux rates produced by the SEBS model were nearly twice (199%) those estimated by the ECMWF model. In comparison with the results observed at Sesheke Meteorological Station, the SEBS evaporative fluxes at Kamanga station were very high and not in good agreement with ECMWF estimates. The possible causes that are behind these discrepancies between the SEBS actual evaporative fluxes and ECMWF estimates at Sesheke and Kamanga stations are also discussed in details at the end of this section .

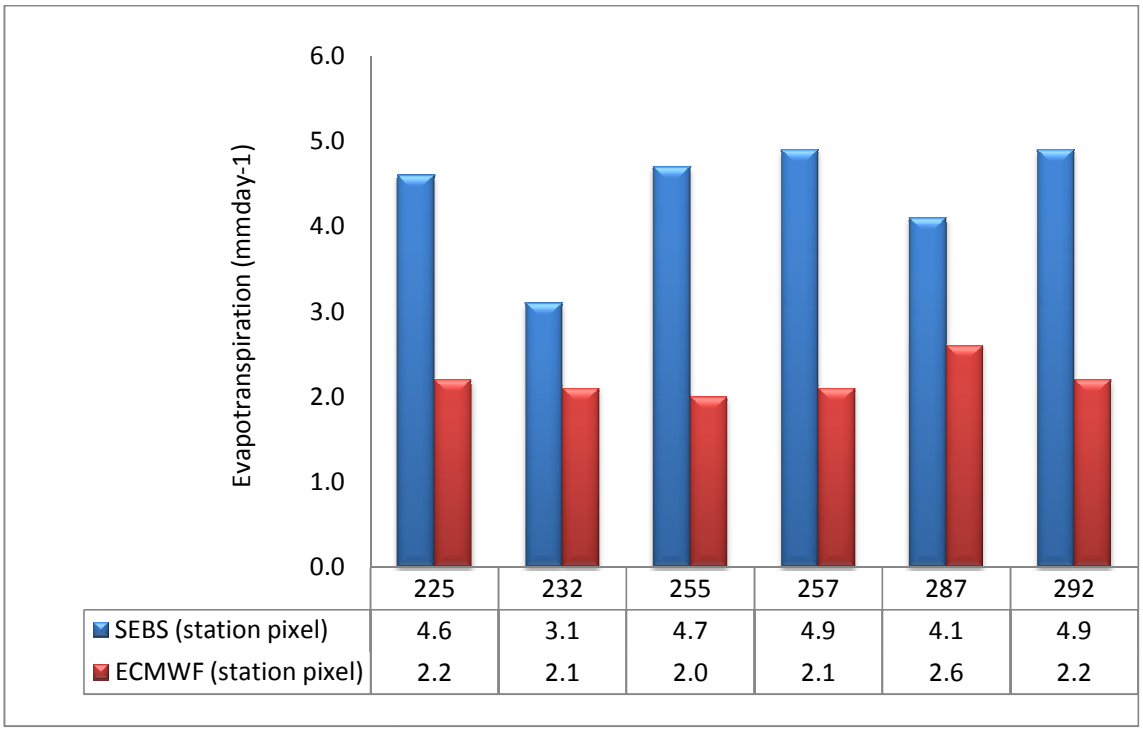

	225	232	255	257	287	292
SEBS (station pixel)	4.6	3.1	4.7	4.9	4.1	4.9
ECMWF (station pixel)	2.2	2.1	2.0	2.1	2.6	2.2

Figure 44: Comparison of the SEBS evaporative fluxes with ECMWF estimates of actual evapotranspiration on hot-dry days (DOY 225-292) at Kamanga station, semi-arid Barotse Sub-basin, South-Western Zambia

The SEBS actual evaporative fluxes were generally in physical agreement (less than PET) with PET on cool-dry and hot-dry days at Sesheke Meteorological Station (Figures 39 and 40). This was expected. The decline in soil moisture that begins in the cool-dry season, soon after the rain season, induces lower rates of actual evaporative fluxes over grass surfaces whereas PET is not affected by this change. Furthermore, the depletion of soil moisture in the hot-dry season due to high atmospheric demand and deep percolation in the semi-arid Barotse sub-basin reduces actual evaporative rates further whereas PET rises significantly because of the increase in energy at the surface (cf. Vogt and Niemeyer, 2001; Suleiman and Richie, 2003). Therefore, the physical agreement between the SEBS fluxes and PET shows that the former responded to the restrictions imposed by soil moisture on cool-dry and hot dry days.

The lack of physical agreement between SEBS evaporative fluxes and PET on warm-wet days was attributed to the effect of change in surface conditions which were beyond the resolution of PET model. The Penman-Montieth PET used in this study take the assumption that the ground is completely covered by short grass, the so called ‘big leaf approach’ (cf. Allen et al., 1998). However, plant species co-exist very often and there is a period when the

vegetation is not 'closed' (Shuttleworth and Wallace, 1985; Kustas and Norman, 1999; Neale and Vinokullo, 2005; Courault et al., 2005). This means that both the soil surface and vegetation leaves evaporate moisture and their relative importance change dynamically as plant species develop (Shuttleworth and Wallace, 1985; Zhang et al., 2008). It is possible that the surface conditions at Sesheke station could have been different from those assumed for the PET on warm-wet days, resulting in the modelled fluxes to be higher than the calculated PET (cf. Hailegorgis, 2006). Thus, it is argued that the modelled actual evaporative fluxes on warm-wet days were not necessarily physically implausible. The systematic occurrence of physically inconsistent SEBS fluxes on warm-wet days rather suggested that surface conditions were different from those assumed for PET of the reference grass surface. This highlighted the uncertainties of evaluating SEBS actual evaporative fluxes against PET in heterogeneous environments on warm-wet days.

The SEBS evaporative rates differed from ECMWF estimates in that the former were mainly higher than the latter. However, it was observed that these fluxes were in better agreement with ECMWF estimates at Sesheke Meteorological Station on a number of days (Figures 38-40) than at Kamanga station (Figures 42-44). The lack of good agreement between the evaporative fluxes modelled by the SEBS and ECMWF were ascribed to a number of factors.

On the one hand, the lack of good agreement between SEBS and ECMWF estimates could have come about because of differences in the parametrisation of turbulent heat fluxes. In addition to this, the SEBS model used in this study was run using the one kilometre spatial resolution of MODIS imagery whereas the ECMWF model has a course resolution of ~50 kilometres at best (Vogt and Niemeyer, 2001). Given that surface conditions (soil moisture and vegetation type) can be highly variable in space and time (Gibson et al., 2011), especially for heterogeneous areas like the semi-arid Barotse sub-basin, the course resolution of the ECMWF model may be questioned if it can adequately capture the spatial variations in the semi-arid Barotse sub-basin (cf. Vogt and Niemeyer, 2001). This means that the resulting evaporative fluxes from the ECMWF model may not be as highly variable as the surface conditions because of its course resolution. It is shown in Figure 41 that ECMWF estimates were less variable compared with the SEBS evaporative fluxes.

On the other hand, modelled evaporative fluxes were higher than ECMWF estimates possibly due to uncertainties associated with surface parameterisation. In this study, a vegetation index

(NDVI) was used to model surface roughness, canopy height, displacement height, fractional vegetation cover and the ground heat flux. It is observed that estimating roughness height for momentum transfer from NDVI is problematic over high vegetation areas such as forests as the value tends to be too small compared to what is actually on the ground (Rauwerda et al., 2002; Su, 2005; Hailegorgis, 2006). Conversely, the value tends to be overestimated over short but very green plant species such as maize and grasses (Hailegorgis, 2006). In this study, it was observed that the estimated roughness values (Tables 8-10) were very low over forested areas compared to reported literature values. For instance, Mücher et al. (2001) reported that roughness can be as high as 1.22 meters over deciduous forests. Furthermore, Alvarez (2007) used vegetation height obtained from LIDAR data to estimate roughness and found that it was as high as 1.29 meters over forests. In the present study, it was also observed that the surface roughness values over grass (Tables 8-10) were slightly higher than known literature values (cf. Wieringa, 1993; Mücher et al., 2001). It is very likely, therefore, that the NDVI-based roughness estimates used in this study affected the accuracy the ET output. It was shown that the estimates of this parameter altered ET results significantly, especially over forested areas (Figure 35). Many other studies (Hailegorgis, 2006; Lin, 2006; Alvarez, 2007; van der Kwast et al., 2009; Gebreyesus, 2009) have also shown that inaccurate estimates of surface roughness alters ET results significantly. This means that estimating roughness using more robust methods can improve the results of the modelled evaporative fluxes. The challenge, however, is that the alternatives such as LIDAR data or detailed roughness maps are often not available.

The use of the fraction vegetation cover, which was derived from NDVI using the method of Sobrino et al. (2003) as given in equation 13, is also likely to have caused higher flux estimates. In this study, fraction vegetation cover was used to calculate the excessive resistance term (kB^{-1}), emissivity (ε) and parameterize ground heat flux (G_o). The use of the fraction vegetation cover as proposed by Sobrino et al. (2003) to calculate the ground heat flux has some drawbacks (Gibson et al., 2011). This is because of the assumption that at NDVI 0.5, taken as the maximum, the fractional vegetation cover becomes unity resulting in a maximum ground heat flux of about five percent of net radiation. However, actual measurements by Gibson et al. (2011) at TERRA overpass have shown that the value was as high as 12 to 16% of net radiation for a fully vegetated surface. They attributed this to solar zenith and azimuth angle in addition to the orientation of the tree rows which allowed bare soil underneath the tress to receive direct radiation. It is also likely that this situation could

have been the case at satellite overpass time in the semi arid Barotse Sub-basin as MODIS TERRA satellite images were used in this study (Table 4). This situation results in the underestimation of the ground heat flux. Consequently higher sensible heat and latent heat fluxes are obtained. In this study, it was observed that maximum NDVI (Tables 8-10; Appendix 4) frequently exceeded the assumed value in the formula by Sobrino et al. (2003). Thus, calibrating the fraction vegetation cover by deriving scene-specific NDVI maximum and minimum, as suggested by Gibson et al. (2011), is likely to improve the estimates of the ground heat flux and the resultant evaporative fluxes.

With regard to uncertainties associated with meteorological input data, the use of average near surface temperature may have contributed to higher flux estimates, especially in the northern parts of the study area. This area is not covered by a functional meteorological station to provide weather data. Thus, average near surface temperatures were used as interpolated surfaces could not be built. It has been shown, however, that the SEBS model is very sensitive to, among other parameters, the input data of air temperature (Badola, 2009; van der Kwast et al., 2009) or land surface and air temperature gradient (Gibson et al., 2011). Therefore, the accuracy of ET estimates over the study area is also likely to increase if distributed near surface temperature validated over a number of ground stations is used.

5.13 Evaluation of the modelled monthly actual evapotranspiration

The comparison of mean monthly actual evaporative rates with PET and rainfall estimates is shown in Figure 45. The estimated rainfall and PET represents long term averages (30 years) at Katima Mulilo Meteorological Station, Namibia (FAO, 2002). The observed rainfall was measured at Sesheke Meteorological Station, Zambia. The two stations are less than ten kilometres apart. It was found that the mean monthly evaporative fluxes were lower than PET in all the months except for January. These fluxes were lower than rainfall only in October, November and December. It was expected that the evaporative fluxes would be lower than rainfall throughout the year given that there were no known irrigation schemes in the study area. However, the reference station at Sesheke was located in a heterogeneous area. It was near the wetlands and water bodies in the south and surrounded by closed to open shrublands. In the application of remote sensing data to calculate ET in heterogeneous environments, the accuracy depends, in part, on the spatial resolution of the sensor data (McCabe and Woods, 2006). In such areas, there is lower confidence in variables obtained from low resolution

sensor data because of the loss of intra-pixel spatial heterogeneity due to the integration of the radiometric signal (Gibson et al., 2011).

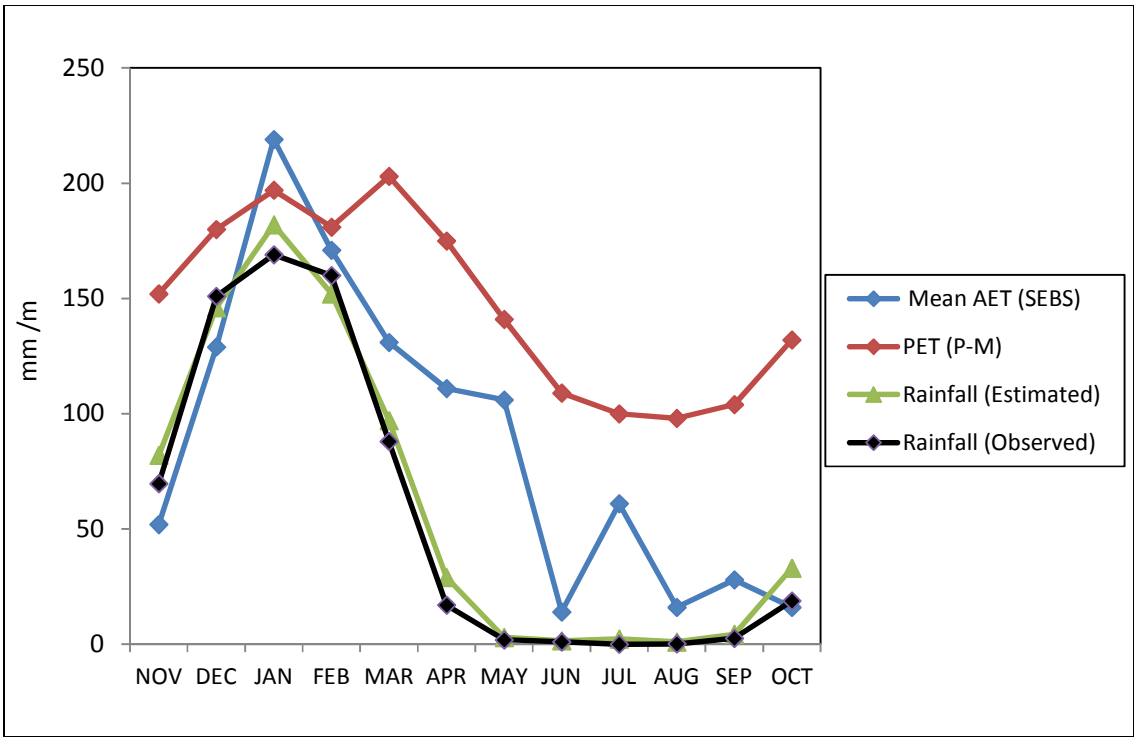

Figure 45: Comparison of modelled monthly actual evapotranspiration with potential evapotranspiration and rainfall at Sesheke Meteorological Station, semi-arid Barotse Sub-basin, South-Western Zambia

Figure 46 shows the comparison of modelled monthly actual fluxes with ECMWF estimates and PET at Sesheke Meteorological Station. The modelled fluxes were physically consistent with PET except in the month of January. It was, however, observed that these monthly fluxes were higher than ECMWF estimates almost throughout the warm-wet and cool-dry seasons (except in November and June). On the other hand, the fluxes were far below the ECMWF estimates in the dry season (August to October).

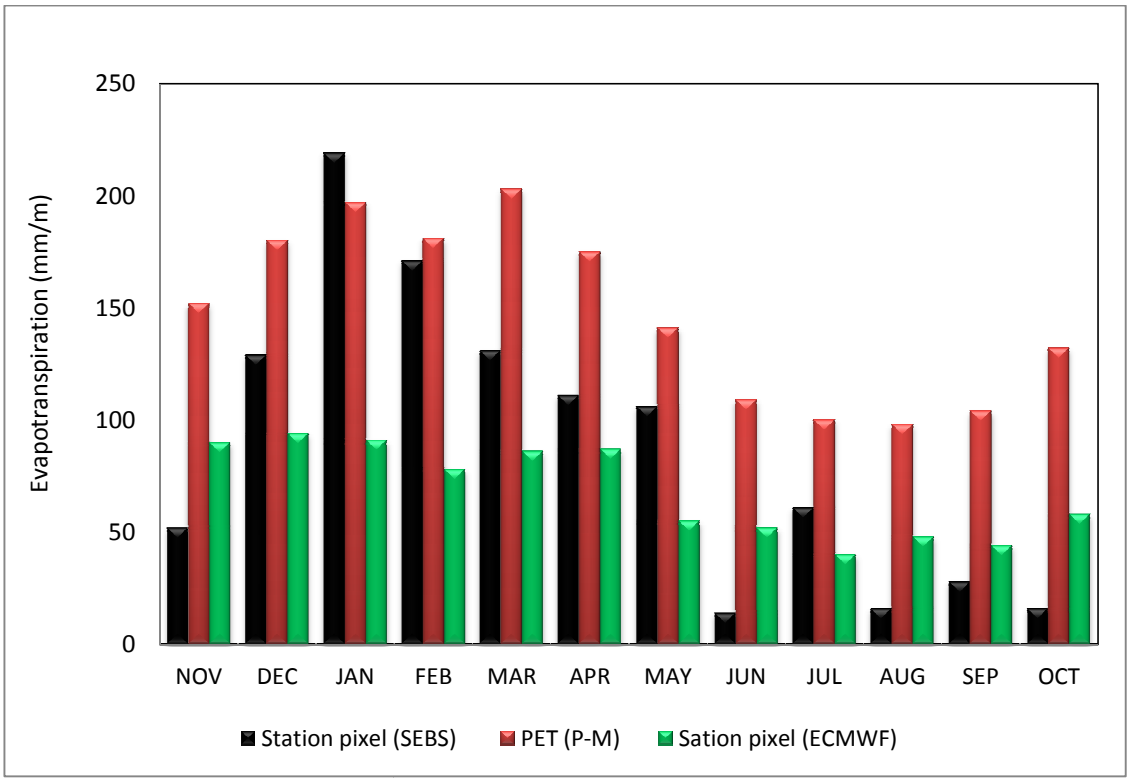

Figure 46: Comparison of modelled monthly actual evapotranspiration with ECMWF estimates and potential evapotranspiration at a monthly time step at Sesheke Meteorological Station, semi-arid Barotse Sub-basin, South-Western Zambia

The modelled monthly evaporative fluxes were also compared with ECMWF estimates at Kamanga station (Figure 47). It was observed that the modelled monthly fluxes were higher than ECMWF estimates in all the months except for June at this station. The SEBS fluxes were very high in comparison with ECMWF estimates especially from November to January (Figure 47). The possible causes of lack of agreement between the mean monthly modelled fluxes and the ECMWF estimates are discussed at the end of this section.

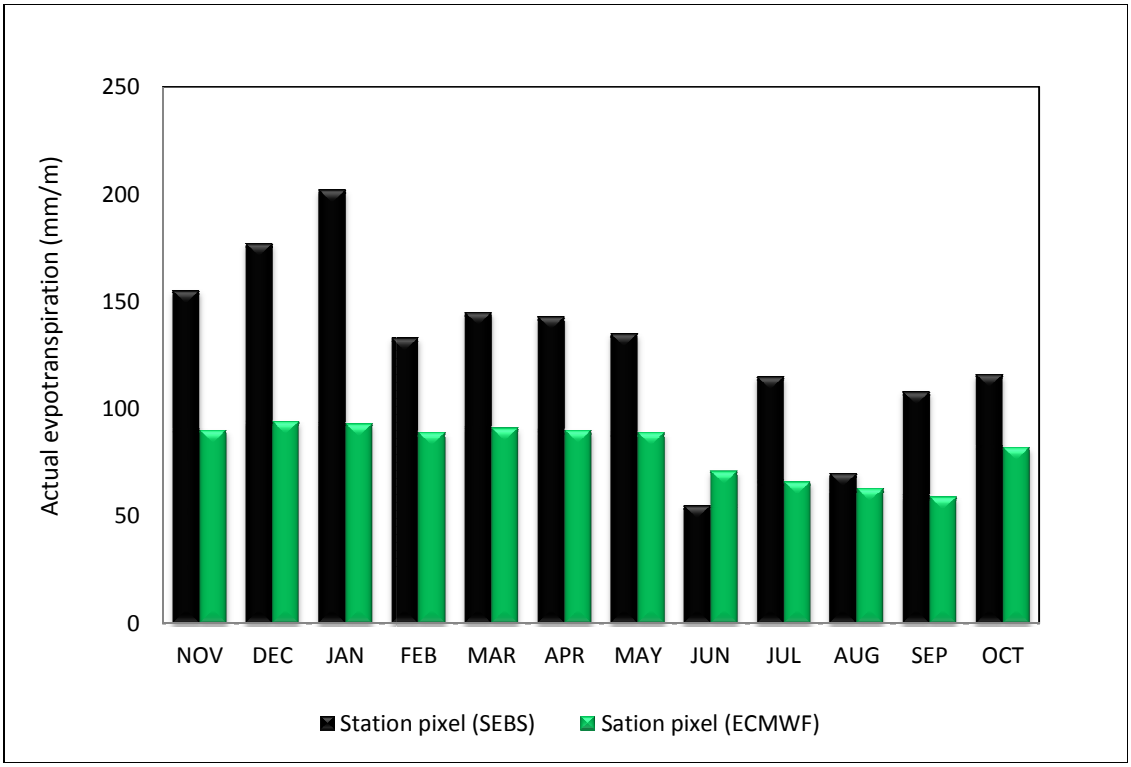

Figure 47: Comparison of modelled monthly actual evapotranspiration with ECMWF estimates at a monthly time step at Kamanga station, semi-arid Barotse Sub-basin, South-Western Zambia

The mean monthly evaporative fluxes were less than the observed rainfall for a few months (Figure 45). Despite the absence of irrigation schemes, the mean monthly fluxes exceeded the amount of rainfall for many months at Sesheke station (cf. Gibson et al., 2010). This was ascribed to the heterogeneous environment around this reference station (cf. McCabe and Wood, 2006; Li et al., 2008; Gibson et al. 2011). The use of few daily ET calculations per month is likely to have also affected the results. As optical remote sensing data is affected by cloudy conditions, a limited number of clear-sky images were available per month, and the rain season (warm-wet days) was the worst affected. However, it is shown in equations 48 and 49 that the accuracy of monthly flux estimates directly depend on the number of daily calculations. The more daily calculations are used the higher the accuracy of the monthly estimates as it helps to cancel out the errors that may be introduced by extreme values (Gokmen, 2011- personal communication). This also means that the accurate estimation of daily fluxes themselves is needed to obtain reliable monthly flux outputs. In this regard, the problems associated with inadequate surface parametrisation may propagate into the estimated monthly fluxes. It was shown that use of NDVI to parameterise surface conditions

affected the accuracy of the estimated daily fluxes. Furthermore, the input data of the sunshine hours is likely to have affected monthly flux results in that errors in these values directly affect the ET estimates. In this study, the sunshine hours were extracted from global models instead of actual measurements from the ground stations. Therefore, the availability of basic meteorological data on the ground is very important for the successful implementation of the SEBS as it helps in the validation some of the input data.

As the population continues to grow, the need to increase food production and provide safe drinking water will exert enormous pressure on scarce and dwindling fresh water resources. For this reason, stakeholders now need detailed information about water resources to prudently safeguard these resources at their disposal and sustain the high standard of living in society. In this regard, research and application of remote sensing data and modelling techniques as used in this study is critical to informed planning, monitoring and management of water resources in water limited areas like the semi-arid Barotse Sub-basin of South-Western Zambia. Despite all the challenges in obtaining suitable reference data, the SEBS algorithm has been proven in this study as a realistic and robust method for estimating the spatial and temporal variability of actual fluxes at a larger scale as compared to point based estimates. Policy and decision makers in Government, private sector and civil society can use this to enhance agricultural food production (e.g determining crop water deficit and requirements), monitor the legal compliance of water use in agricultural areas, and to quantify water resources and determine water use of vulnerable ecosystems at a catchment level (e.g calculating distributed ET to be used in catchment water balance). This is possible as the model quantifies the spatial-temporal actual evaporative fluxes or actual amount of water used by each land cover type.

This study is therefore important in Zambia within the context of the evolving water sector reforms in which water resources management is to be initiated at a catchment level. The experiences, challenges and prospects can thus be drawn from this study by improving upon the methodologies used and applying them in all the Zambian catchments to quantify the evaporative losses and other hydrological fluxes.

CHAPTER 6: CONCLUSION AND RECOMMENDATIONS

The conclusion and recommendations given in this Chapter are summarised as follows:

6.1 Conclusion

The following are the conclusions:

i) The spatial and temporal variability of AET was clearly charaterised over the study area using the SEBS algorithm and MODIS satellite imagery with the advantage over point based estimates in that fluxes attributed to different land cover types were retrieved. This has potential uses such as monitoring water use over crop lands. The estimated fluxes varied by land cover type over warm-wet, cool-dry and hot-dry days. Water bodies, closed to open regularly flooded vegetation and forested areas had higher rates with a low variation over these days whereas mosaic vegetation/cropland and closed to open grassland had the lowest rates of ET with a variation of up 64.1 and 71.1 % respectively between warm-wet and hot-dry days (Objective number 1);

ii) Generating monthly AET from daily fluxes and sunshine data provides a possibility of quickly assessing evaporative losses at a monthly time-scale. However, the accuracy of this method is significantly limited as it depends on the number and accuracy of daily ET calculations used, and availability of reliable sunshine data. The former presents practical difficulties as it is impossible to obtain many clear-sky images especially in the rain season due to cloudy conditions (Objective number 2);

iii) Point-based estimates of ET calculated using FAO-Penman-Montieth method gives the reference ET for a grass surface with constant parameters. These conditions are rarely met at weather stations leading to over and underestimation of ET. At Sesheke station, PET rates were higher on hot-dry days (~6.3 mm day^{-1}) and warm-wet days (~5.7 mm day^{-1}) but lower on cool-dry days (~4.9 mm day^{-1}) (Objective number 3);

iv) Estimated daily fluxes were in physical agreement with PET on cool-dry and hot-dry days. These fluxes, on the other hand, were physically inconsistent on warm-wet days. Due to the possible violation of the assumptions of PET as stated in item (iii) above, however, it difficult to ascertain the accuracy of this comparison. The comparison with ECMWF estimates showed that the SEBS fluxes were in better agreement at

Sesheke station than Kamanga station. At a monthly step, however, the comparison with ECMWF and rainfall estimates indicated that the modelled fluxes were not in good agreement though they were generally below PET. This was attributed to meteorological input data especially air temperature, and surface roughness which seem to be poorly estimated from NDVI over forests (Objective number 4); and

v) With accurate surface parameterisation and meteorological input data, remote sensing and the SEBS model can be successfully used to quantify spatial-temporal evaporative fluxes over heterogeneous areas such as the semi-arid Barotse Sub-basin and contribute towards water resources management.

6.2 Recommendations

The recommendations to UNZA-IWRM Centre are:

(i) Spatially distributed near surface air temperature and soil moisture should be used in the modelling process to get more accurate estimates of biogeophysical parameters and actual evapotranspiration in the semi-arid Barotse Sub-basin;

(ii) An investigation into the best approach for estimating roughness height for momentum transfer in the semi-arid Barotse Sub-basin must be done and the results should be used to improve the accuracy of actual evapotranspiration estimates rather than using empirical relationships with NDVI which saturates at high vegetation densities and the accuracy of the relationship is vegetation and season-dependent;

(iii) Actual measurements of turbulent heat fluxes must be carried out using experimental flux towers so that the results can be used for a decisive validation process;

(iv) As the accuracy of the monthly evaporative fluxes estimated from daily ET in combination with meteorological data is limited by the number of clear-sky images in cloud conditions, especially in the rain season, the use of radar remote sensing data should be incorporated to fill this gap. Alternatively, value compositing should be applied using all the available images that are cloud free and partly clear per month.

(v) High resolution satellite imagery (such as Aster, Landsat and ESA`s future Global Monitoring for Environment and Security (GMES) satellite imagery of the Sentinel 2 and 3) should be used along with MODIS to further characterise ET in the area.

The recommendation to the Government of Republic of Zambia is to rehabilitate existing meteorological stations and set up new ones in catchments with less dense measurements as this will reduce the scarcity of input data and allow for interpolation of variables required for precise quantification of water resources in heterogeneous areas such as the semi-arid Barotse Sub-basin.

REFERENCES

Albertson, J.D., Katatul, G.G., and Wiber, P., (2001), Relative importance of local and regional controls on coupled water, carbon and energy fluxes, Adv. Water Resour., 24,1103-1118, ISSN:0309-1708.

Allen, G.R., Cuenca, H.R., Jensen, E.M., Blantchley, K.R., and Erpenbeck, M.J., (1990), Evapotranspiration and irrigation water requirements, American Society of Civil Engineers, New York (USA), p. 332.

Allen, R.G., Pereira, L.S., Raes, D., and Smith, M., (1998), Crop evapotranspiration. guidelines for computing crop water requirements -FAO Irrigation and Drainage Paper No. 56 FAO, Rome, Italy, p. 300.

Allen, R.G.,Tasumi, M., Morse, A., and Trezza, R., (2005a), A Landsat-based energy balance and evapotranspiration model in Western US water rights regulation and planning. Irrigation and Drainage Systems, 19: 251–268.

Allen, R.G., Tasumi, M., and Morse, A., (2005b), Satellite-based evapotranspiration by METRIC and LANDSAT for western states water management, Presented at the US Bureau of Reclamation Evapotranspiration Workshop, Feb 8-10, 2005 – Ft. Collins, Colorado. ttp://www.idwr.idaho.gov/gisdata/ET/allen_et_al_metric_summary_paper2.pdf.

Allen, R.G., Pruitt, W.O., Raes, D., Smith, M., and Pereira, L.S., (2005c), Estimating evaporation from bare soil and the crop coefficient for the initial period using common soils information, Journal of Irrigation and Drainage Engineering. 131 (1): 14-23.

Allen, R. G., Tasumi, M., Trezza, R., (2007), Satellite-based energy balance for mapping evapotranspiration with internalized calibration (METRIC)-model, Journal of Irrigation and Drainage Engineering, 133 (4): 380-394.

Alvarez, J.A.G., (2007), Effects of land cover changes on the water balance of Palo Verde Wetland, Cost Rica, MSc. Thesis, ITC, The Netherland, pp. 13-72.

Anderson, M. C., Kustas, W. P., and Norman, J. M., (2003), "Up scaling and downscaling – A regional view of the Soil-Plant Atmosphere continuum, Agron. J., 95, 1408–1423.

Angstrom, A., (1929), On the Atmospheric Transmission of Sun Radiation and on Dust in the Air, Geografis. Annal., 2 (3): 130-159.

Archer, D. R., (1971), "Temperature, humidity, sunshine and winds" In Davies, D. H. (ed): Zambia in Maps, University of London Press, London, 22–23.

Aregheore, E.M., (2006), Zambia: Country pasture/forage resource profiles, www.fao.org/ag/AGP/AGPC/doc/countprof/zambia/zambia2/htm.

Badola, A., (2009), Validation of Surface Energy Balance System (SEBS) over forest land cover and sensitivity analysis of the model, MSc thesis, International Institute for Geo-information Science and Earth Observation, The Netherlands, p. 59.

Bastiaanssen, W.G.M., Menenti, M., Feddes, R.A., and Holtslag, A.A.M., (1998a), A remote sensing surface energy balance algorithm for land (SEBAL), Formulation, Journal of Hydrology, 212-213:198-212.

Bastiaanssen, W.G.M., Pelgrum, H., Wang, J., Ma, Y., Moreno, J., Roerink, G.J., and van der Wal, T., (1998b), The Surface Energy Balance Algorithm for Land (SEBAL), Part 2: validation, Journal of Hydrology 212-213: 213-229.

Beven, K.J., (2001), Rainfall-Runoff Modelling, The Primer, John Wiley & Sons, Lancaster, UK, p. 76.

Bicheron, P., Brockmann, C., Schuten., L., Vancutsen, C., Huc, M., Boutemp, S., Leroy, M., Achard, F., Herold, M., Ranera, F., and Arino, O., (2008), The ESA-Globcover Project, MEDIAS-France, pp. 6-43.

Boegh, E., and Soegaard, H., (2004), Remote sensing based estimation of evapotranspiration rates, International Journal of Remote Sensing, 25, 2535-2551.

Bolstad, P.V., and Gower, S. T., (1990), Estimation of leaf area index in fourteen southern Wisconsin forest stands using a portable radiometer, Tree Physiol., 7: 115-124.

Boucher, O., Myhre, G., and Myhre, A., (2004), Direct human influence of irrigation on atmospheric water vapour and climate, clim.Dyn, 22: 597-603.

Bowen, I.S., (1926), The ratio of heat losses by conduction and by evaporation from any water surface, physical Review, 27: 779-788.

Braun, P., Maurer, B., Mueller, G., Gross, P., Heinemann, G., and Simmer, C., (2001), An integrated approach for the determination of regional evapotranspiration using mesoscale modelling, remote sensing and boundary layer measurements. Meteorology and Atmospheric Physics, 76: 83-105.

Brunner, P., Bauer, P., Eugster, M., and Kinzelbach, W., (2004), Using remote sensing to regionalize local precipitation recharge rates obtained from the Chloride Method, Journal of Hydrology., 294: 241– 250.

Brutsaert, W., (1982), Evaporation into the atmosphere: Theory, History, and applications, Reidal Publishing, New York, p. 299.

Brutsaert, W., Hsu, A.Y., and Schmugge, T.J., (1993), Parameterization of surface heat fluxes above forest with satellite thermal sensing and boundary layer soundings, Journal of Applied Meteorology, 32 (5): 909-917.

Brutsaert W., (1999), Aspects of bulk atmospheric boundary layer similarity under free convective conditions, Reviews of Geophysics, 37 (4): 439-451.

Campbell, G.S., and Norman, J.M., (1998), An Introduction to environmental biophysics, Springer, New York, p. 286.

Carlson, T.N., Capehart, W. J., and Gillies, R.R., (1995). A new look at the simplified method for remote-Sensing of daily evapotranspiration. Remote Sensing of Environment, 54, 61-67.

Central Statistics Office (CSO), (2011), 2010 Census of Population and Housing, Preliminary Population Figures, GRZ, Lusaka, p. 17.

Chang, J.H., (1968), Climate and agriculture and ecological survey, University of Hawaii, Aldine Publishing Company, Chicago, (USA), p. 304.

Chen, J.M., Chen, X., Ju, W., and Geng, X.,(2004),Distributed hydrological model for mapping evapotranspiration using remote sensing inputs. Journal of Hydrology, 305: 15–39.

Choudhury, B.J., Ahmed, N. U., Idso, S.B., Reginato, R.J., and Daughtry, C.S.T., (1994), Relations between evaporation coefficients and vegetation indices studied by model simulations, Remote Sensing of Environment, 50 (1): 1-17.

Cohen T., Matos J.P., Boillat J. L., Schleiss A.J. and Portela, M.M., (2010), Semi-distributed hydraulic hydrological modelling of the Zambezi River Basin Challenges and expectations, 11th WaterNet/WARFSA/GWP-SA symposium, Victoria Falls, Zimbabwe, pp. 80-92.

Consoli, S., D'Urso, G., and Toscano, A., (2006), Remote sensing to estimate ET-fluxes and the performance of an irrigation district in southern Italy. Agricultural Water Management., 81: 295–314.

Courault, D., Seguin, B., and Olioso, A., (2005), Review on estimation of evapotranspiration from remote sensing data: From empirical to numerical modelling approaches. Irrigation and Drainage Systems, 19: 223–249.

Crago, R.D., and Brutsaert, W., (1996), Daytime evaporation and the self self-preservation of the evaporative fraction and the Bowen ratio, J.Hydro., 178, 241-255.

Crago, R.D, and Crowley, R., (2005), Complementary relationships for near instantaneous evaporation. Journal of Hydrology, 300: 199–211.

Desanker, P.V., Frost, P.G.H., Frost, C. O., Justice, C.O., and Scholes, R.J., (1997), The Miombo Network: Framework for a terrestrial transect study of land-use and land-cover change in the miombo ecosystems of Central Africa, IGBP Report 41, The International Geosphere-Biosphere Program (IGBP), Stockholm, p. 74.

Dingman, P., (2002), Physical hydrology, Prentice Hall, London, p. 44.

European Centre for Medium Range Weather Forecast (ECMWF), http://www.ecmwf.int/.

Food and Agriculture Organisation (FAO) and Government of Republic of Zambia (GRZ), (1986), Soil map of Zambia,
www.eusoils.jrc.eceuropa.eu/esdb_archive/EUDASM/Africa/lists/si_czm_html.

Food and Agriculture Organisation (FAO), (2002), The FAO Local climate estimator, www.fao.or/sd/2002/EN1803a_en html.

Feddes, R.A., and Lenselink, K.J., (1994), Evapotranpiration, In: Draiange principles and applications, ILRI publication, Wageningen, No.16, 145-173.

Flint, L., (2006), Climate change, vulnerability and the potential for adaptation: case-study – the Upper Zambezi Valley region of Western Zambia, University of Copenhagen, Denmark, p. 17.

Frank, A.B., (2008), Evapotranspiration from northern semiarid grassland, Agronomy journal, 56: 247-260.

French, A.N., Jacob, F., Anderson, M.C., Kustas, W.P., Timmermans, W., Gieske, A., Su, Z., Su, H., McCabe, M.F., Li, F., Prueger, J., and Brunsell, N., (2005), Surface energy fluxes with the Advanced Spaceborne Thermal Emission and Reflection Radiometer (ASTER) at the Iowa 2002 SMACEX site (USA), Remote Sensing of Environment, 99 (1-2): 55-65.

Garatuza-Payan, J., and Watts, C.J, (2003), The use of remote sensing for estimating ET in NW Mexico. ICID Workshop on Remote Sensing of ET for Large Regions, 17 Sept. 2003.

Gash, J.H.C., and Shuttleworth, J., (2007), Evaporation, In: McDonnell, J.J. (Ed.), Benchmark Papers in Hydrology, International Association of Hydrological Sciences (IAHS), Wallingford, p. 131.

Gebreyesus, M. G., (2009), Validation of RS approaches to model surface characteristics in hydrology: a case study in Guarena Aquifer, Salamanca, Spain, MSc thesis, International Institute for Geo-information Science and Earth Observation, The Netherland, p. 65.

Gibson, L. A., Münch, Z., Engelbrecht, J., Petersen, N., and Conrad, J. E.,(2010), Remote sensing as a tool for resources assessment towards the determination of the legal compliance of surface and groundwater use, Water Research Commission, Pretoria, South Africa, WRC Report No. 1690/1/09, 2010.

Gibson, L.A., Münch, Z., and Engelbrecht, J., (2011), Particular uncertainties encountered in using a pre-packaged SEBS model to derive evapotranspiration in a heterogeneous study area in South Africa. Hydrol. Earth Syst. Sci. 15 (1), 295–310.

Gieske, A.S. M., (2003), Operational solutions of actual evapotranspiration, In: Simmers, I., (Ed.), Understanding water in a dry environment: hydrological processes in arid and semi-arid zones, Rotterdam, pp. 65-114.

Global Land Cover (2000), http://www.gvm.jrc.it/glc2000.

Gokmen, M., Vekerdy, Z., and Verhoef, W., (2012a), (Submitted), Assessing groundwater depletion in a semi-arid region using RS-based evapotranspiration and precipitation estimates p. 72.

Gokmen, M., Vekerdy, Z., Verhoef, A., Verhoef, W., Batelaan, O., and van der Tol, C., (2012b), Integration of soil moisture in SEBS for improving evapotranspiration estimation under water stress conditions, In: Remote sensing of environment,121(2012) pp. 261-274.

Gokmen, M., (2011), personal communication on deriving time series of hydrological fluxes, South Africa, 4-14 December, 2011

Gupta, R.P., (2003), Remote Sensing Geology, Springer-Verlag Berlin Herdlberg, ISBN 3-540-43185-3, pp. 1-190.

Hailegiorgis, W.S., (2006), Remote sensing analysis of summer time evapotranspiration using SEBS algorithm: A case study of Regge and Dinkel, The Netherlands, an unpublished M.SC. Thesis submitted to the International Institute for Geo-information Science and Earth Observation, pp. 42-88.

Ham, M.J., and Heilman, L.J., (2003), Experiment test of density and energy-balance corrections on carbon dioxide flux as measured using open-path Eddy Covariance, Agronomy Journal, 95: 1393-1403.

Hemakumara, H.M., Chandrapala, L., and Moene, A.F., (2003), Evapotranspiration fluxes over mixed vegetation areas measured from large aperture scintillometer, Agricultural Water Management, 58: 109–122.

Huntington, T., (2006), Evidence for intensification for the global water cycle: review and synthesis, Journal of Hydrology, 329, pp. 83-95.

Hutchinson, P., (1974), The climate of Zambia, Zambia Geographical Association, Occasional Study No. 7: 95.

Huxman, T., Wilcox, B., Breshears, D., Scott, R., Snyder, K., Small, E., Hultine, K., Pockman, W. and Jackson, R., (2005), Ecohydrological implications of woody plant encroachment Ecology, 86: 308–319.

Irmak, A., and Irmak, S., (2008), Reference and crop evapotranspiration in south central Nebraska: II. Measurement and estimation of actual evapotranspiration, Journal of Irrigation and Drainage Engineering, 134 (6): 700-715.

Irmak, S., (2008), Evapotranspiration, In: Jorgensen, S.E., and Fath, B.D., (eds.), Encyclopaedia of Ecology, Manuscript No. 270, 1st Edition, Elsevier B.V., Oxford, UNL Extension Journal Series No. 1037, pp. 1432-1439.

Irmak, S., (2009), Estimating crop evapotranspiration from reference evapotranspiration and crop coefficients**,** University of Nebraska-Lincoln Extension Neb Guide G1994, p. 4.

Iqbal, M., (1983), An introduction to solar radiation, Academic Press, Canada, Ontario, p. 416.

Jackson, R.D., Reginato, R.J., and Idso, S.B., (1977), Wheat canopy temperature: A practical tool for evaluating water requirements. Water Resource Research 13: 651–656.

Jeanes, K. W., (1991), Landscapes and grasslands of Western Province, Zambia, Dept. of Agriculture, Western Province, p. 14.

Jiang, L. and Islam, S., (2001), Estimation of surface evaporation map over southern Great Plains using remote sensing data. Water Resources Research, 37, 329–340.

Jia, L., Su, Z., Van den Hulk, B., Menenti, M., Moene, A., De Bruin, H.A.R., Yrisarry, J.J.B., Ibenez, M., and Cuesta, A., (2003), Estimation of sensible heat flux using the Surface Energy Balance System (SEBS) and ATSR measurement, physics and Chemistry of the Earth, 28 (1-3): 75-88.

Jia, L., Xi, G., Liu, S., Huang, C., Yan, Y., and Liu, G., (2009), Regional estimation of daily to annual regional evapotranspiration with MODIS data in the Yellow River Delta wetland. Hydrol. Earth Syst. Sci. 13 (10): 1775–1787.

Johnson, H., (ed.), (1977), Encyclopaedia of Science and Technology, vol. 5, MacGraw-Hill Inc, London, p. 1204.

Justice, O.C., Vermote, E., John, R.G., and Townshend, R., (1998), The Moderate Resolution Imaging Spectroradiometer (MODIS): Land Remote Sensing for Global Change Research, Ieee Transaction on Geoscience and Remote Sensing, 36 (4): 1228-1249.

Kabika, J., Marker, P.A., Munck, N. S. M., Nyambe, I. A, Bauer-Gottwein, P., and Larsen, P. F., (2010), Recharge Estimation Using base Flow Recession in the Barotse sub-basin, 11th Waternet WARFSA/GWP-SA Symposium, Victoria Falls, Zimbabwe, 2010, pp. 166-177.

Kaboh-bah, A., Madamombe, C.E., and Rwasoka, D.T., (2011), Estimation of hyper-temporal evapotranspiration over the Middle-Zambezi using the GEONETCAST toolbox and SEBS, in 12th Waternet WARFSA/GWP-SA Symposium, Maputo, Mozambique, 2011, pp. 31-40.

Kaufman, Y.J., Herring, D.D., Ranson, K.J., and Collatz, G.J., (1998), Earth observing system AM1 mission to Earth, Ieee Transaction on Geoscience and Remote Sensing, 36 (4): 1045-1055.

Khan, S.I., Hong, Y., Vieux, B., and Liu, W., (2010), Development and evaluation of actual evapotranspiration estimation algorithm using satellite remote sensing and meteorological observation network in Oklahoma in: International Journal of Remote Sensing, Vol. 31, No. 14, 20 July, 3799-3819, online ©Taylor and Francis,@ www.tandf.co.uk/journal.

Kite, G.W., and Droogers, P., (2000), Comparing evapotranspiration estimates from satellites, hydrological models and field data, Journal of Hydrology, 229 (1-2): 3-18.

Kongo, V.M., Jewitt, G.P.W., 2006), Preliminary investigation of catchment hydrology in response to agricultural water use innovations: A case study of the Potshini catchment – South Africa, Physics and Chemistry of the Earth, 31: 976–987.

Knorr, W., and Schulz, J., (2001), Using satellite data assimilation to infer global soil moisture status and vegetation feedback to climate in: Beniston, M., and Verstraete, M.M., (eds.), (2003), Remote sensing and climate modelling synergies and limitations, Kluwer Academic Publishers, New York, USA, p. 275.

Kustas, W.P., and Daughtry, C.S.T., (1989), Estimation of soil heat flux/net radiation ratio from spectral data, Agric. Forest Meteorol., 49: 205-223.

Kustas, W. P., Perry, E. M., Doraiswamy, P.C., and Moran, M.S., (1994), Using Satellite Remote-sensing to extrapolate evapotranspiration estimates in time and space over a semiarid rangeland basin. Remote Sensing of Environment, 49: 275-286.

Kustas, W.P., and Norman, J.M., (1999), Evaluation of soil and vegetation heat flux predictions using a simple two-source model with radiometric temperatures for partial canopy cover, Agricultural and Forest Meteorology, 94: 13–29.

Lane, S.N., Brookes, C.J., Kirkby, M.J., and Holden, J., (2004), A network-index-based version of TOPMODEL for use with high-resolution digital topographic data Hydrol. Process, 18: 191–201.

Lee, J.H., Timmerman, J., Su, Z., and Mancini, M., (2012), Calibration of aerodynamic roughness over the Tibetan Plateau with Ensemble Kalman Filter analysed heat Flux, Hydro.Earth Syst. Sci. 16: 42291-4302.

Li, F., Kustas, W. P., Anderson, M. C., Prueger, J. H., and Scott, R. L., (2008), Effect of remote sensing spatial resolution on interpreting tower-based flux observations, Remote Sens. Environ., 112, 337– 349, 2008.

Li, X., (2001), Estimation of Urumqi River Basin Evaporation with Remote Sensing, M.Sc. Thesis in Hydrological Engineering, UNESCO-IHE, Delft, p. 44.

Lin, W., (2006), Satellite based regional scale evapotranspiration in the Hebei Plain, Northeastern China, M.Sc. thesis, International Institute for Geo-information Science and Earth Observation, The Netherlands, p. 66.

Liang, S., (2001), Narrowband to broadband conversions of land surface albedo I: Algorithms. Remote Sensing of Environment 76 (2): 213-238.

Lloyd, W.G., (1992), Bowen-ratio measurements, Evapotranspiration measurements of native vegetation, Owens Valley, California, US Geological Survey, Water-Resources Investigations Report 91-4159:5-18.

McCabe, M.F., and Wood, E.F., (2006), Scale influence on the remote estimation of evapotranspiration using multiple satellite sensors, Remote Sens. Environ., 105: 271-285.

MacClatchey, R.A., and Selby, J.E., (1972), Atmospheric transmittance from 0.25 to 38.5 mm: computer code LOWTRAN-2, Air Force Cambridge Research Laboratories, AFCRL-72 0745, Environ. Res. Paper 427.

Malone, R.W., Stewardson, D.J., Bonta, J.V., and Nelsen, T., (1999), Calibration and quality control of the Coshocton Weighting Lysimeters, Transaction of the ASAE/ American Society of Agricultural Engineering, 42 (3): 701-712.

Massman, W.J., (2000), A simple method for estimate frequency response corrections for eddy covariance systems, Agricultural and Forest Methodology, 104: 185-198.

Menenti, M., and Choudhury, B.J., (1993), Parametrisation of land surface evapotranspiration using a location dependent potential evapotranspiration and surface temperature range in: Bolle, H.J. (Ed.), Exchange Processes at the Land Surface for a Range of Space and Time Scales, IAHS, pp. 561–588.

Ministry of Energy and Water Development (MEWD) and Japan International Cooperation Agency (JICA), (1995), The study on National Water Resources Master Plan in the Republic of Zambia , Final Report, Supporting Report-B, Meteorology, Yachiyo Engineering Co. Ltd, pp. 31-47.

Mohamed, A., Kongo, V., Murwira, A., and Makaya, E., (2010), Remote sensing based estimation of evapotranspiration among diffferernt land cover types in the Mkindo catchment, Upper Wami Basin- Tanzania, 11th Waternet WARFSA/GWP-SA, Symposium,Victoria Falls, Zimbabwe, pp. 258-273.

Monin, A. S., and Obukhov, A. M., (1954), Basic laws of turbulent mixing in the surface layer of the atmosphere, Tr.Akad. Nauk SSSR Geophiz. Inst., 24 (151): 163-187.

Montieth, J.L., (1965), Evaporation and environment, 19th Symposia of the society for experimental biology, Cambridge University Press, vol. 19 pp. 205-234.

Monteith, J.L., and Unsworth, M.H., (1990), Principles of environmental physics, Edward Arnold, London, pp. 23-78.

Moran, M.S., (2004), Thermal infrared measurements as an indicator of plant ecosystem health, in: Thermal remote sensing in land surface processes, edited by: Quattrochi, D. A., and Luvall, J.,Taylor and Francis, CRC Press, Boca Raton, USA, 257–282.

Morse, A., Kramber, W.J., Allen, R.G.,and Tasumi, M., (2006), Mapping evapotranspiration using Landsat and the METRIC evapotranspiration model, presented at 2006 ASPRS Annual Meeting–Reno, p. 23.

Mu, Q., Heinsch, F.A., Zhao, M., and Running, S.W., (2007), Development of a global evapotranspiration algorithm based on MODIS and global meteorology data, Remote Sensing of Environment, 111, pp. 519-536.

Muchinda, M.R. (1992), “25 years of meteorological service in Zambia (1967-1992)” Zambia Meteorological Department under UNDP/WMO project

Mücher, C.A., Steinnocher, K., Champeaux, J.L., Griguolo, S., Wester, K., and Loudjani, P., (2001), Land cover characterization for environmental monitoring of Pan-Europe, Wageningen University and Research Centre, Centre for Geoinformation: Wageningen, http://cgi.girs.wageningenur. nl/cgi/projects/eu/pelcom/public/index.htm.

Neale, C.M.U., and Vinokullo, R.K., (2005), A hybrid surface energy balance approach for the estimation of evapotranspiration in agricultural areas, Earth Observation for vegetation monitoring and water management, Napoli, 24-25 October 2005, p. 10.

Norman, J.M., Kustas, W.P., and Humes, K.S., (1995), Source approach for estimating soil and agricultural and forest meteorology, 77 (3-4): 263-293.

Nishida, K., Nemani, R. R., Running, S. W., and Glassy, J. M., (2003), An operational remote sensing algorithm of land surface evaporation, Journal of Geophysical Research-Atmospheres, 108(D9), Art. No. 4270, doi:10.1029/2002JD002062.

Ogunbadewa, E.Y., (2010), Modelling water availability and climate change with satellite remote sensing data, Hydrocomplexity: New tools for solving wicked water problems, Kovacs Colloquium, July 2010, IAHS Publication 338.

Olioso, A., Inoue, Y., Ortega-Farias, S., Demarty, J., Wigneron, J.-P., Braud, I., Jacob, F., Lecharpentier, P., Ottle, C., Calvet, J.C., and Brisson, N., (2005), Future directions for advanced evapotranspiration modeling: Assimilation of remote sensing data into crop simulation models and SVAT models. Irrigation and Drainage Systems, 19: 377–412.

OMI Ozone Monitoring Project website: http://toms.gsfc.nasa.gov/ozone/ozone_v8.htm.

Parodi, G.N., (2006), Introduction to atmospheric correction of the visible and thermal imagery: Basic text, ITC, p. 58.

Parodi, G.N., (2009), SEBS4ILWIS Version 2.0 Flat Manual, ITC, The Netherland, p. 16.

Payero, J.O., Neale, C.M.U., Wright, J.L., and Allen, R.G., (2003), Guideline for validating Bowen ratio date, America Society Agricultural Engineers, 46 (4): 1051-1060.

Peilke, R., (1998), Interaction between the atmosphere and terrestrial ecosystems: influence on weather and climate, Glob. Change Biol. 4: 461-75.

Penman, H. L., (1948), Natural evaporation form open water, bare soil, and grass.Proc. Roy. Soc., 193: 120-146.

Pereira, S.L., Perrier, A., Allen, G.R., and Alves, I., (1996), Evapotranspiration: Review of concepts and future trends. In; Evapotranspiration and Irrigation Scheduling, Proceedings of the international conference, November 3-6, San Antonio, Texas: 109-115.

Perez, P.J., Castelli, F., and Martinez-Cob, A., (2008), A simple model for the estimation of the Bowen ratio from climatic factors for determining latent and sensible heat flux, Agricultural and Forest Meteorology, 148: 25-37.

Priestley, C.H.B., and Taylor, R.J., (1972), On the assessment of surface heat flux and evaporation using large-scale parameters. Month. Weather Rev. 100 (2): 81–92.

Prueger, H.J., Hatfield, J.L., Aase, J.K., and Pikul, J.L., (1997), Bowen-Ratio comparison with lysimeter evapotranspiration, Agronomy Journal, 89 (5): 730-736.

Rahman, H., and Dedieu, G., (1994), SMAC: a simplified method for the atmospheric correction of satellite measurements in the solar spectrum. International Journal of Remote Sensing, 15 (1): 123-143.

Raupach, M.R., (1994), Simplified expression for vegetation roughness length and zero displacement as a function of canopy height and area index, Boundary Layer Meteorology, 17 (1-2): 211-216.

Rauwerda, J., Roerink, G.J., Su, Z., (2002), Estimation of evaporative fractions by the use of vegetation and soil component temperatures determined by means of dual-looking remote sensing, Alterra,Green World Research, Wageningen, pp. 12-47.

Rivalland, V., Demarty, J., Olioso, A., Weiss, M., Rossello, P., Jacob, F., Inoue, Y., and Baret, F., (2005), Evapotranspiration monitoring using remote sensing measurement assimilated in a SVAT Model, geophysical Research Abstracts Vol. 7, 03457, 2005.

Roerink, G.J., Su, Z., and Menenti, M., (2000), S-SEBI: A simplified remote sensing algorithm to estimate Surface Energy Balance, Physics and Chemistry of the Earth (B), 25 (2): 147-157.

Rwasoka, D.T., Gumindoya, W., and Gwenzi, J., (2011), Estimation of actual evapotranspiration using the surface energy balance system (SEBS) algorithm in the Upper Manyame Catchment in Zimbabwe, J. Phys.Chem. Earth, doi:10.1016/j.pce.2011.07.035.

Scholes, R. J., Ward, D. E. and Justice, C. O.,(1996), Emissions of trace gases and aerosol particles due to vegetation burning in southern hemisphere Africa, Journal of Geophysical Research, 101(D19), 23677–23682.

Seguin B., and Ittier B., (1983), Using midday surface temperature to estimate daily evaporation from satellite thermal IR data, International Journal of Remote Sensing Environment, 4: 371–383.

Shan, X., van de Velde, R., Wen, J., He, Y., and Su ,Z., (2007), Regional evapotranspiration over the Arid Inland Heihe River Basin in Northwest China, ESA's Publications Division as Special Publication SP-655, Proceedings of the Dragon Programme final results.

Shuttleworth, W. J., and Wallace, J. S., (1985), Evaporation from sparse crops-An energy combination theory, Quarterly Journal of Royal of Meteorology Society, 11-855-893

Siacinji-Musiwa, J.M., (1999), Conservation tillage in Zambia: Some technologies, indigenous methods and environmental issues. In: Kaumbutho P.G. and Simalenga T.E. (eds.), (1999), Conservation Tillage with Animal Traction, A resource book of Animal Traction Network for Eastern and Southern Africa (ATNESA), Harare, Zimbabwe.

Sichingabula, M., (1998), Rainfall variability, drought and implications of it impacts on Zambia, 1886-1996 in: Servat, E., Hughes, D., Fritsch, J and Hulme, M., (eds.) (1998) Water resources variability in Africa during the XXth Century, IAHS publ. No. 252, pp. 125-134.

Singh, V.P., (1988), Hydrologic system rainfall-runoff modelling, vol. 1, Prentice Hall, ISBN: 0134480511, New Jersey, USA.

Sobrino, J.A., and Raissouni, N., (2000), Toward remote sensing methods for land cover dynamic monitoring. Application to Morocco, Int. J. Rem. Sens. 21 (2): 353–366.

Sobrino, J.A., Kharraz, J.E., Li, Z., (2003), Surface temperature and water vapour retrieval from MODIS data. Int. J. Rem. Sens. 24 (24): 5161–5182.

Su, Z., Schmugge, T., Kustas, W.P., and Massman, W.J., (2001), An evaluation of two models for estimation of the roughness height for heat transfer between the land surface and the atmosphere, Journal of Applied Meteorology, 40 (11): 1933-1951.

Su, Z., and Jacobs, C., (2001), Advanced earth observation: Land surface climate final report, Delft: Beleidscmmissie Remote Sensing (BCRS), UPS report, p. 57.

Su, Z., (2002), The Surface Energy Balance System (SEBS) for estimation of turbulent heat fluxes. Hydrology and Earth System Sciences, 6 (1): 85-99.

Su, Z., Yacob, A., He,Y., Boogaard, H., Wen, J., Gao, B., Roerink, G., and van Diepen, K., (2003), Assessing relative soil moisture with remote sensing data: theory, experimental validation, and application to drought monitoring over the North China Plain, Physics and Chemistry of the Earth, 28 (1-3): 89-101.

Su, Z., (2005), Estimation of the surface energy balance. In: Encyclopedia of hydrological sciences: 5 Volumes. / ed. by Anderson, M.G., McDonnell , and Chichester , J.J., Wiley and Sons, ISBN: 0-471-49103-9. Vol. 2 pp. 731-752.

Su, Z., (2006a), An introduction to the surface energy balance system (SEBS), Lecture notes, Presented at ESA TIGER Capacity Building Facility 1st Training Course on "Advanced optical remote sensing", 22-25 November 2006, Cape Town.

Su, Z., (2006b), Surface radiation budget: measurements and parametrisation, Power point Presentation, Presented at ESA TIGER Capacity Building Facility 1st Training Course on "Advanced optical remote sensing", 22-25 November 2006, Cape Town.

Su, H., Wood, E.F., McCabe, M.F., and Su, Z., (2007), Evaluation of remotely sensed evapotranspiration over the CEOP EOP-1 reference sites, Journal of Meteorological society of Japan, 85A, 439-459.

Shuttleworth, W.J., and Wallace, J.S., (1985), Evaporation from sparse crops-An energy combination theory, Quaterly Journal of the Royal Meteorology Society, 11: 893-855.

Sugita, M., and Brutsaert, W., (1991), Daily evaporation over a region from lower boundary layer profiles measured with radiosondes. Water Resour. Res. 27 (5): 747–752.

Suleiman, A.A, and Crago, R., (2004), Hourly and daytime evapotranspiration from grassland using radiometric surface temperature, Agronomy journal, 96: 384-390.

Suleiman, A.A., and Richie, J.T., (2003), Modelling soil water redistribution under second stage evaporation, Soil Sci.Soc. Am. J., 67 (2): 377-386.

Tasumi, M., Trezza, R., Allen, R.G., and Wright, J.L., (2005), Operational aspects of satellite-based energy balance models for irrigated crops in the semi-arid U.S. Irrigation and Drainage Systems, 19: 355–376.

Thornthwaite, C.W., (1948), An approach toward a rational classification of climate, Geogr. Rev., 38 (1): 55–94.

Timmermans, J., (2011), personal communication on the Surface Energy Balance System, South Africa, 4-14 December, 2011.

Törnros, T., (2010), Precipitation trends and suitable drought index in the arid/semi-arid southeastern Mediterranean region. Globe change: Facing risks and threats to water resources, Friend 2010, IAHS Publication 340: 157-163.

Van den Hurk, B., (2001), Energy balance based surface flux estimation from satellite data, and its application for surface moisture assimilation, Meteorol. Atmos. Phys. 76, 43-52.

van der Kwast, J., Timmermans, W., Gieske, A., Su, Z., Olioso, A., Jia, L., Elbers, J., Karssenberg, D., and de Jong, S., (2009), Evaluation of the Surface Energy Balance System (SEBS) applied to ASTER imagery with flux-measurements at the SPARC 2004 site (Barrax, Spain), Hydrol. Earth Syst. Sci. 13 (7): 1337–1347.

Vogt, J., and Niemeyer, S., (2001), Integration of operationally available remote sensing and synoptic data for surface energy balance modelling and environmental applications on the regional scale in: Beniston, M., and Verstraete, M.M., (eds.), (2003), Remote sensing and climate modelling synergies and limitations, Kluwer Academic Publishers, New York, USA, pp. 329-343.

Wang, K.C., Li, Z.Q., and Cribb, M., (2006), Estimation of evaporative fraction from a combination of day and night land surface temperature and NDVI: A new method to determine the Priestly-Taylor parameter. Remote Sensing of Environment, 102, 293-305.

Wieringa, J., (1993), Representative roughness parameters for homogenous terrain, In: Boundary Layer Meteorology, 63(1993), pp. 323-363.

Wilson, D., Reginato, R., and Hollet, J.K., (1992), Evapotranspiration measurements of native vegetation, Owenes Valley, California, USA. Geological Survey, Water Resources Investigations Report 91-4159: 1:4.

World Meteorological Organization, (WMO), (1992), International Meteorological Vocabulary, Second edition, WMO-No. 182, Geneva.

Zhang, B., Kang, S., Li, F., and Zhang, L., (2008), Comparison of three evapotranspiration models to Bowen ratio-energy balance method for vineyard in an arid desert region of northwest China, Agricultural and Forest Meteorology, 148: 1629-1640.

APPENDICES

Appendix 1: Formulae for calculating net radiation used in the estimation of potential evapotranspiration at Sesheke Meteorological Station, Semi-arid Barotse Sub-basin, South-Western Zambia

Extraterrestrial radiation for daily periods (R_a)

The extraterrestrial radiation for each day of the year and for different latitudes can be estimated from the solar constant, the solar declination and the time of the year by using the below (Allen et al., 1998).

$$R_a = \frac{24(60)}{\pi} G_{sc} d_r [\omega_s \sin(\varphi)\sin(\delta) + \cos(\varphi)\cos(\delta)\sin(\omega_s)]$$

where

R_a extraterrestrial radiation (MJ m^{-2} day^{-1}),
G_{sc} solar constant = 0.0820 (MJ m^{-2} min^{-1}),
d_r inverse relative distance Earth-Sun,
ω_s sunset hour angle (rad),
φ latitude (rad),
d solar decimation (rad).

R_a is expressed in the above equation in MJ m^{-2} day^{-1}. The corresponding equivalent evaporation in mm day^{-1} is obtained by multiplying R_a by 0.408. The latitude, φ, expressed in radians is positive for the northern hemisphere and negative for the southern hemisphere.

The conversion from decimal degrees to radians is given by:

$$[\text{Radians}] = \frac{\pi}{180}[\text{decimaldegrees}]$$

The inverse relative distance Earth-Sun, d_r, and the solar declination, δ , are given by:

$$d_r = 1 + 0.033\cos\left(\frac{2\pi}{365}J\right)$$

$$\delta = 0.409\sin\left(\frac{2\pi}{365}J - 1.39\right)$$

Where, J is the number of the day in the year 1 (1 January) and 365 or 366 (31 December).

The sunset hour angle, ω_s, is given by:

ω_s = arccos [-tan (φ) tan (δ)]

Daylight hours (N)

The daylight hours, N, are given by:

$$N = \frac{24}{\pi}\omega_s$$

Solar radiation (R_s)

If the solar radiation, R_s, is not measured, it can be calculated with the Angstrom formula which relates solar radiation to extraterrestrial radiation and relative sunshine duration:

$$R_s = \left(a_s + b_s \frac{n}{N}\right) R_a$$

where

R_s solar or shortwave radiation [MJ m^{-2} day^{-1}],
n actual duration of sunshine [hour],
N maximum possible duration of sunshine or daylight hours [hour],
n/N relative sunshine duration [-],
R_a extraterrestrial radiation [MJ m^{-2} day^{-1}],
a_s regression constant, expressing the fraction of extraterrestrial radiation reaching the earth on overcast days (n = 0),
a_s+b_s fraction of extraterrestrial radiation reaching the earth on clear days (n = N).

For a_s and b_s parameters, the values $a_s = 0.25$ and $b_s = 0.50$ the recommended where no calibration has not been done (Allen et al., 1998).

Clear-sky solar radiation (R_{so})

The calculation of the clear-sky radiation, R_{so}, when n = N, is required for computing net longwave radiation. The following formula was used:

$$R_{so} = (0.75 + 2\ 10^{-5} z) R_a$$

where z station elevation above sea level (m).

Net solar or net shortwave radiation (R_{ns})

The net shortwave radiation resulting from the balance between incoming and reflected solar radiation is given by:

$R_{ns} = (1\text{-}a)R_s$

where

R_{ns} net solar or shortwave radiation (MJ m^{-2} day^{-1}),
a is albedo, which is 0.23 for the hypothetical grass reference crop (dimensionless),
R_s the incoming solar radiation (MJ m^{-2} day^{-1}).
R_{ns} is expressed in the above equation in MJ m^{-2} day^{-1}.

Net longwave radiation (R_{nl})

The rate of longwave energy emission is proportional to the absolute temperature of the surface raised to the fourth power (Stefan-Boltzmann law). The net energy flux leaving the earth's surface is less than that emitted and given by the Stefan-Boltzmann law due to the absorption and downward radiation from the sky. Thus, the Stefan-Boltzmann law is corrected when estimating - the net outgoing flux of longwave radiation.

$$R_{nl} = \sigma\left[\frac{T_{maxK}^4 + T_{minK}^4}{2}\right](0.34 - 0.14\sqrt{e_a})\left(1.35\frac{R_s}{R_{so}} - 0.35\right)$$

where

R_{nl} net outgoing longwave radiation (MJ m^{-2} day^{-1}),
σ Stefan-Boltzmann constant (4.903 10^{-9} MJ K^{-4} m^{-2} day^{-1}),
$T_{max, K}$ maximum absolute temperature during the 24-hour period (K = °C + 273.16),
$T_{min, K}$ minimum absolute temperature during the 24-hour period (K = °C + 273.16),
e_a actual vapour pressure (kPa),
R_s/R_{so} relative shortwave radiation (limited to ≤ 1.0),
R_s measured or calculated. solar radiation (MJ m^{-2} day^{-1}),
R_{so} calculated clear-sky radiation (MJ m^{-2} day^{-1}).

Net radiation (R_n)

The net radiation (R_n) is the difference between the incoming net shortwave radiation (R_{ns}) and the outgoing net longwave radiation (R_{nl}):

$$R_n = R_{ns} - R_{nl}$$

Appendix 2: Visibility data at satellite overpass time at Katima Mulilo Meteorological Station, Namibia used in Semi-arid Barotse Sub-basin, South-Western Zambia study

No.	DATE	DAY OF YEAR	VISIBILITY (Km)
1.	21-11-2006	325	10.2
2.	30-11-2006	334	10.6
3.	02-12-2006	336	11.0
4.	04-12-2006	338	11.2
5.	12-01-2007	12	11.2
6.	14-01-2007	14	11.0
7.	14-02-2007	45	10.8
8.	18-02-2007	49	10.4
9.	12-03-2007	71	11.0
10.	15-03-2007	74	10.9
11.	16-04-2007	106	10.2
12.	23-04-2007	113	10.1
13.	16-05-2007	136	10.4
14.	23-05-2007	143	10.2
15.	17-06-2007	168	9.9
16.	19-06-2007	170	9.9
17.	10-07-2007	191	9.8
18.	16-07-2007	197	9.9
19.	13-08-2007	225	9.9
20.	20-08-2007	232	9.9
21.	12-09-2007	255	9.8
22.	14-09-2007	257	9.9
23.	14-10-2007	287	10.1
24.	19-10-2007	292	10.6

Source: Namibia Meteorological Services, Katima Mulilo, Namibia

Appendix 3: Formulae for estimating aerosol optical thickness used in the Semi-arid Barotse Sub-basin, South-Western Zambia study

According to Angstrom (1929), aerosol optical thickness for a certain wavelength can be written as:

$$K_{a\lambda} = \beta.\lambda^{-\alpha}$$

Where β is the turbidity coefficient, α is the wavelength exponent taken as 1.3 (Iqbal, 1983), λ is the wavelength (0.55 µm).

According to MacClatchey and Selby (1972), the turbidity coefficient (β) can be estimated form visibility data using the formula give below.

$$\beta = 0.55^{\alpha}\left(\frac{3.91}{\text{vis}} - 0.01162\right)[0.02472(\text{vis} - 5) + 1.32]$$

Where vis is visibility (in kilometers), α is the wavelength exponent 1.3 (Iqbal, 1983)

Appendix 4: The SEBS estimated histogram distribution of NDVI on warm-wet, cool-dry and hot-dry days over the Semi-arid Barotse Sub-basin, South-Western Zambia

A. NDVI distribution on warm-wet days

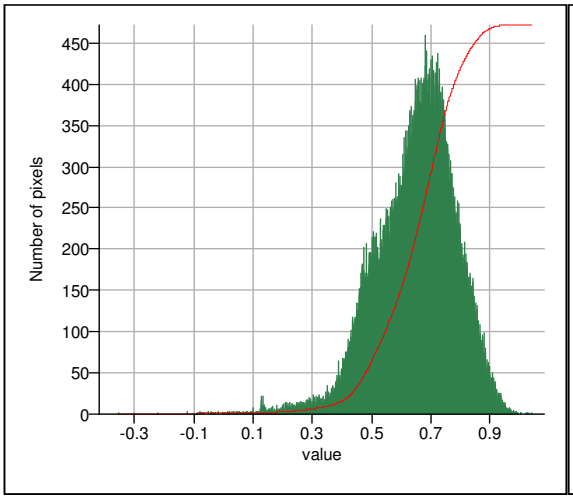

NDVI on DOY 325

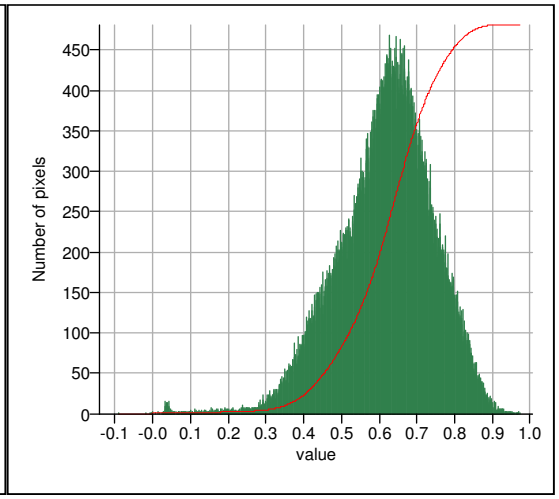

NDVI on DOY 334

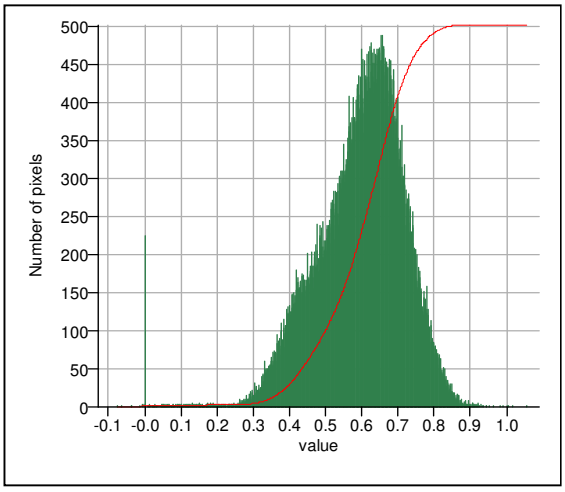

NDVI on DOY 336

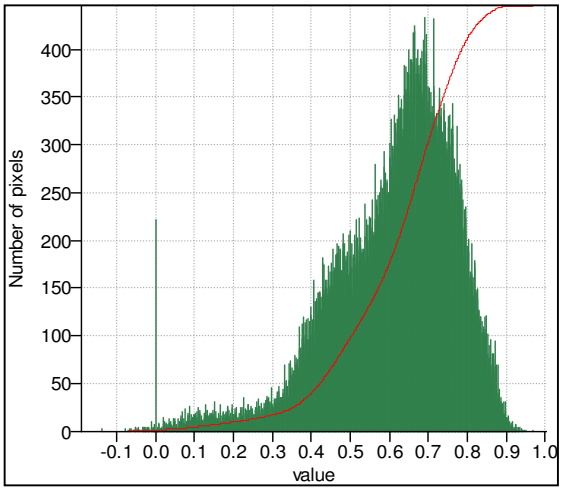

NDVI on DOY 338

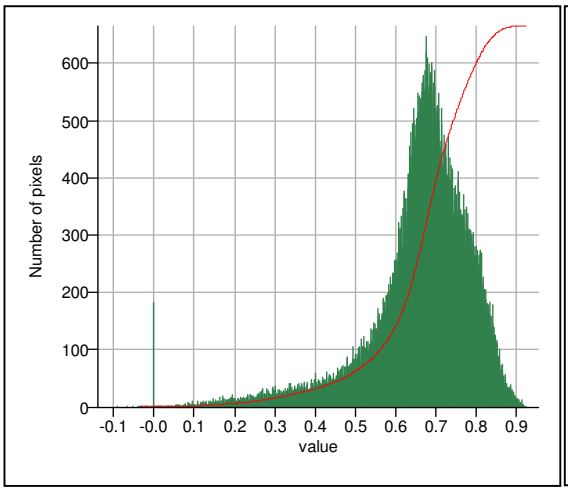

NDVI on DOY 12

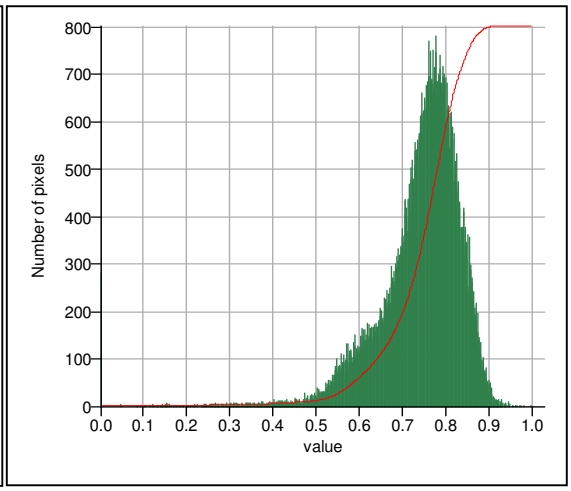

NDVI on DOY 14

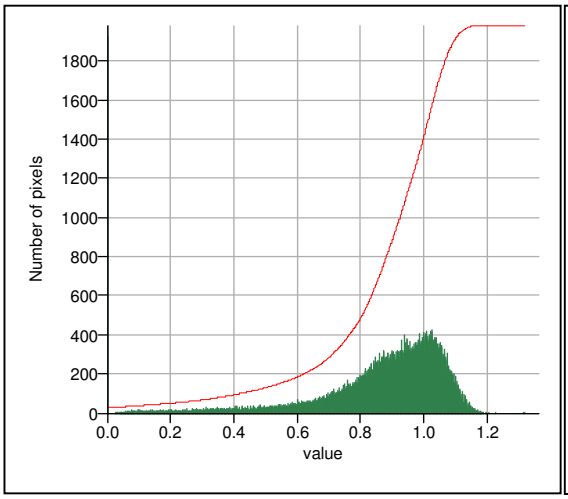

NDVI on DOY 45

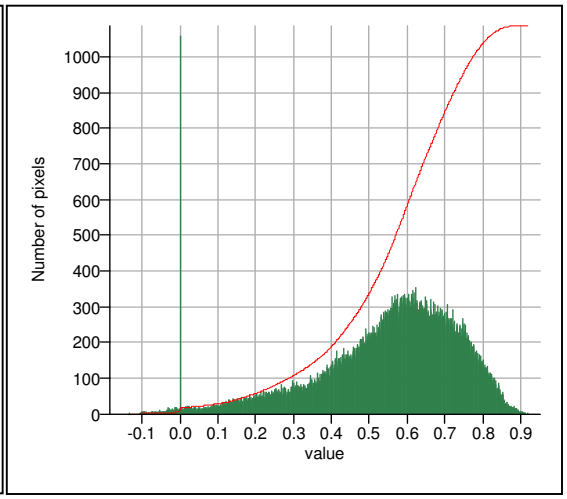

NDVI on DOY 49

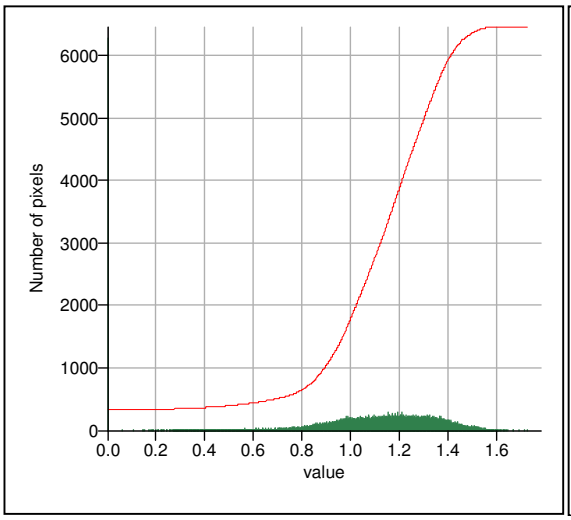

NDVI on DOY 71

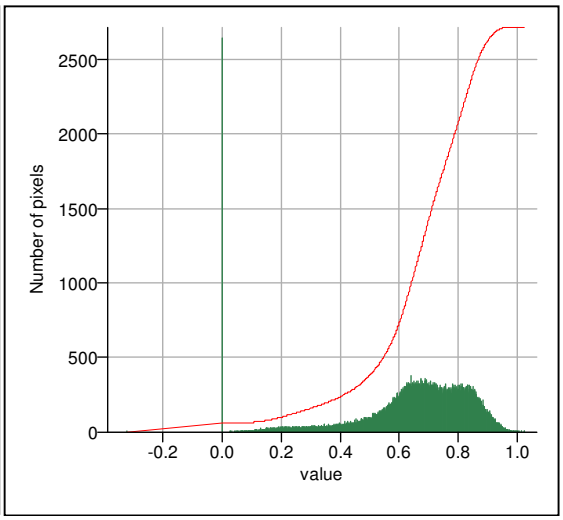

NDVI on DOY 74

B. NDVI distribution on cool-dry days

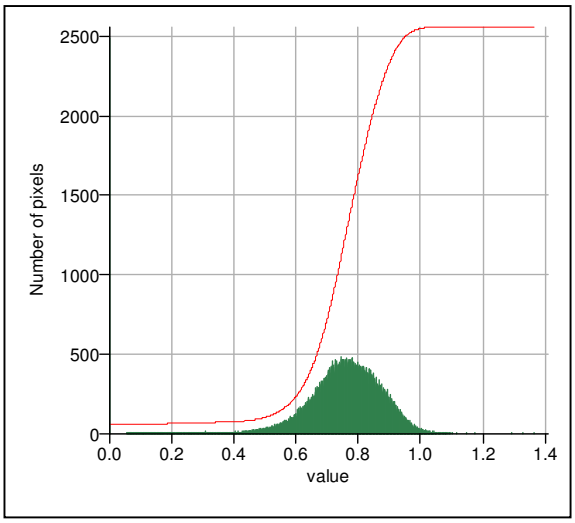

NDVI on DOY 106

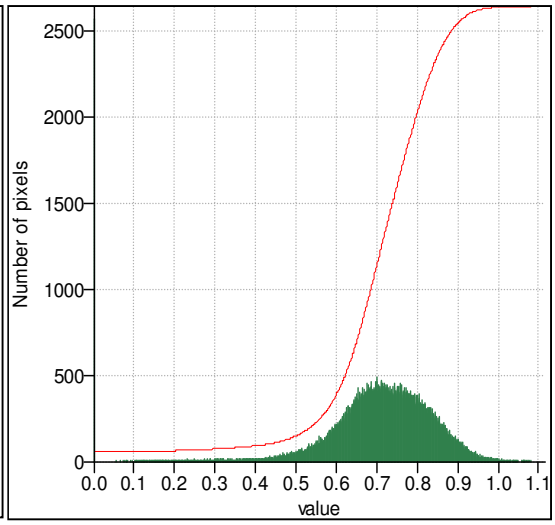

NDVI on DOY 113

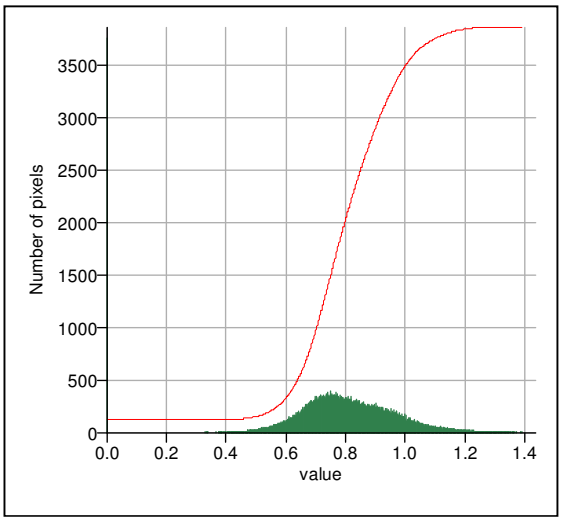

NDVI on DOY 136

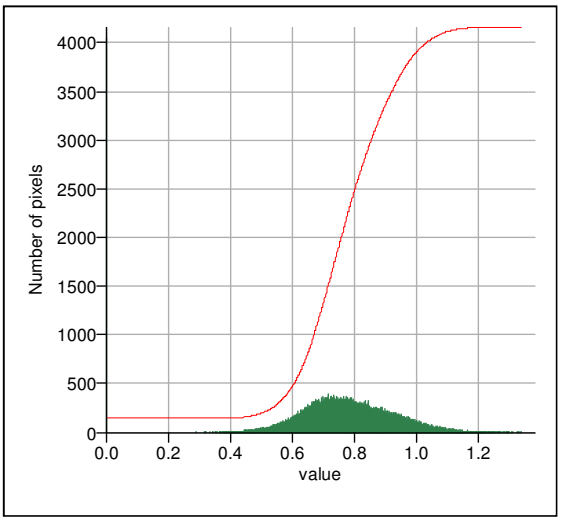

NDVI on DOY 143

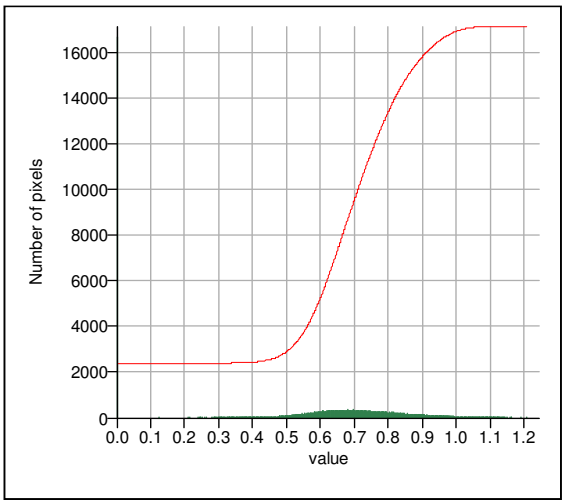

NDVI on DOY 168

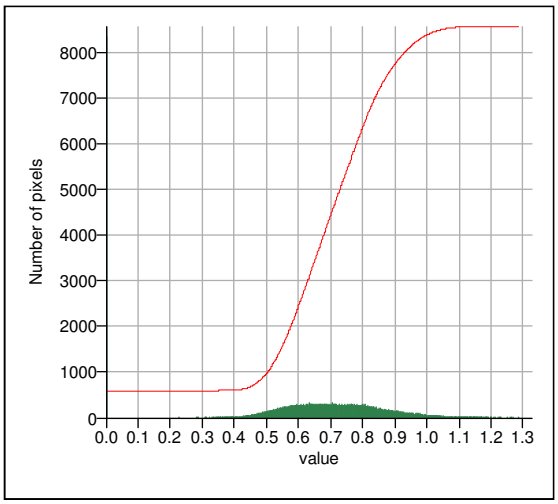

NDVI on DOY 170

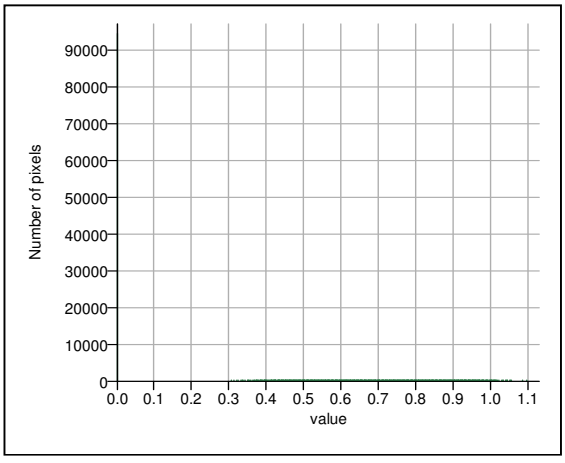

NDVI on DOY 191

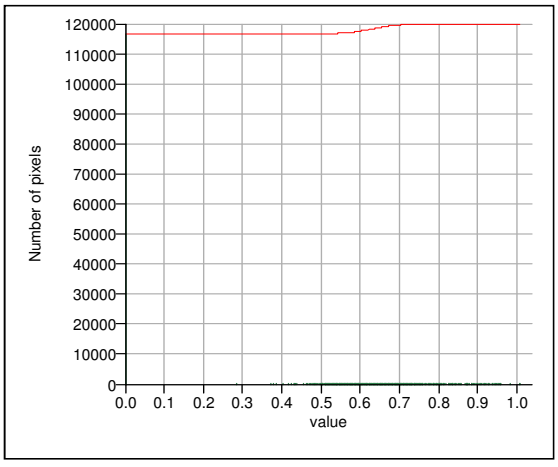

NDVI on DOY 197

C. NDVI distribution on hot-dry days

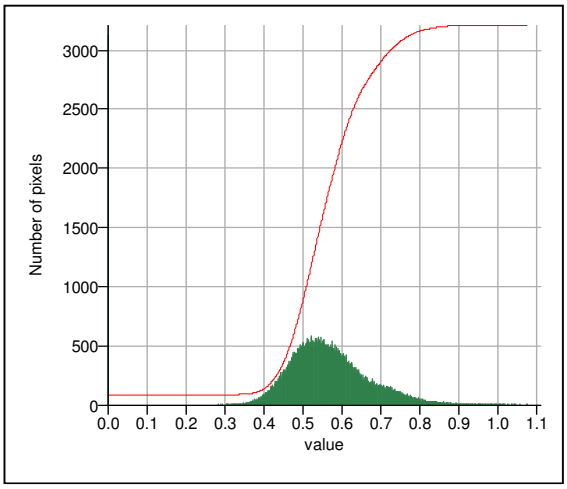

NDVI on DOY 225

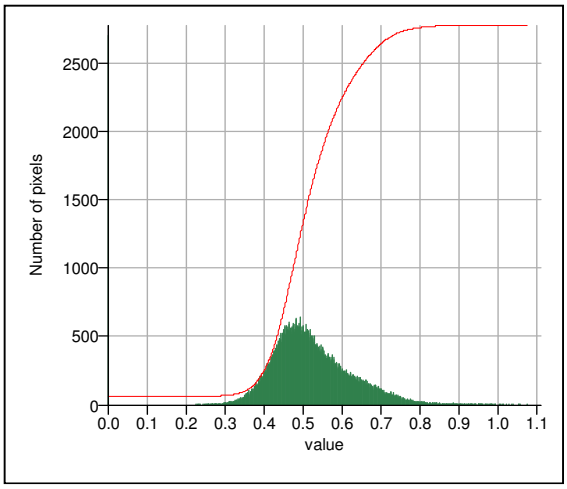

NDVI on DOY 232

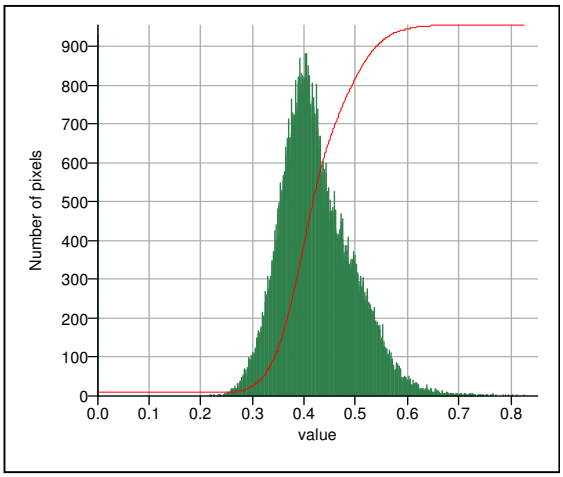

NDVI on DOY 255

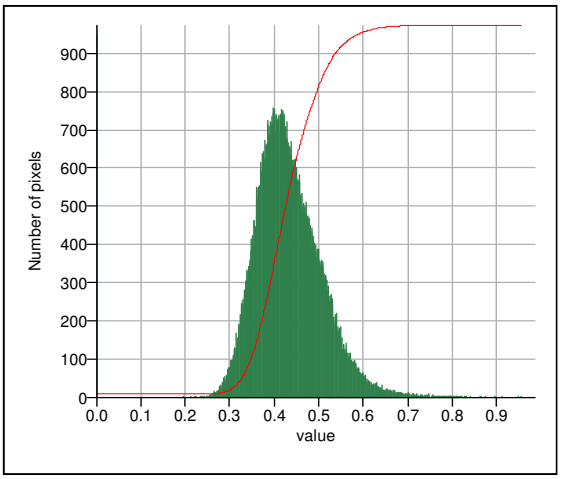

NDVI on DOY 257

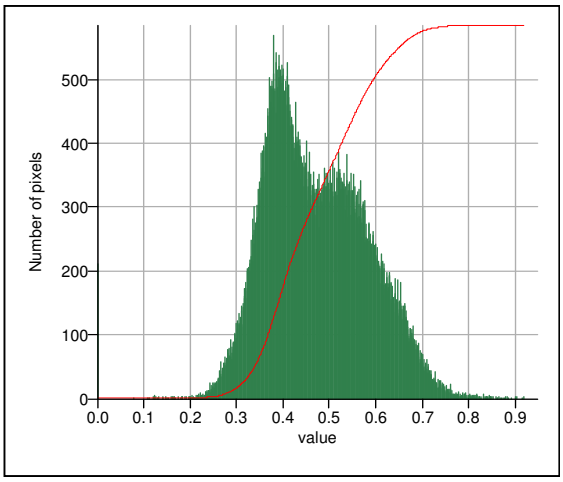

NDVI on DOY 287

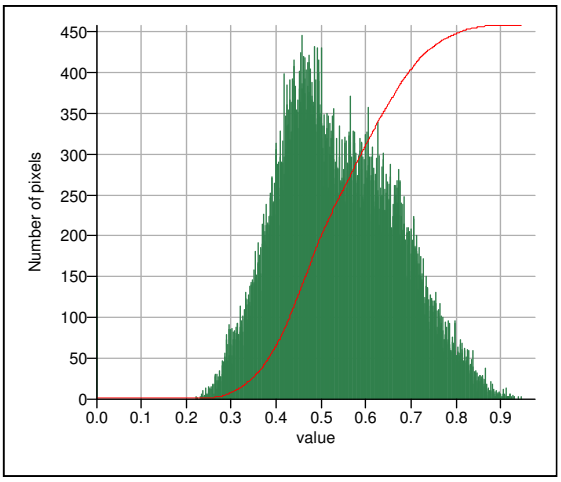

NDVI on DOY 292

Appendix 5: Landuse classes and their associated surface roughness values used in the calculation of ET_landuse Zom in the Semi-arid Barotse Sub-basin, Western Zambia

S/No.	Land cover class	Z_{om} value (m)	Source	Landcover type associated with the value in this study
1	Maize	0.4966	Su, 2005	30
2	Deciduous forest/mixed forest	1.2214	Su, 2005	50, 60 and 120
3	Closed to open shrubland	0.272	Brutsaert, 1982	130
4	Grass	0.034	Wieringa, 1993	140
5	Wetlands	0.0408	Su, 2006a	180
6	Water	0.0002	Brutsaert,1982	210